# Laser Assisted Isotopic Studies using Time of Flight Mass Spectrometer


*Muhammad Saleem*

Department of Physics
Quaid-i-Azam University
Islamabad, Pakistan
2006

This work is submitted as a thesis
in partial fulfillment of
the requirement for the degree of

DOCTOR OF PHILOSOPHY
IN
PHYSICS

Department of Physics
Quaid-i-Azam University
Islamabad, Pakistan
2006

# CERTIFICATE

It is certified that the work contained in this thesis is carried out and completed under my supervision at the Atomic and Molecular Physics Laboratory, Department of Physics, Quaid-i-Azam University, Islamabad, Pakistan.

**Supervisor**

**Prof. Dr. M. Aslam Baig (S.I. & T.I.)**
**Distinguished National Professor,**
Atomic & Molecular Physics Laboratory,
Department of Physics,
Quaid-i-Azam University,
Islamabad, Pakistan.

Submitted through:

**Dr. Pervez A. Hoodbhoy**
Chairman
Department of Physics,
Quaid-i-Azam University,
Islamabad, Pakistan.

***Dedicated***

***To***

*My parents, Wife and kids*
*Bilal and Eman*

# Contents

# Acknowledgement

All praise to the Almighty **Allah**, who enabled me to complete this research work, and my all respect for our dearest Holy Prophet **Muhammad** (*peace be upon him*), whose life is beacon for the salvation of the humanity.

I acknowledge my deepest sense of gratitude to my supervisor Prof. Dr. M. Aslam Baig (S.I., T.I.) for the guidance and encouragement provided to me throughout my research work. I always found him helping, friendly, and encouraging.

I am also thankful to Dr. Raheel Ali for his valuable discussions. I will never forget the working experience with Shahid Hussain and Dr. M. Aslam Zia, along with other colleagues Dr. Shaukat Mahmood, Nek M. Shaikh, Nasir Amin, Samil-ul-Haq, Yasir Yamil, Babar Rashid, Dr. Riaz Muhammad, M. Rafiq, Anwar-ul-Haq, Sarwat Uzair, Mazhar Ali Kalyar and Asif Hameed for their cooperation during my stay here. I am also thankful to Muhammad Sadiq for his valuable help in the Laboratory.

I found no words to thanks my parents who always been a continuous source of love and affection. I also cannot forget my sisters and brother Dr. Khalid Mahmood for their good wishes and prayers for me. I like to acknowledge the patience, which my wife and children, Bilal and Eman showed during the course of research work. Indeed, she faced boredom, when I always come late from the university and had to spend many hours at home pondering on the problems.

I am especially thankful to the Higher Education Commission Pakistan for the award of the scholarship under "Merit Scholarship Scheme 200" and Quaid-i-Azam University for the necessary financial support during the entire period of my research work. I am also thankful to Pakistan Atomic Energy Commission for granting me leave to complete Ph.D. studies.

*Muhammad Saleem*

# Abstract

The present work is devoted to the spectroscopic studies of the lithium isotopes using a locally designed and fabricated atomic beam – Time of Flight mass spectrometer system. Different intermediate states 2p $^2P_{1/2, 3/2}$, 3s $^2S$, 3p $^2P$, 3d $^2D$, 4s $^2S$, 4p $^2P$ and 4d $^2D$ of lithium have been exploited for the isotope separation. The proposed method enabled the isotope separation even if the isotopes have not been selectively excited. Fine structure in the 2p excited state for both the isotopes $Li^6$ and $Li^7$ has been resolved for the first time using this new technique. It is also noticed that the much higher energy density of the exciter laser limits the resolution of the fine structure levels of the lithium isotopes that leads to a loss in the enrichment of $Li^6$ due to the power broadening effect. We have investigated the yield of $Li^6$ exploiting the above mentioned excited states. An efficient pathway for the quantitative enrichment of the $Li^6$ isotope by tuning the exciter laser at the 3p $^2P_{1/2, 3/2}$ state of $Li^6$ have also been proposed in which a concentration up to 60 % is demonstrated from a natural isotopic abundant lithium sample.

In addition, we proposed an alternate technique for the simultaneous measurement of photoionization cross section of the excited states of the isotopes and their corresponding number densities. We report extensive new measurements of the photoionization cross section of the above mentioned excited states. By varying the frequency of the ionizer laser, different regions of the continuum have been investigated and a decreasing behavior of the photoionization cross section by increasing the energy of the ionizer laser is reported experimentally for the first time. The photoionization cross section from the 2p $^2P_{1/2, 3/2}$, 3p $^2P$, 4p $^2P$, 3d $^2D$ and 4d $^2D$ excited states of the lithium isotopes is maximum near the ionization threshold and a smooth decrease in the cross section is observed for the excess energy above threshold. However, for the 3s $^2S$ and 4s $^2S$ excited states, the cross section of the photoionization is lower at threshold and then increases to a maximum value and then decreases. It is also observed that the decrease in the cross section of the 3d $^2D$ and 4d $^2D$ excited states is more hydrogenic than that of the 2p $^2P_{1/2, 3/2}$, 3p $^2P$, and 4p $^2P$ excited states and for the 3s $^2S$ and 4s $^2S$ excited states, it is purely non-hydrogenic.

# List of Publications

1. **Alternate technique for simultaneous measurement of photoionization cross section of isotopes by TOF mass spectrometer**
   **M. Saleem**, N. Amin, S. Hussain, M. Rafiq, S. Mahmood and M. A. Baig
   Eur. Phys. J. D **38** 277 (2006)
2. **Laser isotope separation of lithium by two-step Photoionization**
   **M. Saleem**, Shahid Hussain, M. Rafiq and M. A. Baig
   J. Appl. Phys. **100** 053111 (2006)
3. **Simultaneous measurements of photoionization cross section of lithium isotopes at 3p $^2P_{1/2, 3/2}$**
   **M. Saleem**, S. Hussain, M. Rafiq and M. A. Baig
   J. Phys. B: At. Mol. Opt. Phys. **39** 5025 (2006)
4. **An efficient pathway for the $Li^6$ isotope enrichment**
   **M. Saleem**, Shahid Hussain, M. A. Zia and M. A. Baig
   Appl. Phys. B: Lasers and Optics (2007-in press)
5. **Photoionization cross section measurements from the 2p, 3d and 3s excited states of lithium**
   N. Amin, S. Mahmood, **M. Saleem**, M. A. Kalyar and M. A. Baig
   Eur. Phy. J. D **40** 331 (2006)
6. **Angular Momentum dependence of Photoionization cross section from the excited states of Lithium**
   Shahid Hussain, **M. Saleem** and M. A. Baig
   Phys. Rev. A **74** 052705 (2006)
7. **A Comparative study of RF and DC discharge based Laser Optogalvanic Spectroscopy of Helium Rydberg states**
   S. Hussain, **M. Saleem**, Nek M. Shaikh and M. A. Baig
   J. Phys. D: Applied Physics **39** 3788 (2006)
8. **Photoionization Cross section Measurements of the 3p $^{1,3}P$ Excited states of Helium in the Near-Threshold Region**
   S. Hussain, **M. Saleem**, M. Rafiq and M. A. Baig
   Phys. Rev. A **74** 022715 (2006)
9. **Diagnostics of cadmium plasma produced by laser-ablation**
   Nek M. Shaikh, B. Rashid, S. Hafeez, S. Mahmood, **M. Saleem** and M. A. Baig
   J. Appl. Phys. **100** 073102 (2006)
10. **Measurement of oscillator strength distribution in discrete and continuous spectrum of lithium**
    S. Hussain, **M. Saleem**, M. Rafiq and M. A. Baig
    Phys. Rev. A **75** 022710 (2007)
11. **Diagnostics of Copper Plasma Produced by the Fundamental, Second and Third harmonics of a Nd: YAG Laser**
    B. Rashid, S. Hafeez, Nek M. Shaikh, **M. Saleem**, R. Ali and M.A. Baig
    International J. Modern Physics B (2007-in press)

# List of figures

# List of Tables

# Chapter 1

# INTRODUCTION

## 1.1 Review

Fusion reactors are ultimately the future source of energy and deuterium tritium (D-T) reaction is considered to be a most suitable reactor fuel. Deuterium comprises 0.02 % of natural hydrogen and can be obtained from the seawater (30 g/m$^3$), but tritium does not exist naturally because of its radioactivity with a half-life of 12.36 years, which however can be produced artificially to fuel a fusion reactor. The lithium isotopes (7.5 % $Li^6$ and 92.5 % $Li^7$) have different nuclear properties of thermal neutron absorption. Due to the large absorption cross-section for the thermal neutron, the less abundant $Li^6$ isotope can be used as a tritium breeding material. Therefore, one has to enrich $Li^6$ in order to use it as the tritium breeding material. The classical methods of isotope separation on a large technical scale, such as the thermal diffusion (Ehrfeld 1983) or the gas-centrifuge techniques (Villani 1979) are expensive because they demand costly equipment and consume much energy. In addition, some other novel techniques exist, which are based on isotope-selective excitation/ionization by lasers called AVLIS (Bokhan *et al* 2006) and the laser enhanced chemical reactions (Zare 1977, Cantrell *et al* 1979, Alpine and Evans 1985, Symons 1985, Myers 1987, Arisawa *et al* 1983). Ion cyclotron resonance (ICR) heating is also one of the promising techniques (Dawson *et al* 1976) used for isotope separation. The large impetus for the development of efficient new methods for isotope separation is due to the increasing demands for the use of isotopes in medicines, biology, geology and hydrology as well as in nuclear industry. It is therefore worthwhile to think about some new and efficient techniques of isotope separation on a medium scale.

Laser isotope separation promised a popular method for the enrichment of the $Li^6$, owing to its high selectivity and low cost. Shimazu *et al* (1977) suggested that the two-step selective photoionization may leads to lithium isotope separation. A unique feature of this technique is its exceptionally high selectivity, which makes it potentially useful for

applications in environmental monitoring, nuclear industry, geophysics and ultra trace analysis. Isotope shifts and hyperfine structures form the basis of the isotopic selectivity. The line width of the exciter laser therefore determines the selectivity of an isotope of interest using multi step ionization. The technique however requires an ultra narrow line width exciter laser because of the small isotopic shift of the lithium isotopes. These types of lasers may include the cw dye lasers (Hollberg 1990), narrow line-width copper vapor laser (CVL) pumped-dye lasers (Duarte and Piper 1984, Bass *et al* 1992, Singh *et al* 1994, Maruyama *et al* 1996) and narrow line-width tunable external cavity semiconductor lasers (Zorabedian 1995, Duarte 1995). The cw dye lasers are relatively complex, expensive and require fairly sophisticated engineering for building and maintenance. One advantage, however, is that they can yield relatively high cw powers in a single longitudinal mode. CVL pumped dye lasers can also deliver very narrow line-widths and tenability. This type of laser has been operated only in a handful of laboratories around the world. A relatively inexpensive alternate is the tunable external cavity semiconductor diode lasers that can yield a narrow line-width single longitudinal mode but with very low average powers.

In this thesis, we have demonstrated another experimental approach with which we can resolve the very close lying energy levels even if they have not been selectively excited. This technique is a combination of a well-collimated atomic beam source and a linear Time of Flight (TOF) mass spectrometer. The TOF mass spectrometer is a very sensitive ion detector (Castaldi *et al* 1998) and has the advantage over other ion detectors like thermionic diode (Niemax 1985) and triple-crossed-atomic beam apparatus (Nygaard *et al* 1975) that it can resolve the isotopic masses on the time axis. It made possible simultaneous measurement of the spectroscopic properties of the selected isotopes (Demtröder 1998, Saleem *et al* 2006). It has been widely used for the measurement of the photoionization cross section of the excited states (Lievens *et al* 1996, Philipsen *et al* 2000, Gisselbrecht *et al* 1999) as well as for the ground states of different elements (Sato *et al* 1985, Huang *et al* 1999, Wehlitz *et al* 2002, Van der Hart and Greene 1998.

## 1.2 Laser-Atom Interaction

An atom possesses discrete and continuum energy states. When the laser light interacts with an atom, the outermost electron in some initial discrete state $|i\rangle$ absorbs the photon energy $h\upsilon$ and jumps to the next energy state $|f\rangle$ provided that the photon energy is in resonance with the energy difference between the states involved i. e;

$$E_f - E_i = \hbar\omega$$

Here $\omega$ is the frequency of the absorbed photon. Similarly, when an electron jumps from some higher energy state to a lower energy state, it emits a photon of energy corresponding to the energy difference of the involved states. The absorption of a photon in an atomic system is shown in figure (1.1).

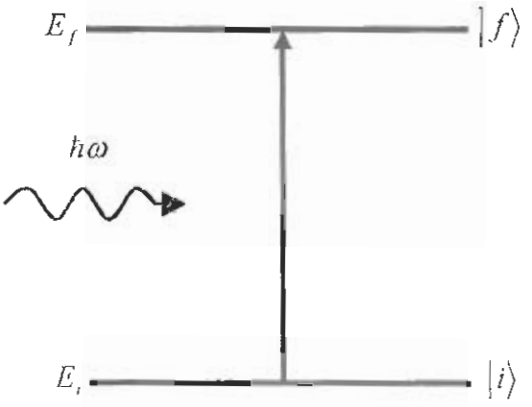


Figure 1.1 *Interaction of laser radiation with atom*

Due to some inherent properties of the laser light, such as mono-chromaticity, directionality, coherence and high intensity, new fields of research have emerged such as photoexcitation, photoionization, laser-induced breakdown studies, laser cooling and multi-photon excitation processes. Laser radiation can be absorbed in any atomic or molecular system through many processes like multi-step and multi-photon absorption. A description of these processes is presented in the next sections.

### 1.2.1 Multi-step excitation/ionization

In the single photon absorption, a photon is absorbed by an atom and gets excited from $|i\rangle$ to the $|f\rangle$ state. In multi-step absorption, an atom can simultaneously absorb photons

of different colors depending upon the lifetime of the intermediate levels. The simplest example is the two-step photoabsorption.

In the two-step absorption, the intermediate state is a real state. In this process two photons of different frequencies, $\hbar\omega_1$ and $\hbar\omega_2$ interact with an atom and are simultaneously absorbed. First photon $\hbar\omega_1$ is absorbed and excites the atom from the ground state $|i\rangle$ to the first excited state $|k\rangle$, which is considered as an intermediate state. The second photon $\hbar\omega_2$ excites the atom from the state $|k\rangle$ to the final excited state $|f\rangle$. This process is depicted in the figure (1.2).

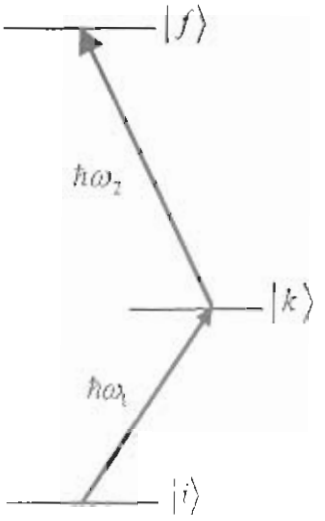


Figure 1.2 *Two-step photoabsorption processes*

The transitions following this process, obey the single-photon dipole selection rules and one can approach high Rydberg states by selecting different intermediate states. The transition probability per unit time is expressed as (Thorne 1988 and references therein) for the electric dipole approximation:

$$P_{ij} = \frac{\pi\rho(\omega_{ij})}{3\varepsilon_0\hbar^2}\left|\langle f|er|i\rangle\right|^2 \qquad (1.1)$$

Here $\rho(\omega_{ij})$ is the radiation density per unit interval of the angular frequency. The transition probability depends on the electric dipole matrix element $\left|\langle f|er|i\rangle\right|^2$. This

term is non-zero only when the angular momentum between the initial and the final state change by ± 1 i. e.

$$\Delta \ell = \pm 1,$$

$$\Delta S = 0,$$

$$\Delta J = 0, \pm 1, \quad 0 \leftrightarrow 0 \ \textit{forbidden}$$

Here $\ell$ is the orbital angular momentum, $J$ is the total angular momentum and $S$ is the multiplicity of the concerned state. All the transitions in the multi-step excitation process follow these dipole transition selection rules.

The intermediate state should have opposite parity to that of the initial and final states. The conditions for the effective excitation of the final state $|f\rangle$ through the ladder of real intermediate states is that the laser-pulse duration $\tau$ must be shorter than the lifetime of the intermediate state $|k\rangle$ and the second laser should come within the lifetime of the excited state $|k\rangle$. Following are some advantages of using multi-step photoabsorption:

1. Transitions that lie in the VUV regions can be achieved using dye lasers in the visible and near ultraviolet regions.
2. The stepwise excitation provides the maximum probability of exciting the atoms to the high-lying states.
3. The time resolution of the order of the lifetimes of the intermediate excited state can be obtained.

A disadvantage of this technique is that one requires as many lasers as the number of steps to access the final excited states.

### 1.2.2 Multi-photon excitation/ionization

The availability of the intense laser sources opens the area of the multiphoton absorption. Two-photon absorption is the simplest example, which is similar to the two-step process but the intermediate state is a virtual state. Two-photon absorption was theoretically predicted by Goppert-Mayer in 1931 and was experimentally observed after the invention of lasers in 1961 using a ruby laser as the light source. The figure (1.3) shows a two-photon transition where the intermediate state is a virtual state.

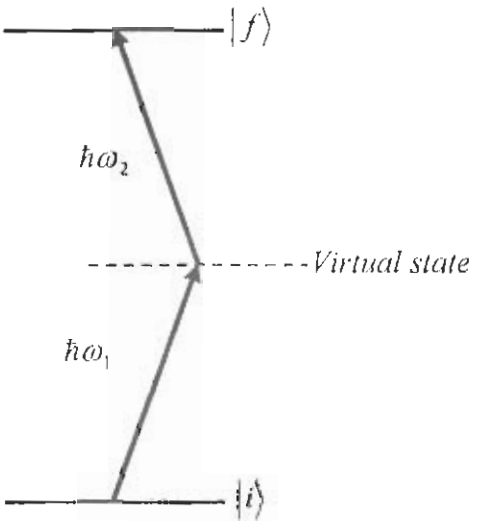


Figure 1.3 Two-photon photoabsorption processes

Two photon absorption are expressed as

$$E_f - E_i = \hbar(\omega_1 + \omega_2)$$

Here $\omega_1$ and $\omega_2$ may be the same or different frequencies. The corresponding probability of the two-photon absorption, $\sigma_{if}$ ignoring the Doppler effect, is given by

$$\sigma_{if} = \frac{I_1 I_2}{(2\hbar^4 \Gamma_{if})} \left| \sum_k \left[ \frac{(d_{ik} e_1)(d_{kf} e_2)}{\omega_{ki} - \omega_1} + \frac{(d_{ik} e_2)(d_{kf} e_1)}{\omega_{kf} - \omega_2} \right]^2 \right| \qquad (1.2)$$

Here the summation is over all the intermediate state $|k\rangle$ accessible from the initial state $|i\rangle$, $I_1$ and $I_2$ are the intensities of $\omega_1$ and $\omega_2$, $d_{ik}$ is the electric dipole matrix elements between the states $|i\rangle$ and $|k\rangle$ and $\Gamma_{if}$ is the half-width at maximum intensity of the $|i\rangle \rightarrow |k\rangle$ transition. The term $(d_{ik} e_1)$ is the projection of the transition dipole moment matrix element onto the light-wave polarization vector. The equation (1.2) can be obtained either by calculating the probability of the two-photon transition using the perturbation theory (Dirac 1958), or from the expression for the imaginary part of the third order nonlinear susceptibility (Bloembergen and Levenson, 1976) for a quantum system in the light field. If $\omega_1$ and $\omega_2$ are chosen such that they come close to a real intermediate state then from the above equation a sharp increase in the probability is expected.

Equation (1.2) predicts that the two-photon transition probability is non-vanishing only if both the dipole matrix elements $d_{ik}$ and $d_{kf}$ are non-zero and that can be non-zero only for $\Delta\ell = \pm 1$. Since two photons are involved in the transition, therefore, the selection rules for two-photon process are

$$\Delta L = 0, \text{ or } \Delta L = \pm 2$$

The initial $|i\rangle$ and final $|f\rangle$ states should have the same parity. Therefore, the states, which are not possible to access through the single photon process, can be approached through the two-photon excitation. The two-photon transition is polarization dependent, such that if two-photon transition is carried out through two parallel right circularly polarized lights, only $\Delta L = \pm 2$ transitions will be observed. However in the case if one of the beams is counter circularly polarized only $\Delta L = 0$ transitions will be observed.

The two-photon process has some major advantages over conventional single photon excitations. First, one can use the visible light to access the energy states that are lying in the UV-region. Second, one can study the transitions between the states of same parity, i.e., the states, which are forbidden in the case of single photon transitions, are accessible in the two-photon process. Among the other advantages is the minimization of the Doppler broadening using counter-propagation of lasers for two-photon absorption process and thus achieving high-resolution data.

## 1.3 Fine Structure Levels

The structure originated due to the interaction between the magnetic field of the orbiting electron and the magnetic moment associated with its spin is known as the fine structure splitting. All the energy states of the valence electrons in the alkali elements (except for those with $\ell = 0$) split into two components; one state corresponding to the total angular momentum number $j = \ell + 1/2$ and the other to $j = \ell - 1/2$. The interaction causing this splitting is termed as spin-orbit interaction. The energy shift due to this interaction is given (Bransden and Joachain 1983) as:

$$\Delta E = \frac{1}{2}\lambda_{nl}\left[ j(j+1) - l(l+1) - \frac{3}{4} \right] \tag{1.3}$$

The constant $\lambda_{nl}$ is proportional to the expectation value of $\frac{1}{r}\frac{dV(r)}{dr}$ and is given by

$$\lambda_{nl} = \frac{\hbar^2}{2m^2c^2}\left[\frac{1}{r}\frac{dV(r)}{dr}\right] = \hbar^2\,\xi(r) \qquad (1.4)$$

Here $V(r)$ is the effective central potential in which the valence electron moves. The magnitude of $\lambda_{nl}$ can be estimated by using $V(r)$ as calculated by the Hartree-Fock method. It is observed that for a given atom the splitting decreases with the increasing $n$ and $\ell$ values.

Using the Hartree-Fock potential, $\lambda_{nl}$ is found to be positive, and the state with $j$ = 3/2 has greater energy than that with $j$ =1/2. This is true for all the terms of lithium, and for the lower lying states of other alkalis. The one-electron selection rules for the transitions between the fine structure components are

$$\Delta\ell = \pm 1$$

$$\Delta j = 0, \pm 1 \quad with\ 0 \leftrightarrow 0\ forbidden$$

## 1.4 Hyperfine Structure and Isotopic Shift

Michelson in 1891 and Fabri and Perot in 1897 discovered hyperfine effects, which produces shift in the energy levels that are usually much smaller than those corresponding to the fine structure. These effects can be classified in to two types, those which give rise to the splitting of the electronic energy levels, called hyperfine structure and those that slightly shift the energy levels but with out giving rise to the level splitting are called isotope shift.

The hyperfine structure is a small perturbation in the energy levels of atoms or molecules due to the magnetic dipole-dipole interaction, arising from the interaction of the nuclear magnetic dipole with the magnetic field of the electron. Therefore, due to the electron's spin, there is also hyperfine splitting for s electrons, which have zero orbital angular momentum. The nuclear spin $I$ and the total angular momentum $J = L + S$ gets coupled, giving rise to the grand total angular momentum $F = J + I$. The hyperfine splitting is then expressed as (Yang and Hamilton 1996):

$$\Delta E_{hfs} = -\mu_I\, B_J = \frac{a}{2}\left[F(F+1) - I(I+1) - J(J+1)\right]$$

Here $a = \frac{g_I \mu_N B_J}{\sqrt{J(J+1)}}$

Here $\mu_N$ the magnetic dipole moment of the nucleus.

Pauli and Peierls (1931) pointed out that the difference in the nuclear volume (nuclear charge distribution) between the isotopes can produce an isotpe shift. Bransden and Joachain (1983) represented the energy shift between the isotopes as:

$$\delta E \cong \frac{4}{5} \frac{Ze^2}{4\pi\varepsilon_0} R^2 \frac{Z^4}{a_\mu^3 n^3} \frac{\delta R}{R}$$

Where R is the radius of the isotope and $\delta R$ is the difference in the radii of the two isotopes. Thus the isotope with the larger radius has the higher energy value. Also the isotopic shift $\delta E$ increases when Z increases and n decreases, so that the most important volume effects occur for low lying $s$ states.

## 1.5 Photoionization Cross Section

The probability of photoionization of atoms to an ionic state is proportional to the photoionization cross section. Photoionization is a dipole transition between the initial $\Psi_i$ and final $\Psi_f$ states. The only difference from the discrete electronic excitation is that the final state lies in the continuum. This means that for each energy $E > 0$, there is a solution of the Schrödinger equation of the form $e^{ikr}$. This solution does not decay at infinity, but oscillates periodically and corresponds physically to an electron asymptotically free. Transition probability is controlled by the dipole transition moment

$$M_{fi} = \langle \Psi_f | r | \Psi_i \rangle$$

and the cross section is proportional to the sum of the squares

$$\sigma \propto \sum_f |M_{fi}|^2$$

over all final states available. Angular momentum and the parity selection rules imply $\ell_f = \ell_i \pm 1$, so for the n$s$ orbital ionization only the $ns \to \varepsilon p$ channel gives a contribution, while ionization of a *nd* orbital occurs through two channels $nd \to \varepsilon f$ and $nd \to \varepsilon p$. Generally, the $\ell_f \to \ell_i + 1$ transition contributes dominantly. The interaction, and hence the cross section will be larger when the vacated orbital and the photoelectron

wave are in the same spatial region. The variation of a photoelectron wave with the photon energy gives rise to considerable variations in the cross section. The photoionization cross section gives a direct picture of the orbital levels.

The cross section is usually highest near the ionization threshold and after that decreases with increasing the excess photon energy. As the kinetic energy of the photoelectron increases, its wavelength decreases and the electron wave becomes more oscillatory. As a consequence, the positive and negative parts of the dipole matrix element with the vacated orbital tend to cancel one another, and the cross section suffers rapid decay. The rate of the decay can be characteristic of the atomic orbital.

Different theoretical and experimental techniques have been developed for the determination of the photoionization cross section of the ground as well as the excited states of atoms and molecules. We have demonstrated an alternate technique for the simultaneous measurement of photoionization cross section of the excited states of the isotopes. The technique is described in the chapter 5.

## 1.6 Gaussian Beam

The radial distribution of a laser radiation oscillating in the fundamental mode has a gaussian profile. The transverse distribution of the intensity of a simple gaussian beam is of the form

$$I = I_0 \, e^{-\frac{2r^2}{\omega^2}}$$

Here $I_0$ is the maximum intensity and $\omega$ is the beam radius (or waist) inside of which 86.5 % of the energy is concentrated, as shown in the figure (1.4). A detailed description of the Gaussian beam has been treated by Demtröder (1998).

When a Gaussian beam is focused by a lens of focal length $f$, the spot size in the beam waist (at the focus) for $f >> \omega_1$ is

$$\omega_0 = \frac{f\lambda}{\pi \omega_1}$$

Where $\omega_1$ is half the spot size of the laser beam on the focusing lens. To avoid the diffraction losses, the diameter d of the lens should be $d \geq 3\omega_1$. The Gaussian beam then expands and diverges from the focus point.

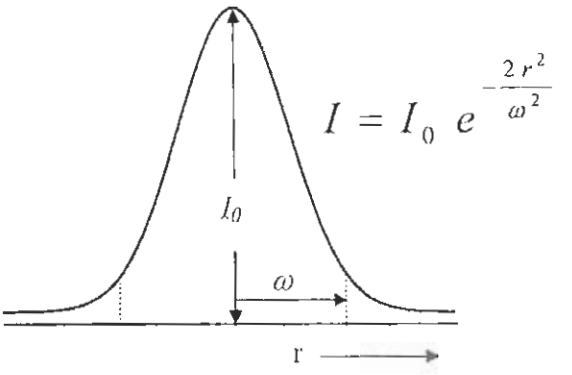


Figure 1.4 *Radial distribution of Gaussian beam*

The diameter of the expanded Gaussian beam can be calculated at any distance z from the focus point as

$$\omega(z) = \omega_0 \sqrt{1 + \left(\frac{\lambda z}{\pi \omega_0^2}\right)^2}$$

$$= \omega_0 \sqrt{1 + \frac{z^2}{z_R^2}}$$

Where $z_R = \frac{\pi \omega_0^2}{\lambda}$ is known as Rayleigh range, as shown in the figure (1.5). It is also referred to as the depth of focus when focusing a Gaussian beam. The length of the Rayleigh distance depends on the spot size and therefore on the focal length of the focusing lens. At $z = z_R$,

$$\omega(z) = \sqrt{2}\omega_0$$

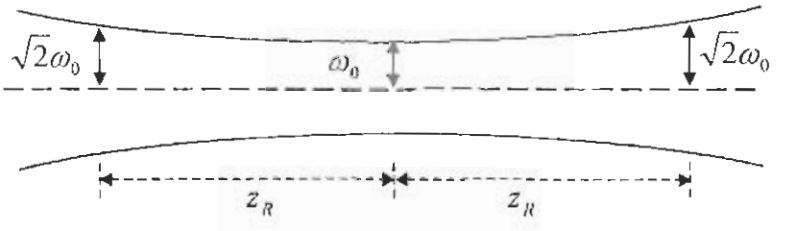


Figure 1.5 *Gaussian beam parameters associated with the minimum beam waist.*

## 1.7 Layout of the Thesis

In this work we have investigated the enrichment of $Li^6$ exploiting seven excited states of lithium. The second chapter contains the experimental set up which has been used for all the experimental studies in this work. The third chapter is about the design, construction and the performance of the TOF mass spectrometer and the atomic beam apparatus. In the fourth chapter, investigations about the enrichment of $Li^6$ from the different excited states of lithium are presented and the fifth chapter contains the simultaneous measurements of the photoionization cross section of the excited states being exploited in the enrichment process.

# Chapter 2

## Experimental Setup

The experimental setup for measuring the photoion yield as a result of two-step ionization of the excited stated of atoms is described. The setup consists of a vacuum chamber, which accommodates a locally developed atomic beam apparatus and a Time of Flight mass spectrometer, an exciter and ionizer laser, and the data recording system. The apparatus has been used to carry out all the experiments described in this thesis.

Figure (2.1) shows a schematic diagram of the experimental setup for the selective two-step photoionization spectroscopy/spectrometry of isotopic lithium atoms. It consists of a vacuum chamber for an in-house built atomic beam source and a Time of Flight (TOF) mass spectrometer, Nd:YAG laser (Brilliant-B, Quantel), a narrow line-width dye laser TDL-90 (Quantel), a home made open cavity dye laser pioneered by Hanna *et al* (1975) and a digital storage oscilloscope (TDS 2024) interfaced with the computer for spectrum analysis. The 90 % of the laser energy at 532 nm was used to pump the TDL-90 dye laser while the remaining 10 % was used to pump the Hanna type open cavity dye laser.

A spectroscopically grade pure lithium sample with natural isotopic abundance of 7.5 % $Li^6$ and 92.5 % $Li^7$ was filled in the atomic beam oven which was then vaporized by a cylindrical resistive heater that surrounds the oven. The oven temperature was maintained at ≈ 600 K, which was monitored by a Ni-Cr-Ni thermocouple with an accuracy of ± 2%. The lithium atomic beam source was placed precisely below the ionization/extraction region of the TOF mass spectrometer, from where a well-collimated atomic beam, after passing through a set of collimating apertures, travels from the bottom to the top of the vacuum chamber. A locally developed TOF mass spectrometer was used for the separation and detection of the lithium isotopic ionic masses. The operating chamber pressure was maintained at ≈ $10^{-6}$ Torr at the interaction region. The laser used to excite the lithium atomic levels is termed as exciter and the laser used for their subsequent ionization from the excited levels is termed as the ionizer. At the center of the ionization/extraction region of the TOF mass spectrometer, the lithium atomic beam was

irradiated with the exciter laser beam, followed by the ionizer laser beam with some delay. The relative delay between the exciter and the ionizer laser pulses can be controlled and varied by an optical delay line, which is necessary to optimize the photoion signals. The two laser beams were introduced into the vacuum chamber from opposite directions. As a result of two-step photoionization, the ionic species were accelerated twice and allowed to travel in the field free region of the TOF mass spectrometer where the isotopic masses were separated and ultimately detected on the channeltron. The current signal from the channeltron was recorded on the oscilloscope (TDS 2024) via a 50 Ω feed-through, which was necessary for capturing the fast signals. The digital oscilloscope was computer interfaced to transfer the data to the computer for subsequent processing and analysis. The wavelength calibration of the isotopic peaks was achieved by simultaneously recording the output TOF signals and the etalon fringes from a 5 mm thick fused silica Fabry-Perot etalon (FSR 0.67 $cm^{-1}$) via three boxcar averagers (SR250). Two boxcars were simultaneously used to register the isotopic signals of $Li^6$ and $Li^7$ and the third for capturing the etalon fringes. Each data point is an average of three laser shots. The isotopic signals were recorded with the scanning speed of 0.003 nm/s of the exciter laser in order to capture every event change in the photoion signals of $Li^6$ and $Li^7$. The neutral density filters were used to adjust the intensity of the exciter and the ionizer lasers beams independently. In order to measure the exciter and the ionizer laser energies, an energy meter (R-752 universal radiometer with P-444 Pyroelectric Probe, DigiRad USA) was used with an accuracy of ± 3%. A detailed description of the experimental elements is described below.

## 2.1 Laser System

The laser system comprises two types of lasers: solid state Nd: YAG laser and a dye laser. The SHG (second harmonic generation) of the fundamental wavelength of Nd: YAG laser at 532 nm was used to pump the dye laser. A brief description of both types of lasers is given below.

### 2.1.1 Nd: YAG Laser

We have used a Q-switched Nd: YAG (Brilliant-B Quantel) laser source for pumping two dye lasers, the TDL-90 (Quantel) and a home made open cavity Hanna type. The

Nd:YAG laser (Brilliant-B) is coupled with SHG and THG modules for producing laser at 532 and 355 nm with the corresponding energies 450 and 200 mJ respectively with pulse duration of 5ns and 10 Hz repetition rate. The output laser energy can be controlled by the flash lamp – Q switch delay circuit. We have pumped both the dye lasers with 532 nm (SHG of Nd:YAG laser) for the entire experiments conducted in the present studies.

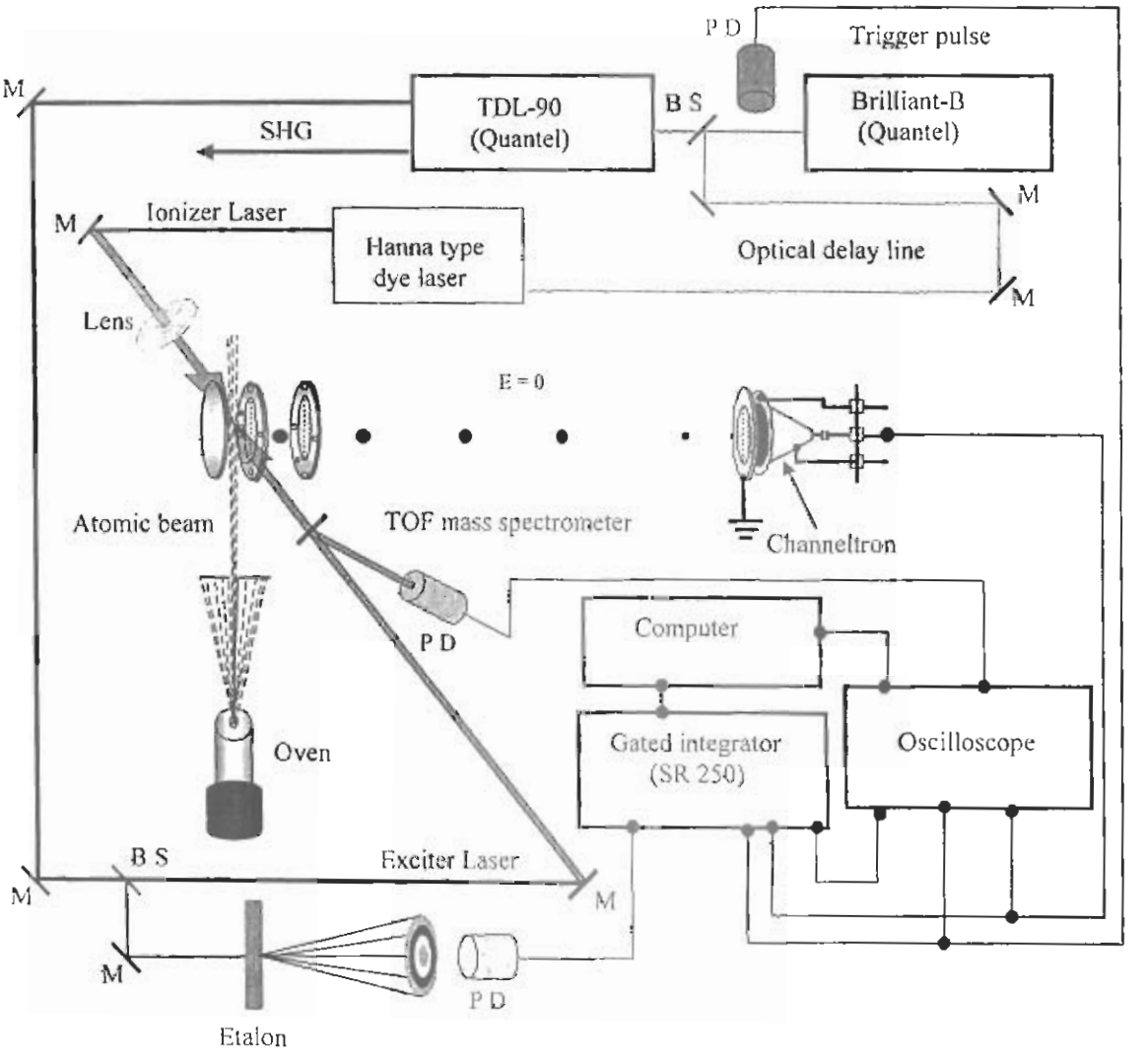


M = Mirror  B S = Beam splitter  P D = Photodiode

Figure 2.1 *Experimental setup for laser assisted isotopic studies of the lithium*

## 2.1.2 Dye Laser

A dye laser is a type of laser, which uses solution of some particular dye as an active lasing medium. The most useful feature of dye lasers is their tunability i.e. the

wavelengths emitted by the dye lasers can be varied over a wide range depending on the dye material, dye solution concentration, pumping source etc. Like other types of active medium of lasers, when a dye solution is pumped with any light source (Flash lamps, Lasers etc) they emit fluorescence over a broad range of wavelengths (Sorokin and Lankard 1966, Schafer *et al* 1966). Taking advantage of this broad fluorescent width, one can use a wavelength-dispersive optical element such as a diffraction grating or prism at one end of the dye laser resonator to perform selective tuning (Duarte and Piper 1984). Such tuning can yield different wavelengths at extremely narrow line width. Dye lasers can be operated in both pulsed and CW modes depending on the pumping source. We have used two dye laser systems in our experiments; TDL-90 (Quantel) and open cavity Hanna type (Hanna *et al* 1975).

### 2.1.2.1 TDL-90 (Quantel)

TDL-90 dye laser uses a high resolution grating in grazing incidence to tune over a wide range of wavelength with narrow linewidth. It uses a special cavity configuration for low level of fluorescence and a prism beam expander for narrowing the laser linewidth. Schematic of the prism beam expander is shown in figure (2.2).

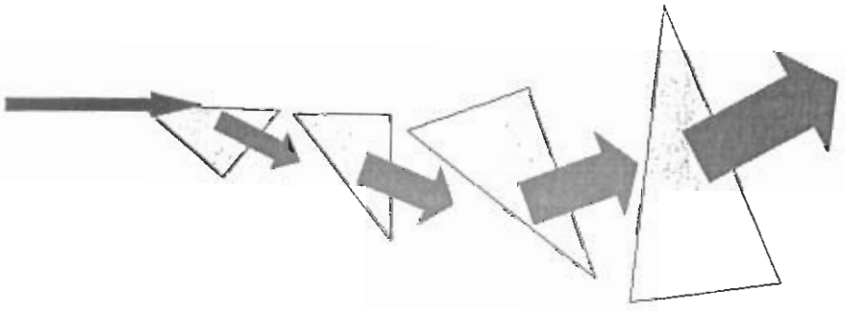

Figure 2.2 *Multi-prism beam expander*

The TDL-90 dye laser is computer interfaced for scanning the wide range of wavelengths with a very small scanning step. It provides the auto tracking option for the UV laser radiation to scan the dye laser over the highly excited states of the atoms. This dye laser delivers the laser light over a wide range with the line width ~ 0.1 $cm^{-1}$ (measured using

an etalon of FSR 0.67 $cm^{-1}$). The complete optical layout of the TDL-90 is shown in the figure (2.3).

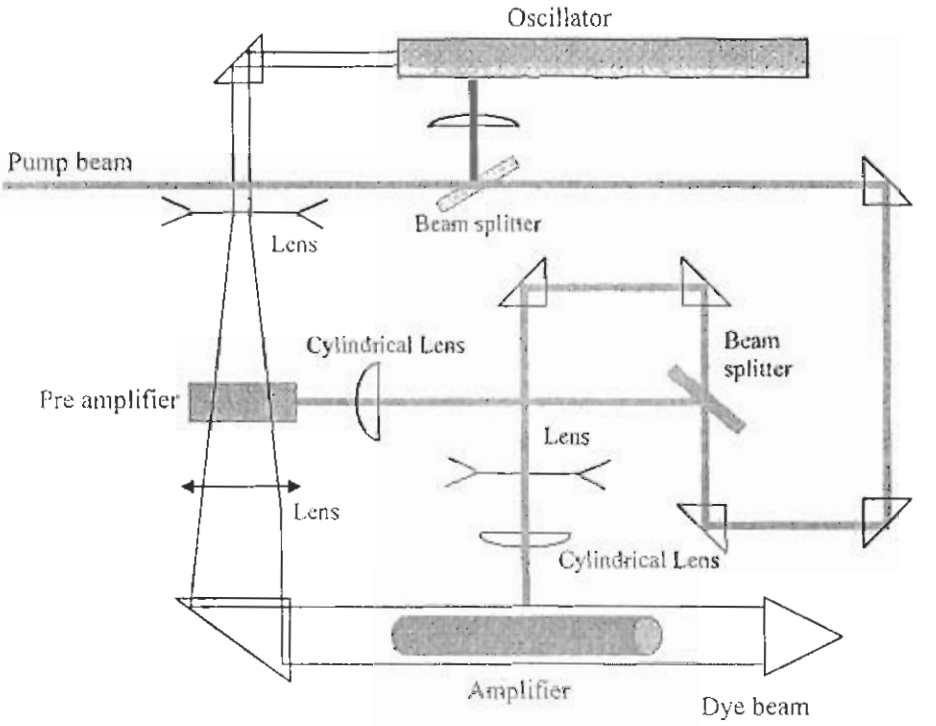


Figure 2.3 *Optical lay out of TDL-90 (Quantel) dye laser*

### 2.1.2.2 Open cavity Dye Laser

Hänsch (1972) introduced a very exciting feature of a dye laser i.e. narrow bandwidth. A telescopic cavity for the beam expansion was used to illuminate the grating. Thus by using the dispersive characteristics of the grating used in the Littrow configuration, a linewidth of about 0.08 $cm^{-1}$ at $\lambda \sim 600$ nm was achieved. Further narrowing of the linewidth was achieved by using an intracavity etalon. Hanna *et al* (1975) reported the linewidth in the range of 0.08 $cm^{-1}$ to 0.2 $cm^{-1}$ with an improved single prism laser cavity design. Another way of illuminating the grating is at a grazing incidence angle. Using such a configuration, Shoshan *et al* (1977) and Littman and Metcalf (1978) have reported a linewidth of the order of 0.08 $cm^{-1}$ at $\lambda \sim 600$ nm.

However, there are two disadvantages in the use of single prism cavities as these employed the prism at a high angle of incidence, which causes significant optical power

loses. Moreover, in the case of an open cavity the output is coupled with a high component of amplified spontaneous emission and the closed cavity leads to reduced efficiency. Duarte and Piper (1980) reported a dye laser with a linewidth of the order $0.05cm^{-1}$ (at $\lambda \sim 510$ nm) and an efficiency of 14 % using a multiple prism beam expander.

We have used the Hanna type open cavity dye laser with linewidth ~ 0.3 $cm^{-1}$ throughout our experiments, which is formed between a flat mirror and a 2400 lines $mm^{-1}$ holographic grating, as shown in the figure (2). The pumping beam (532 nm) was focused on a dye cell through a quartz cylindrical lens of a 10 cm focal length. The dye cell was tilted at a 15° for the prevention of the parasitic lasing. A right angle prism expander was used to expand the beam before striking the holographic grating (2400 lines/mm). As a result the beam illuminates the maximum area of the grating. The grating used was placed in Littrow configuration that serves as wavelength selector as well as an end reflector. The perfect alignment of the cavity and the area of the grating illuminated ensure the generation of the narrow bandwidth dye lasers.

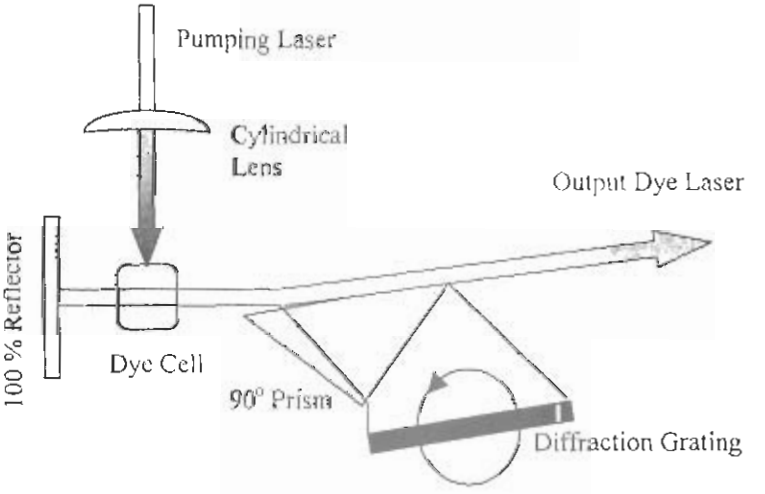


Figure 2.4 *A Hanna type open cavity dye laser cavity*

## 2.2 Data acquisition system

The digital oscilloscope TDS 2024 was used to acquire the TOF signals. When the exciter laser was scanned, two gated integrator (SR 250) were used to get the averaged output signals of both the isotopes. The SR 250 consists of a gate generator; a fast gated

integrator and exponential averaging circuitry. The unit generates a gate when triggered internally or externally. The delay of this gate can be adjusted from a few nanoseconds to 100 milliseconds and its width can be varied from 2 ns to 15 μs. The fast-gated integrator integrates the input signal during the gate. The output from the integrator is then normalized by the gate width to provide a voltage that is proportional to the average of the input signal during the sampling gate. This signal is further amplified according to the front panel sensitivity setting. By averaging many noisy samples of a signal, the average is made to converge to the mean value of the signal as noise averages out to almost zero. In order to trigger the oscilloscope and the gated integrator, a photodiode BPX65 was used. The laser pulse from the same photodiode was used as the reference pulse for the measurement of the time of flight of the isotopic masses.

# Chapter 3

## Design and Fabrication of Atomic Beam Apparatus and Time of Flight Mass Spectrometer

A design and construction of an atomic beam apparatus in conjunction with a linear Time of Flight (TOF) mass spectrometer for isotopic studies is presented. The atomic beam source consists of a cylindrical shape oven enclosed by a cylindrical heater for producing vapor pressure in the oven. The atomic beam source is simple, versatile and can be operated at a stable temperature up to 1000 K. The Time of Flight mass spectrometer provides a two-stage acceleration and one-meter field free length for separating isotopic masses. Interaction of a laser with an atomic beam produces ions, which are resolved and detected by the TOF mass spectrometer and the observed signals are correlated with the flight times for different isotopic masses. The optimum performance of this system has been demonstrated by the isotopic separation of lithium. The designed and fabricated system has been used for the studies of the ionization yield of a particular isotope and the measurements of the absolute photoionization cross-section of different excited states of the lithium isotopes $Li^6$ and $Li^7$.

### 3.1 Atomic Beam Apparatus

A well collimated atomic beam is an extremely powerful tool for the investigation of many fundamental problems in modern physics. An atomic beam system consists typically of an oven containing a source of atoms, an exit hole and a set of apertures to attain a well collimated atomic beam. Fraser (1931) and Ramsey (1956) described the design parameters e.g. exit hole size, effusion rate, collimation, shape and size, beam flux, velocity distribution, density, and intensity of an atomic beam. Estermann (1946) described the physical concepts as well as the design of well-collimated beams. Aushev *et al* (1982) described the properties of the lithium atomic beam like angular dispersion, divergence, directivity and the type of flow of the atoms. Ross and Sonntag (1995) described in detail the high temperature metal atomic beam sources, different types of flow of atoms along with the materials used for the construction of atomic beam ovens, and the collimation apertures. The controlled atomic beams can be used for the construction of the objects and devices of a few nanometers in size (Maissel and Glang 1970). Giormaine and Wang (1960) attained a high directivity and beam intensity using

long parallel tubes instead of an exit hole. High directivity atomic beams are used for isotope separation by the laser deflection method, laser selective excitation/ionization of ions, and the TOF mass spectrometer. The advantages of producing an atomic beam with reduced transverse velocity components are the reduction of collisions and Doppler broadening, which causes the broadening of the spectral lines.

We have designed an atomic beam source to produce a well-collimated and directed atomic beam of particles. The directivity of an atomic beam depends upon the mode of flow, the geometry of the exit hole and the collimating apertures. The high-resolution spectroscopy needs a transparent flow of a beam of atoms in which there are ideally no collisions. This type of flow depends upon the vapor density of the element inside the oven, the diameter and wall thickness of the exit hole. The atomic flow from the exit hole is transparent if the mean free path ($\lambda$) in the oven is larger than the diameter 'a' of the exit hole and the thickness 't' of the aperture wall is less than 'a'. The mean free path (Ramsey 1956) is given by

$$\lambda = 7.321\times10^{-20}\frac{T}{P\,\delta} \quad (cm) \tag{3.1}$$

Where $\delta$ is the cross section for atomic collisions ($cm^2$), $T$ is the absolute temperature of the oven (K) and $P$ is the vapor pressure (Torr).

The atomic beam source is a cylindrical stainless steel oven with an exit hole of 2 mm diameter and 0.5 mm wall thickness, to allow the atoms to diffuse from the source in the transparent mode. A cross-sectional view of the oven assembly is shown in figure (3.1). The stainless steel 304 is chosen (Compbell and Shewood 1967, Weissler and Carlson 1979) for the construction of all the components including the oven and the cylindrical housings because it is a good vacuum material. The inner diameter of the oven cylinder is 9 mm and the depth is 75 mm for sample loading. A thermo-coax wire (*Philips*) is wrapped around the cylindrical housing in such a way that the induced magnetic field is cancelled out in the vicinity of the heater. The filled and open circles in figure (3.1) represent the flow of current in the opposite direction. The heater assembly is then fixed in a ceramic (Alumina, $Al_2O_3$) cylinder, which is a bad conductor of heat and electricity having a high melting point of 2300 K (Ross and Sonntag 1995). The alumina cylinder is then fixed in a stainless steel cylindrical base, which is placed at the center of the vacuum

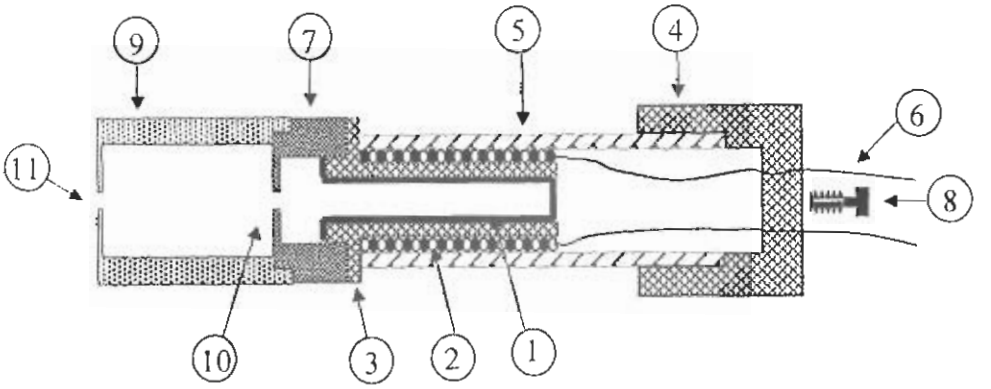


1) Oven (SS)
2) Thermo coax heating wire
3) Cylindrical housing (SS)-1
4) Cylindrical housing (SS)-2
5) Ceramic housing (alumina)
6) Power cables
7) Cup with exit hole
8) Assembly holding screw
9) Collimation cup
10) Oven exit hole
11) Collimation aperture

Figure 3.1 *Cross sectional view of the atomic beam apparatus with detail of its components.*

chamber so that the exit hole of the oven is aligned just below the center of the ionizing region of the TOF mass spectrometer. Water cooling is not required inside the vacuum chamber, which keeps the system neat, clean and easy to fabricate. However, the outer chamber was water cooled by wrapping copper tubes around it. In order to get a well collimated atomic beam a collimation cup having 2 mm aperture is placed at about 65 mm above the exit hole of the oven. This design allows the container (oven) to replenish without disturbing the entire arrangement and alignment.

For the high resolution spectroscopic studies, the pressure of particles inside the oven $\approx 10^{-6}$ Torr is sufficient (Gomide 1997). Our atomic beam system can be operated continuously for several hours under stable conditions up to 1000 K that is sufficient to maintain a vapor pressure of most of the alkali and alkaline earth elements for the spectroscopic investigations.

We produced the atomic beam of lithium for its isotope separation at 600 K. At this operating temperature, the mean free path for the lithium is $\approx$ 4 meter that ensures transparent flow of atoms through the exit hole (Ramsey 1956, Compbell and Shewood 1967). The number of atoms per second that exit the oven, is given (Ramsey 1956) by

$$Q = \frac{1}{k}\frac{n_o \langle \upsilon \rangle A_s}{4} \tag{3.2}$$

Where $n_o$ is the atomic density inside the oven, $\langle \upsilon \rangle$ is the average velocity of the atoms in the oven, $A_s$ is the area of the oven aperture, and $1/k$ is a factor that depends on the diameter and width of the aperture, equal to 1 in our case. For lithium at 600 K, $n_o$ = $5.5\times10^{11}$atoms/cm$^3$ (Dushman 1966), $\langle \upsilon \rangle = 1.4\times10^5$cm/s and $Q \sim 5.7\times10^{14}$ atoms/sec. The vapor pressure for lithium at 600 K is taken from the vapor pressure curves reported by O'Hanlon (1989). The divergence of the atomic beam is ≈ 61 mrad as measured from the spot of the lithium atomic beam on a glass strip fixed ≈ 290 mm above the last aperture. The measured divergence is in good agreement with the calculated value by Bernhardt (1976)

$$\theta = \frac{2(2r)}{l} \tag{3.3}$$

Where r is the radius of both the collimating apertures, and $l$ is the distance between them. The temperature has been measured using a Ni-Cr-Ni thermocouple with ± 2 % accuracy.

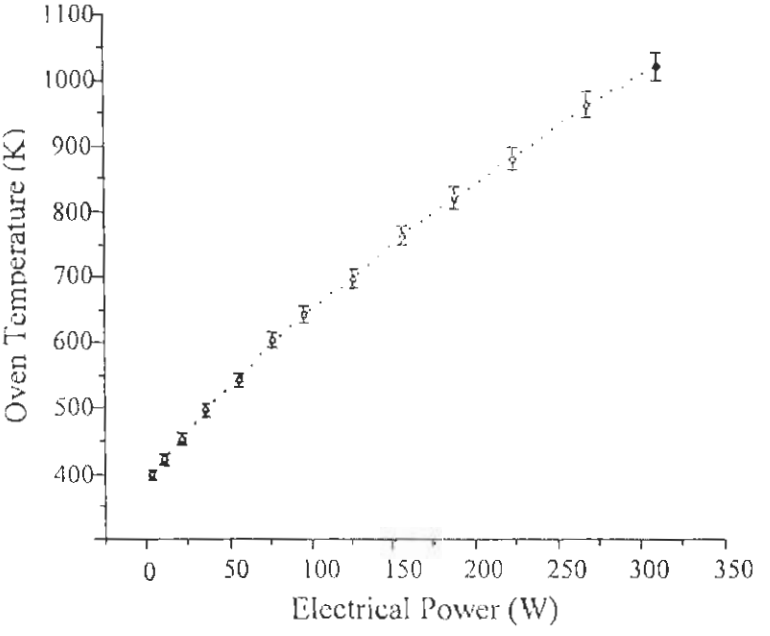


Figure 3.2 *Thermal characteristics of the atomic beam oven*

Figure (3.2) shows the variation of the oven temperature as a function of applied electrical power, which shows almost a linear increase in the temperature with the applied electric power.

## 3.2 Time of Flight Mass Spectrometer

A time-of-flight mass spectrometer (TOF-MS) is a valuable tool for mass analysis. In a number of applications and in conjunction with the ionization schemes, TOF-MS is being used with great success (Payne *et al* 1994). Among the many important features of a TOF-MS, one of the most important is its ability to simultaneously determine all the ionic masses with any mass-to-charge ($m/q$) ratio without moving any of its parts or scanning fields. As a result, the TOF-MS is freed from many of the constraints faced by sequentially scanning instruments (like magnetic sector and quadrupole mass spectrometers) and enjoys precision, sensitivity, and resolution. Time-of-flight (TOF) mass analyzers are also recognized for their excellent speed of analysis, producing full mass spectra for every shot when coupled to a pulsed ionization source. Thus a shot-to-shot variation in the spectra can be monitored directly. Another advantage of the TOF mass spectrometer is its accuracy that depends on the electronic circuits rather than on the mechanical alignment, that makes the construction simple and easy. The first time of flight mass spectrometer was suggested by Stephens (1946) and constructed by Cameron and Eggers (1948). Later on, Wiley and McLaren (1955) devolved a two stage acceleration TOF mass spectrometer with improved resolution.

### 3.2.1 Design Parameters

A linear two stage TOF mass spectrometer consists of a vacuum chamber containing an ion production/extraction region 's', an acceleration region 'd', a field free drift region 'D' and an ion detector at the end of the field free region. The ions are produced as a result of laser matter interaction, which are accelerated twice and then entered in the field free region where they are separated according to their mass to charge ($m/q$) ratio and ultimately detected at the detector (see figure 3.3). Our designed TOF mass spectrometer operates in pulsed mode as the ion source is pulsed and the accelerating fields are constant. The lighter ions arrive at the detector earlier than the heavier ones. Assuming that all the ions possessing zero initial kinetic energy at the time of their birth, the total

flight time of any ion can be evaluated using the equations of motion (Wiley and McLaren 1955) as:

$$T(U_i = 0, s_0) = \sqrt{\frac{m}{2U_f}}\left\{2s_0\sqrt{k_0} + 2d\frac{\sqrt{k_0}}{\sqrt{k_0}+1} + D\right\} \tag{3.4}$$

Where $U_f = qs_0E_s + qdE_d$ is the total energy of the ions after getting acceleration in extraction/acceleration regions, and $k_0 = 1 + \frac{dE_d}{s_0E_s}$. Equation (3.4) can thus be used to calculate the flight time of an ion of particular ($m/q$) ratio. The accuracy of the flight time calculations of a particular ion depends upon the accuracy with which we can measure the extracting/accelerating voltages. After calibrating the spectrometer once, the flight time of the isomass peaks in the recorded spectrum are measured and the corresponding mass can be identified immediately employing the equation

$$m = \frac{2U_f}{\left\{2\sqrt{k_0}s_0 + 2\frac{\sqrt{k_0}}{(\sqrt{k_0}+1)}d + D\right\}^2}T^2 \tag{3.5}$$

The resolution of a TOF mass spectrometer is defined in the time domain (Guilhaus 1995) as

$$R = \frac{m}{\Delta m} = \frac{T}{2(\Delta t)_{FWHM}} \tag{3.6}$$

Where $T$ is the total flight time and $\Delta t_{(FWHM)}$ is the width of the ionic signal peak. Equation (3.6) therefore shows that the resolution can be enhanced by increasing the time of flight of an ion or by narrowing peak signal width $\Delta t_{(FWHM)}$. Ideally this could be done simultaneously, but system parameters usually affect $T$ and $\Delta t_{(FWHM)}$ in opposite manners, hence all the peak-broadening factors have to be considered to achieve the required resolution. If all the ions are formed simultaneously at the same plane whose normal is parallel to the axis of the flight tube, at the distance $s_0$ from the extraction grid $G_1$ with zero initial velocity, the flight time then would be the same for all the ions possessing same ($m/q$) ratio, then the resolution will be limited only by the detection system. However, the actual situation is different as the detected isomass signal peaks are

always broadened in time, which is mainly ascribed to initial space distribution, initial energy spread and temporal distribution of the ions.

Initial space distribution of ions arises because every ionizing source has a finite width at the focus point so that the ions produced near the repeller plate P experience a larger potential gradient $E_{s_{max}}$ ($s_{max} = s_0 + \Delta s/2$) and thus accelerated to higher kinetic energy than those formed close to the extraction grid because of a small potential gradient $E_{s_{min}}$ ($s_{min} = s_0 - \Delta s/2$). This results in a difference in the energy, $\Delta U = q\,(s_0 \pm \Delta s)\,E_s$ of the isomass ions produced and due to this energy difference, the ions formed closer to the repeller plate will enter the field-free drift region later than the ions formed closer to the extraction grid. However, after some time the isomass ions will catch up each other and the plane where the isomass ions catch up, $\Delta U$ vanishes, that corrects the initial spatial distributions, called the space focus plane, where isomass ions reach at the same point. This plane of catch up can be found by setting

$$\frac{dT(0,s_0)}{ds} = 0$$

This yield

$$D = 2s_0 k_0^{\frac{3}{2}} \left( 1 - \frac{1}{(k_0 + \sqrt{k_0})} \frac{d}{s_0} \right) \tag{3.7}$$

This shows that $k_0$ makes it possible to achieve the space focusing of the ions at the plane where the detector is already located. Equation (3.6) shows that for the best resolution T ($0,s_0$) should be maximum. Thus in order to find the condition for T (0,s) to be maximum, the second derivative of equation (3.4) yield

$$\left( \frac{d^2T}{ds^2} \right)_{0,s_0} = \frac{d}{s_0} - \frac{(k_0 - 3)}{k_0} \frac{D}{2s_0} \tag{3.8}$$

This is called the second focusing condition as $T(0,s_0)$ is maximum for $k_0 > 3$. In contrast, the space focus condition for the single-field system ($d = 0$, $k_0 = 1$) is purely geometric i.e. $D = 2s_0$ which is not possible to achieve. Also $T(0,s_0)$ will always be minimum for the single-field system, thus lowering the resolution. The advantage of a dual accelerating region TOF mass spectrometer over the single accelerating region TOF mass

spectrometer is that one has an additional control parameter, $E_d$. It makes the double field source easier to adjust thereby yielding a better resolution.

An initial energy spread arises because of the same or different initial kinetic energies in different directions at the time of birth i.e. towards or away from the detector will have different final velocities after acceleration and arrive at the detector at different times, causing the broadening of the isomass peaks. If an ion-1 initially having a velocity directed away from the detector is decelerated by the field $E_s$ until it comes to rest and then it starts its motion towards the detector, i.e. in the direction of the field $E_s$. Thus comparing the ion born at the same place but with a velocity directed towards the detector, the ion-1 lags behind the ion-2 by the 'turn around time' (as shown in figure 3.3c). Therefore, each mass-to-charge ($m/q$) ion packet arriving at the end of an optimum drift length will have a time width $\Delta t$, given by

$$\Delta t \geq \frac{2\sqrt{2mU_0}}{qE_s}$$

The turn around time can be decreased by decreasing the initial velocity distributions of the ions. This can be done using a higher extraction field $E_s$, which in turn reduces $k_0$, hence contradicts the primary space focus condition and therefore cannot be useful. The effect of initial energy spread of ions can also be reduced by cooling atoms through supersonic expansion, by applying a pulsed field to the extracting/accelerating plate 'P' with a minimal delay after the ionizing laser pulse, called time lag focusing (Wiley and McLaren 1955), or by using an ion reflection mirror (Mamyrin *et al* 1973).

Temporal distribution of the ion formation also causes the broadening of the ion pulse. Two ions of the same ($m/q$) ratio with zero kinetic energy that are formed at the same distance from detector but at different times will start their journey towards the detector and arrive at the detector with a time difference of $\Delta t$, causing the isomass peak broadening, which can be reduced by using a laser of narrow pulse duration.

In addition, the coulombic repulsion of like-charge ions, ion collisions with other atoms/molecules in their path due to poor vacuum, instabilities in the electronic recording device, jitter in the triggering, synchronization of ion extraction events, non-ideal acceleration fields, fringe electric fields around the backing plate and grids, electric field

lenses and the response time of the detector may also contribute in the isomass peak broadening which ultimately limits the resolution of the TOF mass spectrometer.

## 3.2.2 Fabrication

The essential elements of a TOF mass spectrometer are shown in the figure (3.3). It consists of a vacuum chamber, a grid assembly, a flight tube and an ion detector. The grid assembly (figure 3.3 d) is comprised of a backing plate P which is a flat circular stainless steel plate (thickness 0.5 mm and diameter 50 mm) and two grids $G_1$ and $G_2$ fabricated from a 65 lines per square inch tungsten mesh (95 % optical transmission) sandwiched between two flat (0.5 mm thick) stainless steel circular rings (outer diameter 50 mm and inner diameter 25 mm). Grid scattering has dramatic effects on both the sensitivity and the resolution of the instrument (Bergmann *et al* 1989, Selby *et al* 2001). When an electric field is applied to a grid, a small electrostatic lens is produced at each opening. If the grid is not ideally flat i.e. there are wrinkles in the grid, then the ion scattering limits the resolution. Therefore, special care is needed while assembling the grids. Teflon is used as insulation spacers between the backing (repeller) plate and the grids. Voltage $V_s$ is applied between the plate P and the grid $G_1$ while $V_d$ is applied between the grids $G_1$ and $G_2$ by two different stabilized high voltage power supplies whereas grid $G_2$ is body grounded.

The entire grid assembly is mounted on a flange and installed in a chamber (230 mm in diameter, 460 mm height) that is connected with a tube (67 mm inner diameter, one meter long), called the flight tube. The electrical connections are attained with locally made feed-throughs. At the opposite end of the flight tube a channeltron (Galileo, USA) is connected which is used for the ion detection. A grid is placed in front of the detector to create a truly field free drift region in the flight tube. Stainless steel 304 is used for the construction of all the components including the chamber, the grid assembly and the flight tube. Vacuum of the order of $1\times10^{-6}$ Torr is maintained by a diffusion pump (Edwards) that is equipped with a liquid nitrogen baffle. The atomic beam source is precisely placed beneath the ionization / extraction region of the TOF mass spectrometer from where a well collimated atomic beam emerging from the downside passes through the ionization / extraction region and interacts with the exciter and ionizer lasers in

orthogonal, as shown in figure (3a). The diameter of the atomic beam at the interaction region is ≈ 4.5 mm calculated from the beam divergence.

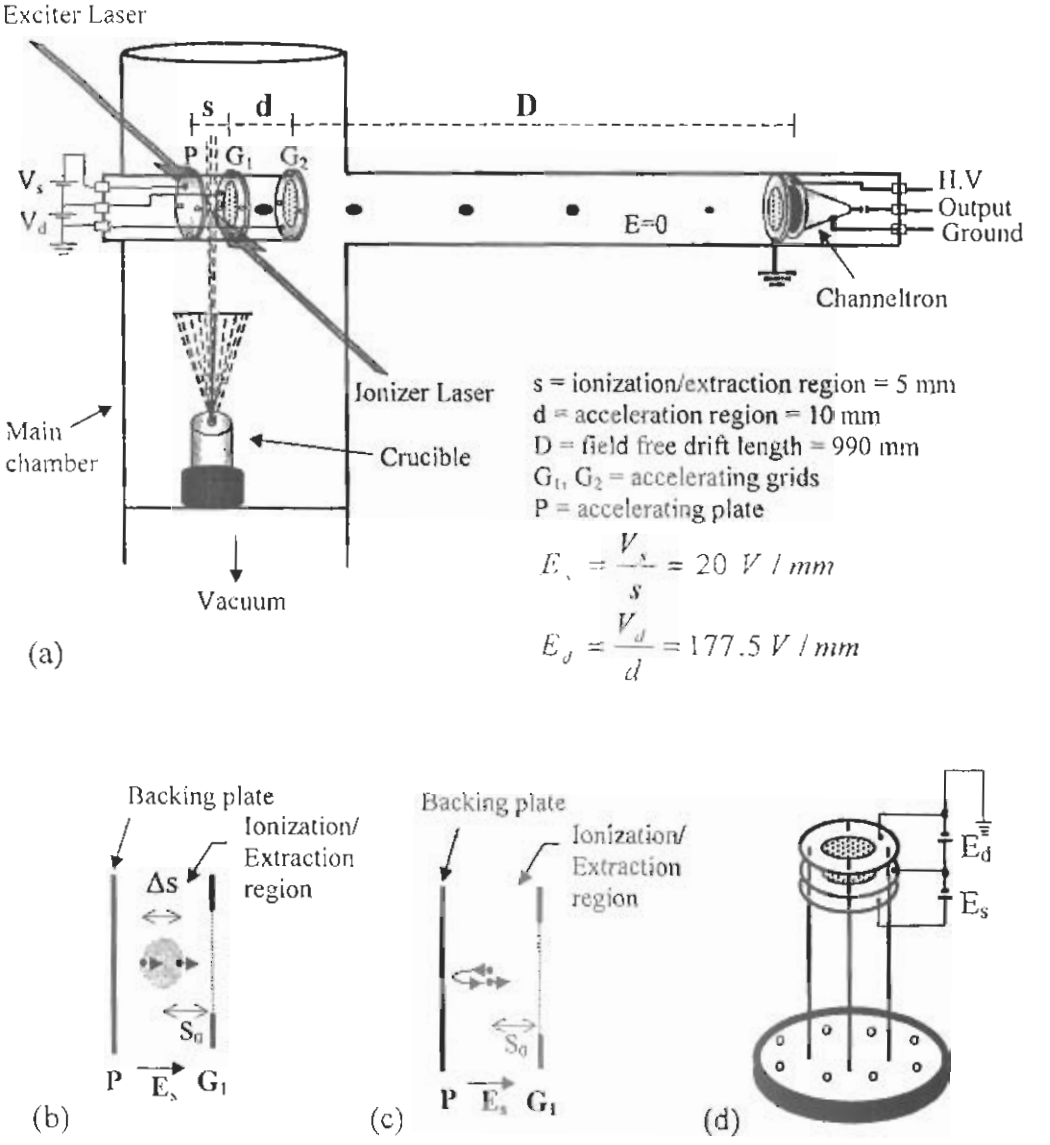


Figure 3.3 *(a) Schematic diagram of the atomic beam-TOF mass spectrometer*
*(b) Spatial distribution of ions*
*(c) Initial velocity distribution of ions*
*(d) Ion accelerating grid assembly*

In order to demonstrate the performance of the whole system, lithium photoions were produced as a result of two step photoionization. The lithium atomic beam with natural isotopic abundance is illuminated with the exciter laser at 670.8 nm and the ionizer laser at 335.4 nm. The ionizer laser was focused with a plano convex lens of the focal length of 250 mm. An extended view of the laser interaction with the atomic beam is shown in the figure (3.4).

The photoions thus produced are separated and detected by the TOF mass spectrometer. The TOF distribution of lithium isotopes is shown in figure (3.5), where the laser pulse is used as the reference to measure the time of flight of the isotopes. The isotopic abundance or relative concentration of all the element presents in an atomic beam can be measured accurately provided the ion detector (channeltron) of the TOF mass spectrometer is operating in a linear mode.

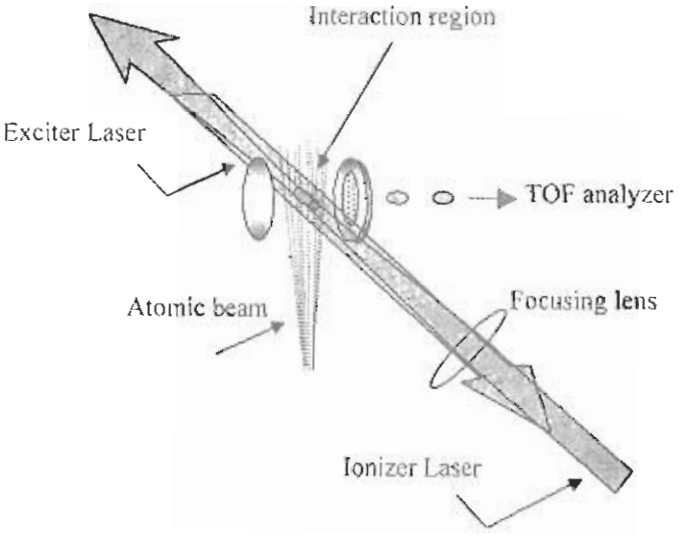


Figure 3.4 *Expanded view of interaction volume of exciter/ionizer laser with the lithium atomic beam*

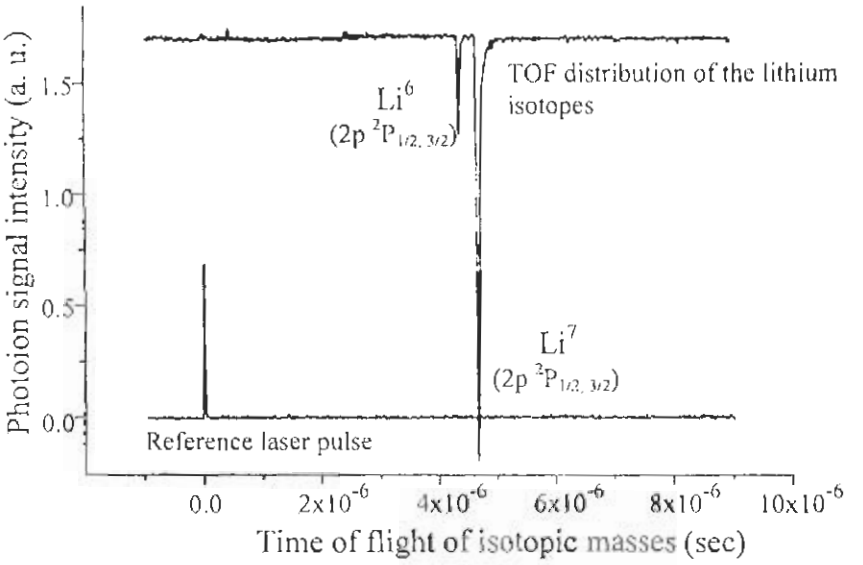


Figure 3.5 *TOF distribution of the lithium isotopes $Li^6$ and $Li^7$, produced as a result of the two step photoionization. The laser pulse is used to measure the flight time of the isotopic masses.*

Figure (3.6 a,b) represents the behavior of the TOF detector for measuring the relative abundance of lithium isotopes as a function of the detector voltage. This detector behavior is registered by focusing the laser at 532 nm (30 mJ, 5 ns), which produces breakdown in the lithium atomic beam and subsequently ionizes all the species according to their abundance present in the focal volume (Ready 1965).

It is evident from the figure (3.6 a, b) that the relative concentration of $Li^7$ decreases whereas that of $Li^6$ increases with the increase in the concentration of $Li^6$ at a fix ion number density of both the isotopes in the interaction region. This shows that the detector is unable to magnify the isotopic signals according to their natural abundance. This study helps us to operate the TOF detector in the linear mode. The integrated intensities (area under the curve) of both the isotopes were calculated, which shows that the abundance of $Li^6$ and $Li^7$ measured by our experiment is 8 % and 92 %, which is very close to the already reported values as 7.5 % and 92.5 % (natural abundance of lithium isotopes) while the detector was operating at 1300V.

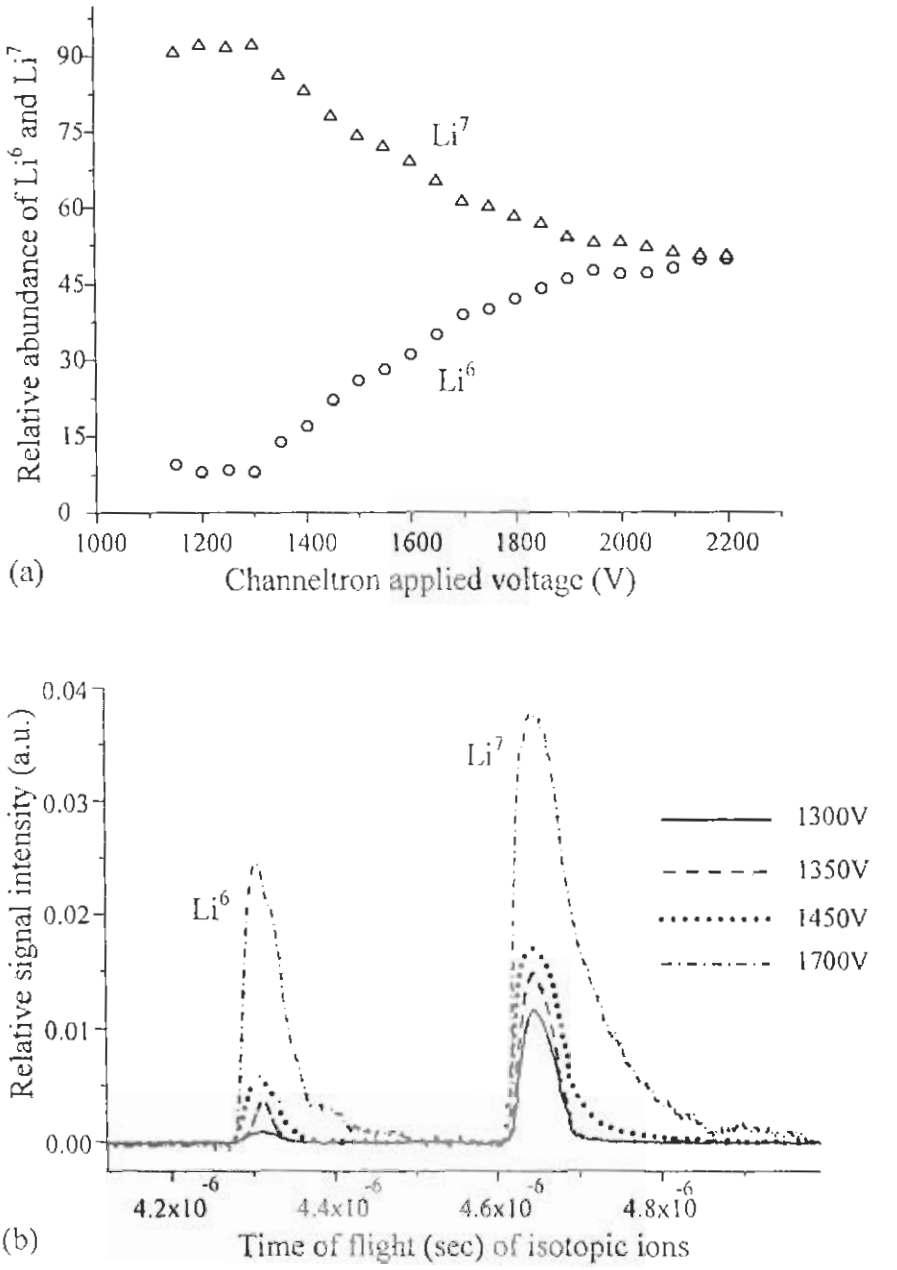


Figure 3.6 (a) *The effect of the TOF detector voltage on the measurement of the relative abundance of the lithium isotopes.*
(b) *Relative signal intensity of the lithium isotopes at different TOF detector applied voltages.*

# Chapter 4

## Laser Isotope Separation of Lithium

The ionization yield of the lithium isotopes $Li^6$ and $Li^7$ utilizing two-step photoionization in combination with an atomic beam-TOF mass spectrometer are presented in these studies. The 2p $^2P_{1/2, 3/2}$, 3s $^2S$, 3p $^2P$, 3d $^2D$, 4s $^2S$, 4p$^2P$ and 4d $^2D$ excited states of lithium have been exploited to investigate the yield of the $Li^6$ isotope. It is observed that the enrichment of the $Li^6$ isotope can be enhanced up to over 60 % by tuning the exciter laser to the 3s $^2S$ and 3p $^2P$ excited states of the $Li^6$ isotope.

Lithium is the first element of alkali group having one outer s-electron with the ground state $^2S_{1/2}$. It is a soft, silvery and highly reactive metallic element. It has two isotopes $_3Li^6$ and $_3Li^7$ with natural abundances as 7.5 % and 92.5 %. Both the isotopes are important for fusion and fission reactors. $Li^6$ is particularly important for producing tritium (T), which is used as the fuel in the fusion reactor.

Shimazu *et al* (1977) proposed that the two-step selective photoionization might lead to lithium isotope separation. In this technique, the isotope of interest is uplifted to a particular excited state, from where it is photoionized by the absorption of a second photon during the lifetime of the excited state. The resulting photoions of the particular isotope can be collected for its practical use. The two-step photoionization technique has been widely used (Arisawa, *et al* 1982 a, 1982b, Karlov *et al* 1978, 1979, Olivares *et al* 1999, 2002, Yamashita and Kashiwagi 1979, Mariella 1982, Li *et al* 1983, Xiwen *et al* 1992, Arisawa *et al* 1983) for the isotope separation and the enhancement of the concentration of the light isotope $Li^6$ using the 2p $^2P_{1/2,3/2}$ excited state. Karlov *et al* (1978, 1979) applied two-step selective photoionization for the isotope separation of Nd, Sm, Eu, Gd, Dy, Er, Li and U etc. Yamashita and Kashiwagi (1979) registered a patent for the lithium isotope separation in which they suggested the use of the two-step photoionization for the enrichment of the lithium isotopes, whereas Mariella (1982) described the same technique for the lithium isotope separation with the additional suggestion of using solar radiation to photoionize the selected excited isotope. Arisawa *et al* (1982 a) employed the same technique for lithium isotope separation using a very narrow linewidth exciter laser (~ 0.04 $cm^{-1}$) and obtained the highly enriched $Li^6$ up to 90

% by tuning the exciter laser to the $^2P_{1/2}$ excited state of $Li^6$. Arisawa *et al* (1982 b) also investigated an efficient recovery of the isotopic ions of lithium by the charge exchange process in laser-produced plasma of lithium. Olivares *et al* (1999, 2002) applied the two-step photoionization technique, where they used ultra narrow linewidth diode laser (~0.000033 $cm^{-1}$) for the selective excitation of lithium isotope, which were subsequently photoionized with the fourth harmonic (266 nm) of a Nd:YAG laser. They resolved the fine and hyperfine levels of both the isotopes $Li^6$ and $Li^7$. Other experimental techniques, like laser deflection method and the magnetic deflection of polarized atomic beam have been utilized by Li *et al* (1983) and Xiwen *et al* (1992) for the enrichment of $Li^6$. Chemical methods (Symons 1985) of the lithium isotope separation have the capability to enrich $Li^6$ on large scale and laser enhanced chemical reaction (Arisawa *et al* 1983, Myers *et al* 1987) suggested an efficient means of lithium isotope separation. Balz *et al* (1987) suggested the separation of the lithium isotopes by double resonance enhanced multiphoton ionization of $Li_2$.

Most of the above mentioned methods require narrow line width laser for the first excitation step. We propose an alternate technique; a combination of an atomic beam and a Time of Flight (TOF) mass spectrometer to separate the isotopes. This technique works quite satisfactorily even if the isotopes have not been selectively excited. The experimental data presented in this thesis is a step forward in the ongoing investigations of lithium isotopic separation (Saleem *et al* 2006). Almost all the above cited work on the enrichment of the $Li^6$ isotope is based on the 2p $^2P_{1/2, 3/2}$ excited state of the lithium. We, have therefore used the 2p $^2P_{1/2, 3/2}$ excited state of lithium for studying the enrichment of $Li^6$. In addition, the 3s $^2S$, 3p $^2P$, 3d $^2D$, 4s $^2S$, 4p $^2P$ and 4d $^2D$ excited states of lithium have been exploited for the first time to investigate the yield of the $Li^6$ isotope.

## 4.1 Ionization yield of both the lithium isotopes from the 2p $^2P_{1/2, 3/2}$ excited state

The natural isotopic abundant lithium atomic beam was irradiated with the exciter laser at 670.8 nm to populate the 2p excited level via single photon excitation and subsequently photoionized by absorbing photons of the ionizer laser at 335.4 nm. The exciter dye laser (TDL-90, Quantel) was charged with the LDS698 dye prepared in ethanol. The ionizer laser at 335.4 nm was achieved by frequency doubling of the exciter laser with a BBO

crystal. Both the exciter and the ionizer lasers were separated by a Pellin Broca prism. The exciter laser was scanned from the $2p\ ^2P_{1/2,\ 3/2}$ excited state of $Li^6$ to that of $Li^7$, while keeping the ionizing laser fixed. Three boxcar averagers were simultaneously used to record the photoions signal of the $Li^6$, $Li^7$ and the etalon fringes. Figure (4.1) shows the resolved spectrum of the $2p\ ^2P_{1/2,\ 3/2}$ fine structure levels of the $Li^6$ and $Li^7$. This figure depicts the dependence of the photoion signals of both the isotopes on the exciter laser frequency. It is evident that the $2p\ ^2P_{3/2}$ excited state of $Li^6$ and $2p\ ^2P_{1/2}$ of $Li^7$ have not been excited separately as the line width of our exciter laser (~ 0.1 $cm^{-1}$) is wider than the energy spacing (~0.015 $cm^{-1}$) between them. However, the use of a TOF mass spectrometer enabled us to resolve these levels because it resolves the ionic masses on the time axis without knowing how they have been produced. The etalon fringes made it possible to measure the isotopic shift and the fine structure energy spacing of the lithium isotopes.

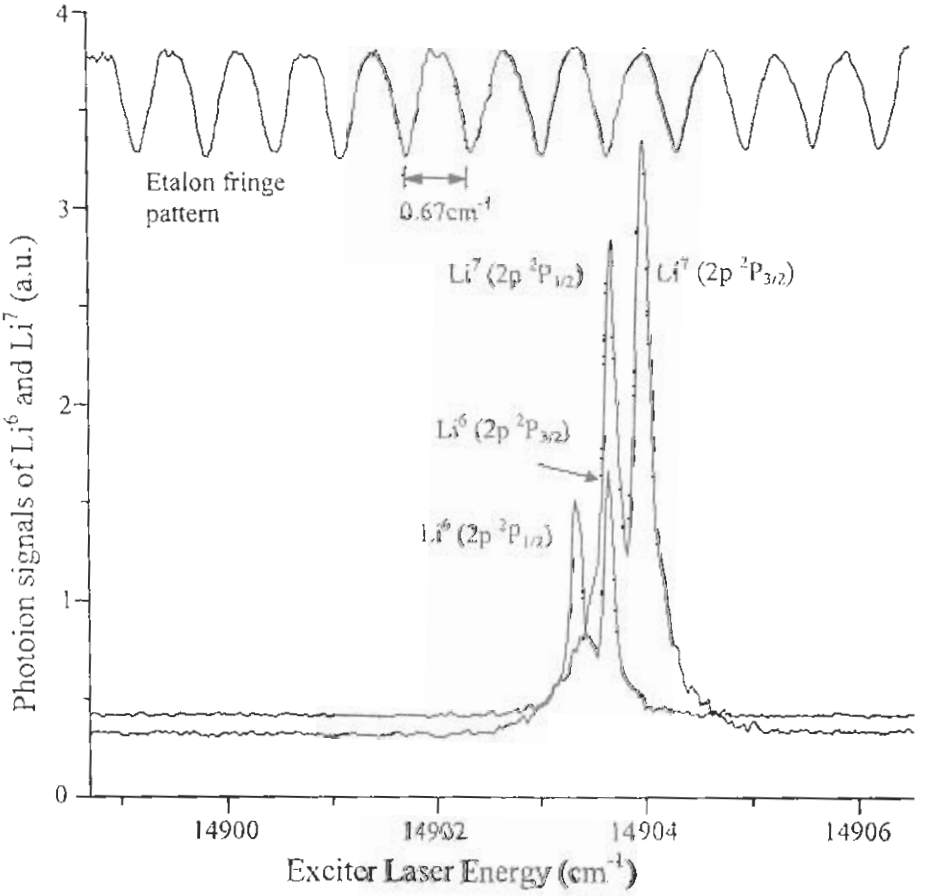


Figure 4.1 *Dependence of the photoion signals of $Li^6$ and $Li^7$ on the exciter laser frequency in the case of natural isotopic abundant lithium sample*

We measured the energy spacing between the $2p^2P_{1/2}$ and $2p^2P_{3/2}$ excited states of the $Li^6$ and $Li^7$ from the center of gravity of each isotopic signal peak to be 0.34 $cm^{-1}$ and the average isotopic shift between both the lithium isotopes at 2p as 0.35 $cm^{-1}$, which is in good agreement with the known values (Lorenzen and Niemax 1982, Windholz 1995, Sansonetti et el 1995, Yan and Drake 2002, Walls *et al* 2003).

It is also noticed from the figure (4.1) that the isotopic signal intensity dominates for the transition when $\Delta J$ changes in the same direction i.e. the transition from 2s $^2S_{1/2}$ to 2p $^2P_{3/2}$ for both the isotopes is dominating the 2s $^2S_{1/2}$ to 2p $^2P_{1/2}$ transition in accordance to the dipole selection rules and relative signal intensity rules (Cowan 1981, Sobel'man 1972). We have observed an interesting phenomenon of power broadening due to the exciter laser as its energy density is varied from 2.38 $mJ/cm^2$ to 0.16 $mJ/cm^2$ as shown in figure (4.2).

It is evident that the energy density of the exciter laser affects the resolution of the fine structure levels of both the isotopes and these get resolved as the energy density of the exciter laser is gradually decreased. Therefore, much higher energy density of the exciter laser not only limits the resolution of the fine structure levels of the lithium isotopes but also leads to a loss in the enrichment of $Li^6$ due to the power broadening effect.

We have also recorded the TOF isotopic signals of the lithium isotopes on the oscilloscope by scanning the exciter laser frequency. The photoions of both the isotopes were calculated from the recorded data using the relation

$$\frac{Q}{e} = \frac{\left(\frac{TOF\ voltage\ signal \times \Delta t}{R}\right)}{e} \qquad (4.1)$$

Here $(TOF\ voltage\ signal \times \Delta t)$ gives the integrated area under the isotopic signal peak, $R$ is the terminating resistance at the oscilloscope, $\Delta t$ is the FWHM pulse width of the photoion signal peak in seconds and $e$ is the elementary charge of the electron. In order to measure a truthful number density of the isotopic masses, the corresponding photoions $\frac{Q}{e}$ were divided with the gain of the channeltron (Galileo, USA), which is used as the ion detector in the TOF mass spectrometer.

Figure (4.3) shows the variation of the photoion signals of both the isotopes $Li^6$ and $Li^7$ verses the exciter laser frequency. This figure shows that an identical trend prevails in recording the isotopic signals on the oscilloscope as has been recorded by the boxcar averager. The photoions of both the isotopes, shown in figure (4.3) were used to calculate the percentage concentration of $Li^6$ in the collected mass. Figure (4.4) shows the concentration of $Li^6$ that has been obtained by this method. Arisawa *et al* (1982 a) also pointed out that with an ultra narrow linewidth of the exciter laser (~ 0.036 $cm^{-1}$), the isotopic abundance of $Li^6$ can be enhanced up to 90 % by tuning the exciter laser to the $2p\ ^2P_{1/2}$ of $Li^6$. In our proposed method with the exciter laser line width ~ 0.1 $cm^{-1}$, the isotopic abundance of $Li^6$ in the collected mass can be enhanced up to 50 %. Narrow linewidth lasers are excellent for selectivity but higher yields of the enriched isotopes are difficult to achieve. However, with the proposed method, a much higher yield of the enriched isotope is expected even if the linewidth of the exciter laser is greater than the fine/hyperfine width.

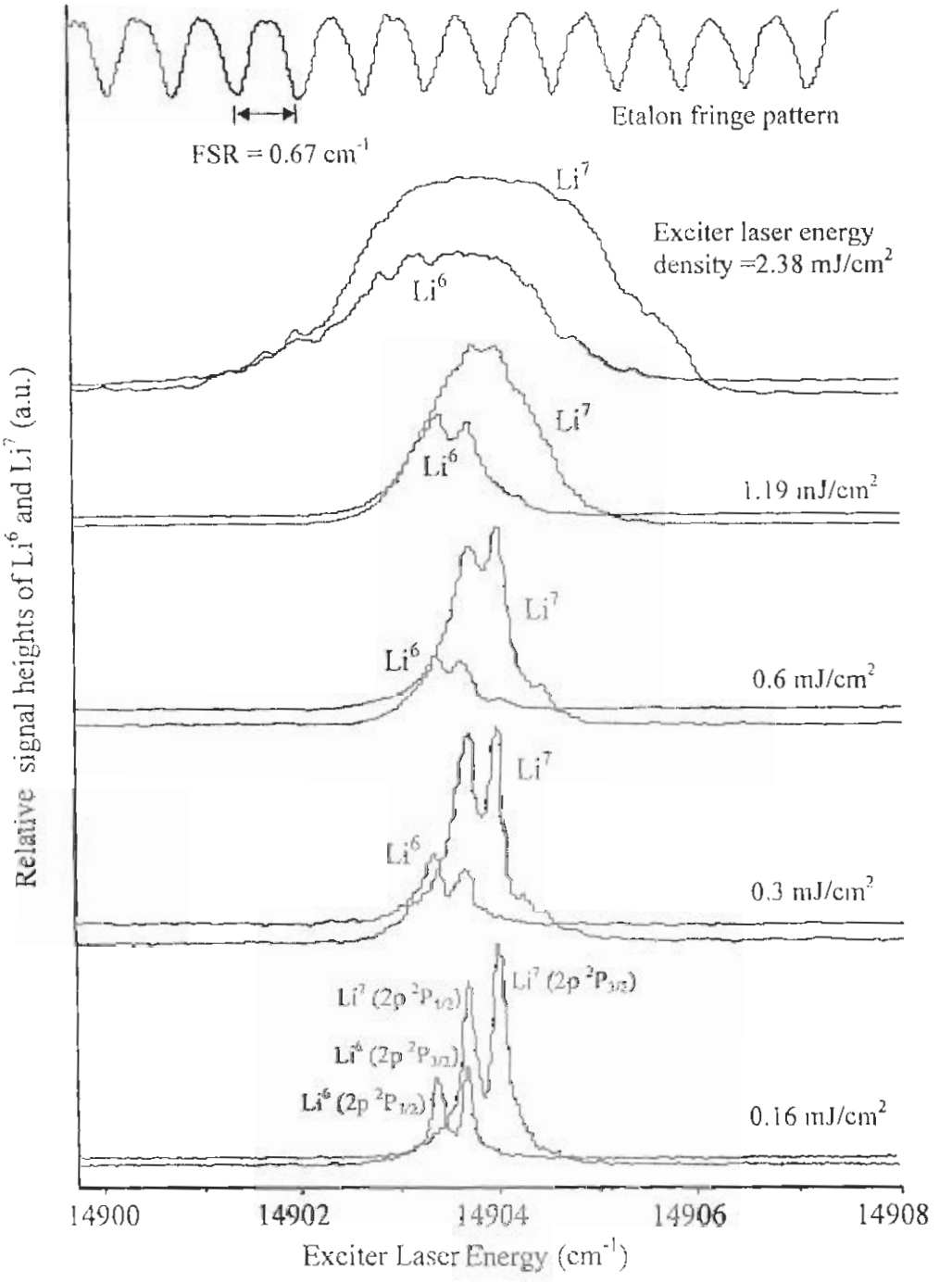


Figure 4.2 *Power broadening effect in relation to the energy density of the exciter laser (Energy density of the ionizer laser 1 J/cm$^2$).*

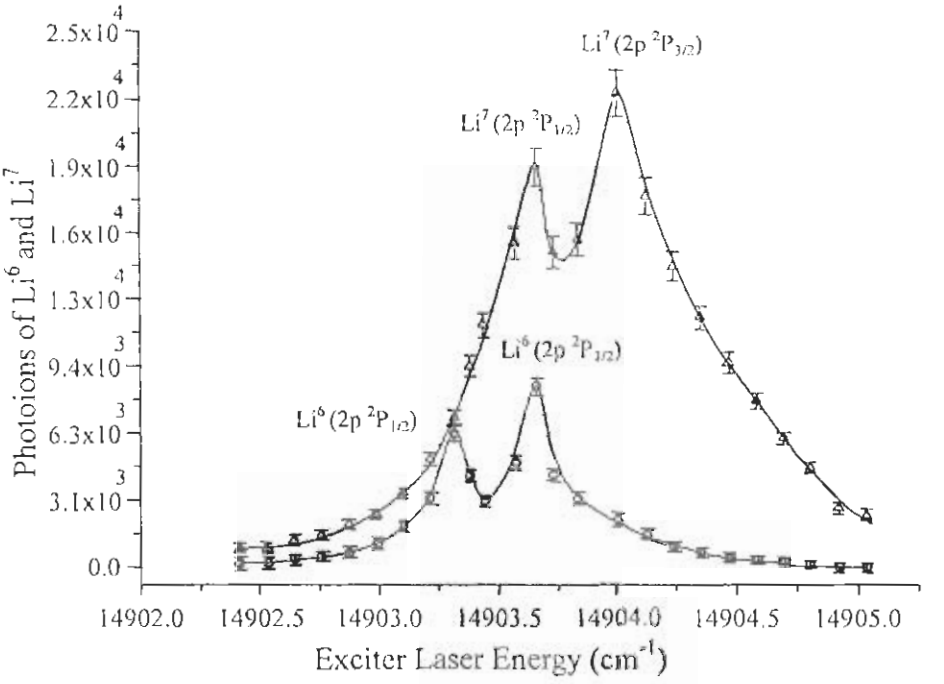


Figure 4.3 *Dependence of the photoions of the lithium isotopes on the exciter laser frequency. Each data point is calculated using equation (4.1) from text. The error bars (5%) are due to the energy fluctuations of the exciter/ionizer lasers. (Exciter laser line width ~ 0.1 cm$^{-1}$, exciter laser intensity: 0.16 mJ/cm$^2$, ionizing laser intensity 1J/cm$^2$).*

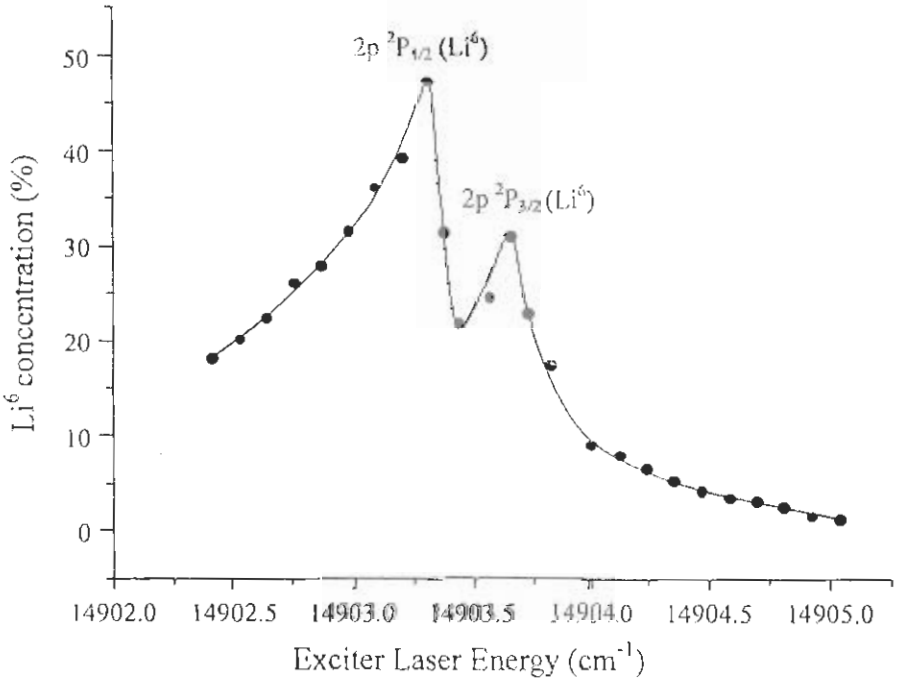


Figure 4.4 *Dependence of the enrichment of the Li$^6$ on the exciter laser wavelength (Exciter laser line width ~ 0.1 cm$^{-1}$, exciter laser intensity: 0.16 mJ/cm$^2$, ionizing laser intensity 1J/cm$^2$).*

## 4.2 Ionization yield from the 3s $^2$S, 3p $^2$P, 3d $^2$D, 4s $^2$S, 4p $^2$P and 4d $^2$D excited states of lithium isotopes

The 3s $^2$S, 3p $^2$P, 3d $^2$D, 4s $^2$S, 4p $^2$P and 4d $^2$D excited states of lithium have been exploited for the first time for the ionization yield of $Li^6$ and $Li^7$ isotopes. Since the ground state of the lithium atoms is 2s $^2$S, therefore the 3s $^2$S, 3d $^2$D, 4s $^2$S and 4d $^2$D excited states can be populated only via two photon absorption by using the exciting laser wavelengths at 735.13, 639.32, 571.23 and 546.1 nm and the 3p $^2$P and 4p $^2$P excited states were populated by the single photon absorption at 323.4 and 274.2 nm respectively. The exciting wavelengths were achieved by charging the dye laser (TDL-90 Quantel) with different dyes given in the table (4.1). The exciting wavelengths at 323.4 and 274.2 nm were generated by frequency doubling of 646.8 and 548.4 nm respectively using BBO crystal.

Table 4.1

*List of the exciting laser wavelengths used to excite the 3s $^2$S, 3p $^2$P, 3d $^2$D, 4s $^2$S, 4p $^2$P and 4d $^2$D excited states of lithium using dye laser TDL-90 pumped with the SHG of the Nd:YAG laser.*

| Exciting wavelengths | Dyes | Solvent |
|---|---|---|
| 735.13 nm | Pyridine - 2 | PC (Propylene Carbonate) |
| 639.32 nm / 646.8nm | DCM | Methanol |
| 571.23 nm | Rhodamine 590 | Methanol |
| 546.1 nm / 548.4 nm | Flourescene 548 | Methonol + NaOH |

The 3s, 3p, 3d excited states were subsequently photoionized by the ionizing laser wavelengths at 614, 735 and 765 nm respectively, whereas the 4s, 4p, and 4d excited states were photoionized with the fundamental wavelength of Nd:YAG lasing at 1064 nm to produce isotopic ions in order to investigate the yield of $Li^6$ as a function of the exciter laser frequency. The ionizing laser wavelengths at 614, 735 and 765 nm were achieved by charging a home made Hanna type (Hanna *et al* 1975) dye laser with the dye Rhodamine 640 dissolved in methanol and Pyridine-2 dissolved in PC, which was pumped with SHG of the same Nd:YAG laser.

The exciter laser was scanned from the lower to higher frequency for all the aforementioned excited states to explore their behavior for the enrichment of $Li^6$, while

keeping the ionizer laser fixed. The resulting photoion signals of $Li^6$, $Li^7$ and the etalon fringes (FSR 0.67 $cm^{-1}$) were simultaneously recorded by three boxcar averagers (SR-250). Figures (4.5a - 4.10a) shows the spectrum of the boxcar averaged output signals originated from the 3s, 3p, 3d, 4s, 4p and 4d excited states. Evidently, these figures depict the dependence of the photoion signals of both the lithium isotopes from all the mentioned excited states as a function of frequency of the exciter laser. Figures (4.5a - 4.10a) shows that the linewidth of the exciter laser (~ 0.1 $cm^{-1}$) was not sufficiently narrow to selectively excite the $Li^6$ or $Li^7$ from all the involved excited states, however the TOF mass spectrometer enabled the isotope separation because of the different masses of $Li^6$ and $Li^7$. The beauty of the TOF mass spectrometer is that it separates the ions according to their mass to charge ratio with out knowing the way of their production. Utilizing this feature, we have recorded the variations in the photoionic signals of both the lithium isotopes as a function of exciter laser frequency, as shown in the figures (4.5a to 4.10a).

The variation in the TOF signals of both the lithium isotopes were also recorded on an oscilloscope by scanning the exciter laser from the excited state of $Li^6$ to that of $Li^7$ for all the above mentioned six excited states, at fixed ionizer laser frequency. The photoions of both the isotopes were therefore calculated using the TOF isotopic signals originating from all the involved excited states. Figures (4.5b - 4.10b) shows the variation of the photoions of the $Li^6$ and $Li^7$ originating from the 3s, 3p, 3d, 4s, 4p and 4d excited states as a function of the exciter laser frequency. The same trend has been found in the isotopic signals and the number of the photoions of $Li^6$ and $Li^7$ originating from all the excited states either recorded by the boxcar averager or the oscilloscope.

When the exciter laser was tuned to any of the above mentioned excited state of $Li^7$, it yields the maximum concentration of $Li^7$ in each of the six cases as shown in the inset (1) of the figures (4.5b – 4.10b). Whereas, the inset (2) shows different concentrations of $Li^6$ achieved from different excited states when the exciter laser was tuned to the excited state of $Li^6$.

As described in chapter 1, the isotopic shift decreases with an increase in the principle quantum number $n$ and the angular quantum number $l$. Therefore, due to the broad line width of our exciter laser (~ 0.1 $cm^{-1}$) the possibility of the selective excitation of $Li^6$ or

$Li^7$ from the higher excited states further reduces. The fine and hyperfine structure mixing of the excited states of both the isotopes with increase in the *n* and *l* values also affects the isotope separation.

The 3s $^2S$ and 4s $^2S$ excited states have no fine structure components because of the absence of the spin orbit interaction. However, the interaction of the magnetic moment of electron (due to its spin S =1/2) with the magnetic moment of the nucleus (due to the nuclear spin I = 1 for $Li^6$ and I = 3/2 for $Li^7$) leads to hyperfine splitting of both the states. The 4s $^2S$ excited state seems to have larger hyperfine structure (figure 4.8a) than the 3s $^2S$ excited state (figure 4.5a) for both the lithium isotopes. The hyperfine structures of both the lithium isotopes mix together and as a result ultra narrow linewidth laser is required for the excitation of the individual isotope. The proposed method, however, made it possible to enrich a particular isotope up to some extent even with comparatively broadband exciter laser. When the exciter laser was tuned to the 4s $^2S$ excited state of $Li^6$, the concentration of $Li^6$ just approaches to that of $Li^7$ (inset 2 of figure 4.8b) due to the large hyperfine structure mixing of both the isotopes. When the exciter laser was tuned to the 3s excited state of $Li^6$ (inset 2 of figure 4.5b), the concentration of $Li^6$ exceeds to that of $Li^7$.

In the case of the 3p and 4p excited states of lithium, the energy spacing between the fine structure components (doublets) due to spin orbit interaction decreases with an increase in *n* and *l* quantum numbers. In addition, both the doublets persists the hyperfine structure due to the non-zero nuclear spin of both the isotopes. Because of this decrease in the fine structure splitting, the possibility of mixing of the fine and hyperfine structure increases. Figure (4.6a) shows that the 3p excited state seems to have less fine/hyperfine structure mixing as compared with the 4p excited state (figure 4.9a). Therefore when the exciter laser of linewidth (~ 0.1 $cm^{-1}$) was tuned to the 3p excited state of $Li^6$, the concentration of $Li^6$ exceeds to that of $Li^7$ (inset 2 of figure 4.6b), which may be attributed to a less mixing of the fine/hyperfine structure in comparison with the 4p excited state (inset 2 of figure 4.9b). Therefore, when the exciter laser was tuned to the 4p excited state of $Li^6$, the concentration of the $Li^6$ just approaches to that of $Li^7$, which is due to the strong mixing of the fine/hyperfine structure.

The 3d and 4d excited states of the lithium also persists both the fine and hyperfine structures. The 4d excited state (figure 4.10a) seems to have much broader fine/hyperfine structure mixing in comparison with the 3d excited sate (figure 4.7a). Due to this reason, when the exciter laser was tuned to the 4d excited state of $Li^6$, we observed complete overlapping of both the isotopic peaks. As a result, the concentration of $Li^6$ does not approach even to that of $Li^7$ (inset 2 of figure 4.10b). However, when the exciter laser was tuned to the 3d $^2D$ excited state of $Li^6$, the concentration of $Li^6$ approaches to that of $Li^7$ (inset 2 of figure 4.7 c) that is attributed to small fine/hyperfine structure mixing.

The percentage yield of the $Li^6$ isotope was calculated from the photoions of both the lithium isotopes originating from all the aforementioned excited states as shown in the figures (4.5b to 4.10b) and are reproduced in the figures (4.5c - 4.10c). It is evident that when the exciter laser was tuned to the 3s (figure 4.5c) and 3p (figure 4.6c) excited states of $Li^6$, the concentration of $Li^6$ exceeds to that of $Li^7$ and gets enhanced up to over 60 %. In order to decide which level can be efficiently used for the quantitative yield of $Li^6$, the photoionization cross section of all the aforementioned excited states have been measured, the details are given in chapter 5.

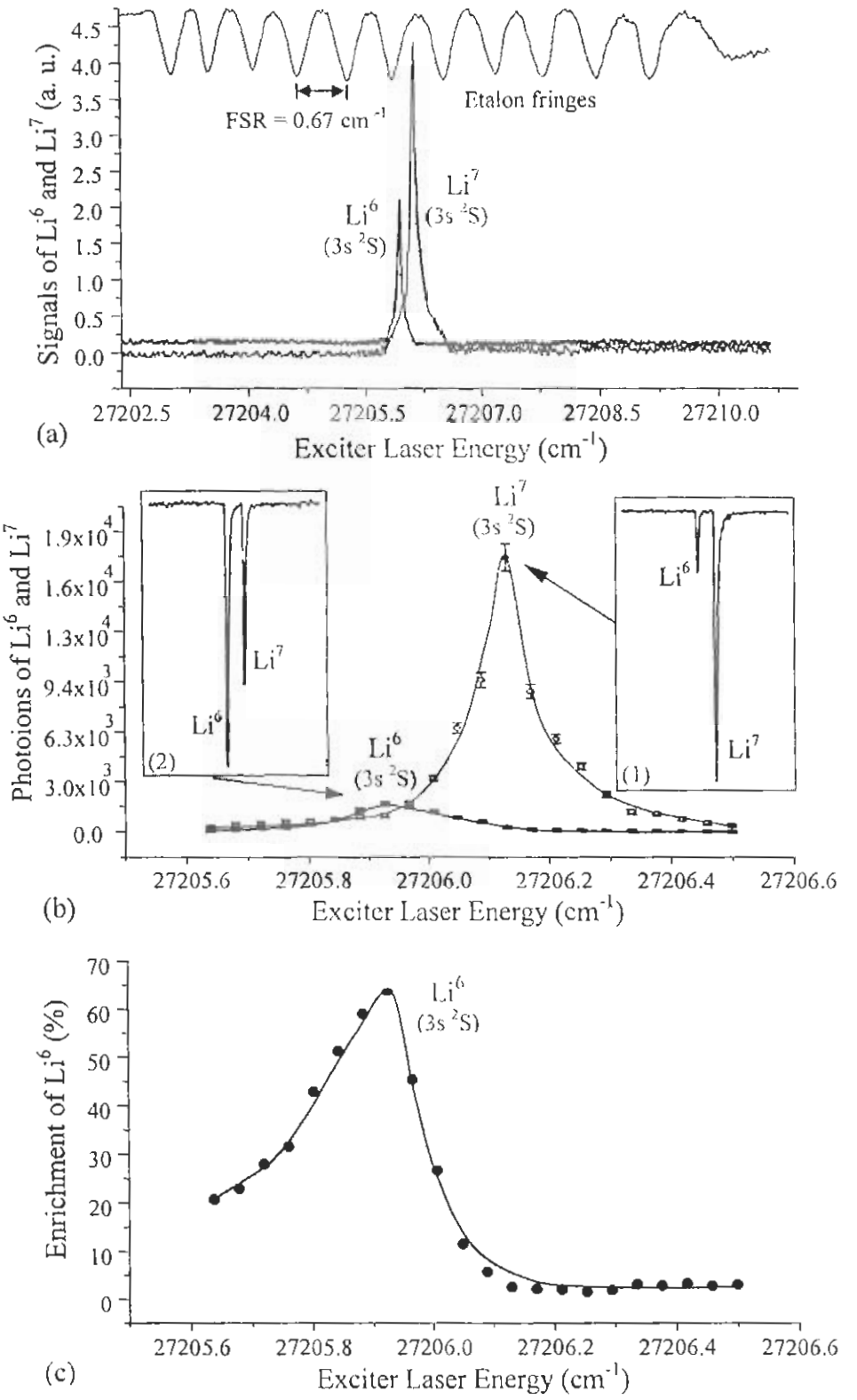


Figure 4.5 *(a) Boxcar averaged signals of both the lithium isotopes, (b) Photoions of both the isotopes and (c) concentration of $Li^6$ as a function of the exciter laser exploiting the $3s\ ^2S$ excited state of lithium.*

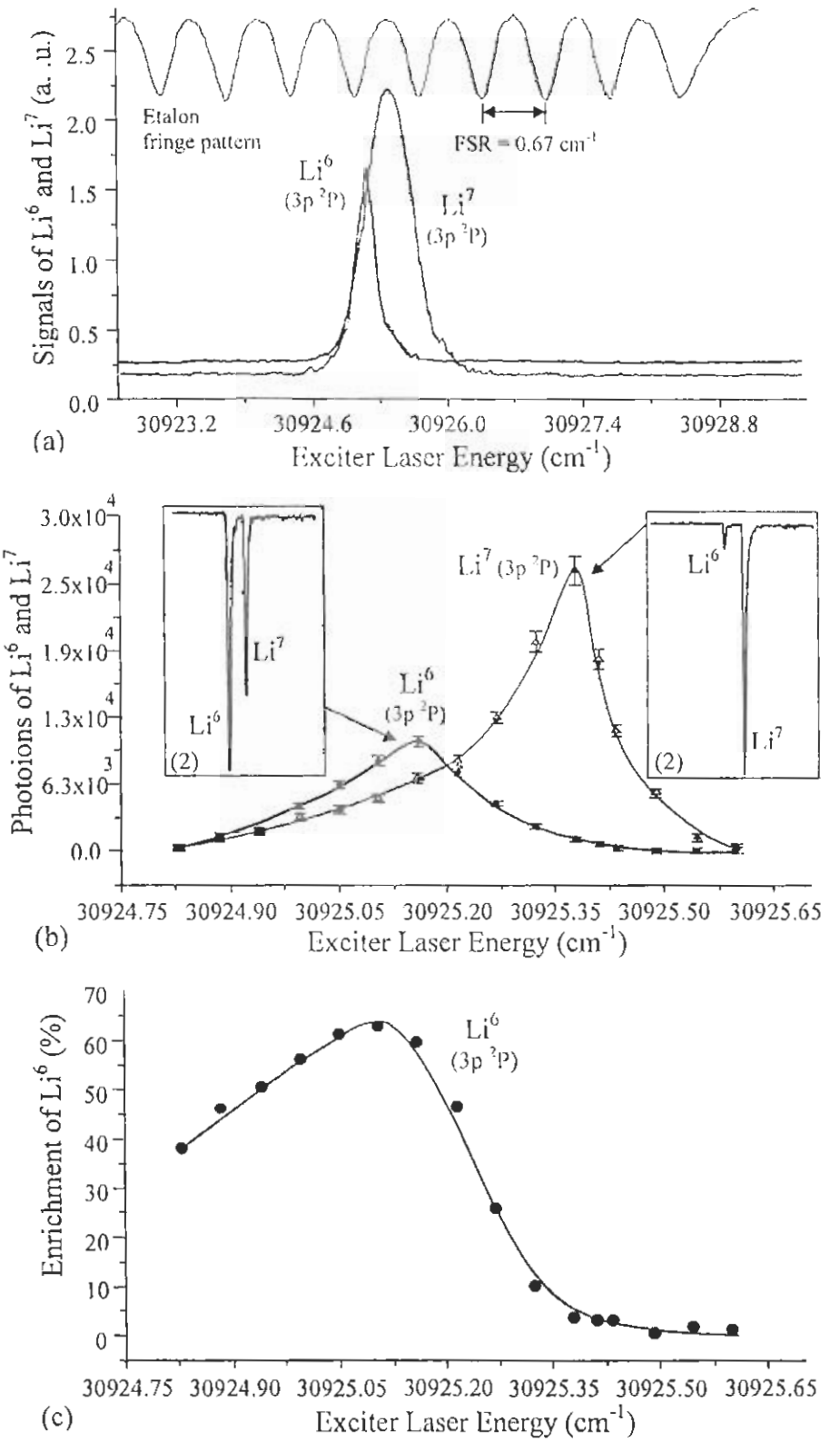


Figure 4.6 *(a) Boxcar averaged signals of both the lithium isotopes, (b) Photoions of both the isotopes and (c) concentration of $Li^6$ as a function of the exciter laser exploiting the $3p\ ^2P$ excited state of lithium.*

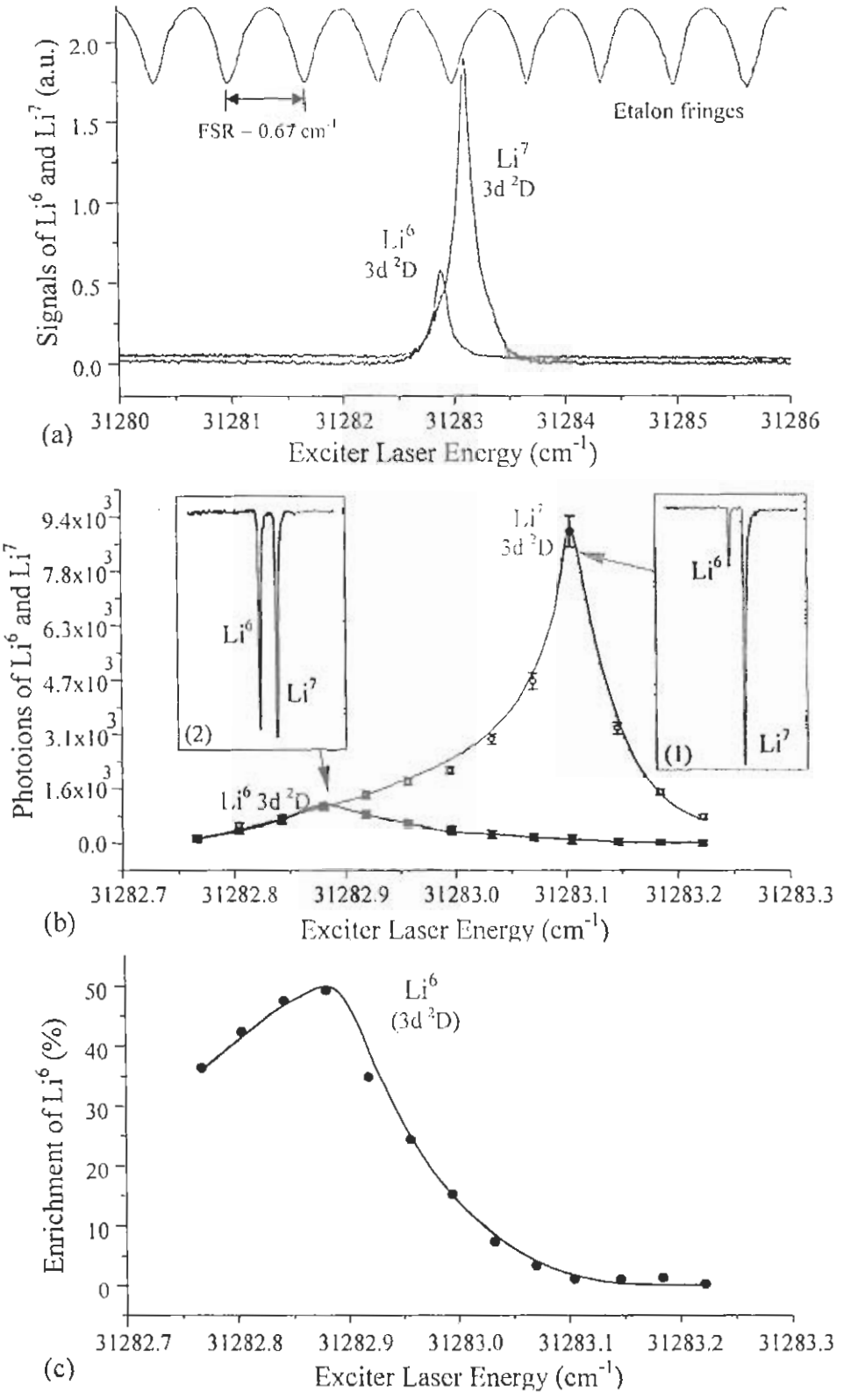


Figure 4.7 *(a) Boxcar averaged signals of both the lithium isotopes, (b) Photoions of both the isotopes and (c) concentration of $Li^6$ as a function of the exciter laser exploiting the $3d\ ^2D$ excited state of lithium.*

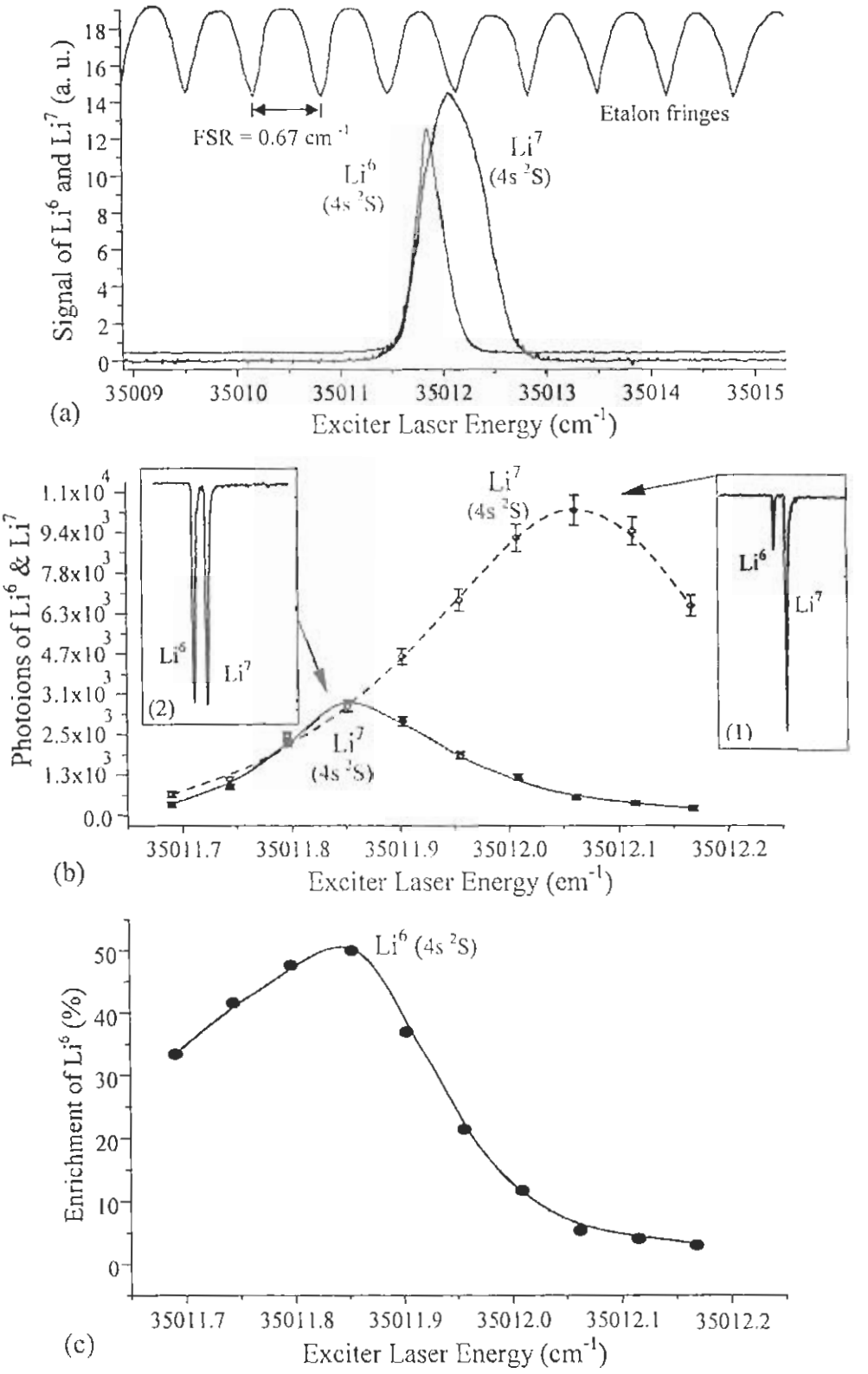


Figure 4.8 *(a) Boxcar averaged signals of both the lithium isotopes, (b) Photoions of both the isotopes and (c) concentration of $Li^6$ as a function of the exciter laser exploiting the $4s\ ^2S$ excited state of lithium.*

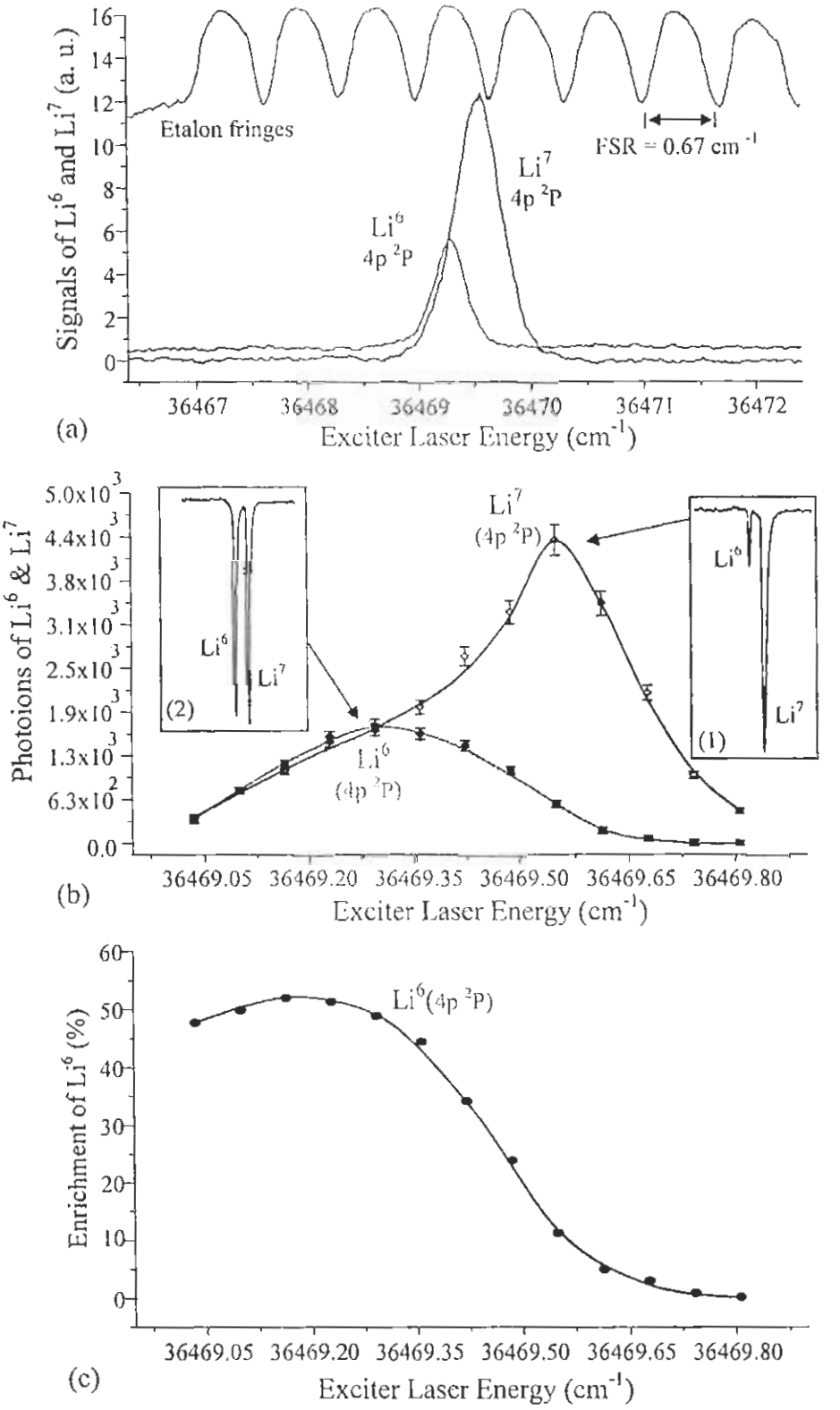


Figure 4.9 *(a) Boxcar averaged signals of both the lithium isotopes, (b) Photoions of both the isotopes and (c) concentration of $Li^6$ as a function of the exciter laser exploiting the $4p\ ^2P$ excited state of lithium.*

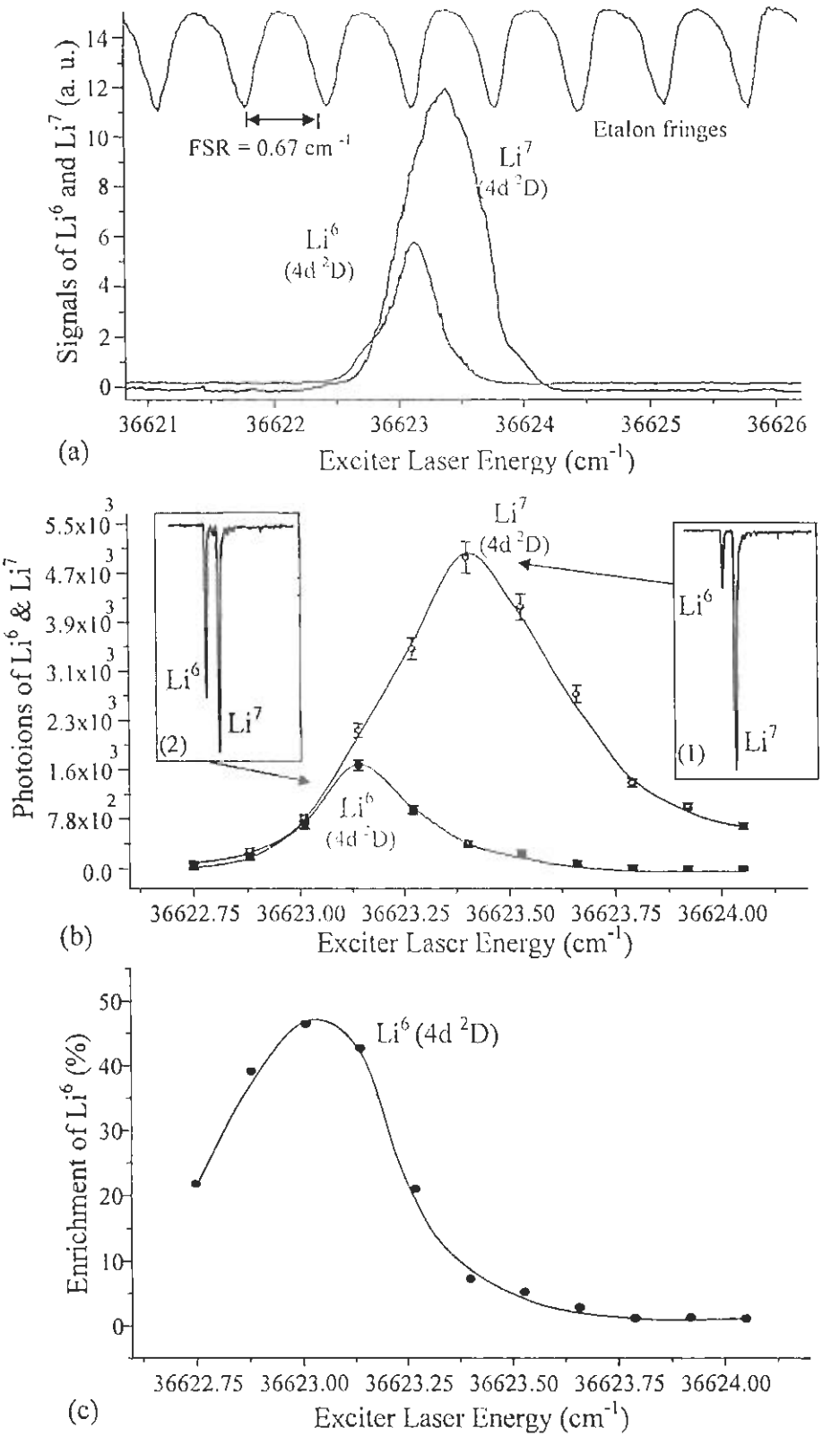


Figure 4.10 *(a) Boxcar averaged signals of both the lithium isotopes, (b) Photoions of both the isotopes and (c) concentration of $Li^6$ as a function of the exciter laser exploiting the 4d $^2$D excited state of lithium.*

# Chapter 5

## Simultaneous measurements of the photoionization cross section of lithium isotopes

We have experimentally demonstrated an alternate technique for the simultaneous measurement of the photoionization cross section of the excited states of isotopes. Saturation technique has been utilized to deduce the values of the cross section and the number densities of the corresponding isotopes. We have made new measurements of the photoionization cross-section of the lithium isotopes from the 2p $^2P_{1/2,3/2}$, 3s $^2S$, 3p $^2P$, 3d $^2P$, 4s $^2S$, 4p $^2P$ and 4d $^2D$ excites states using different ionizing laser wavelengths above the first ionization threshold in order to probe different regions of the continuum.

The photoionization cross section of the ground states are well known for many atoms (Marr 1967 and Berkowitz 1979, 2003), but for the excited states comparatively little experimental data are available. The excited states photoionization is of great importance in controlled thermonuclear research plasmas and in the regions of high temperature, such as stellar atmospheres. This type of process is also useful in understanding radiative recombination, the inverse process of the photoionization.

Theoretical determination of the photoionization cross section are found to be very sensitive to the nature of the wave functions involved in the calculations. Hartree-Fock wave functions have been used extensively for the calculation of the photoionization cross section of the ground states (Stewart 1954, Seaton 1951) as well as of the excited states (Msezane and Manson 1984, Chang and Kim 1982, Nahar and Manson 1989, Zhou *et al* 1993). Burgess and Seaton (1960) developed a general formula for the calculation of the photoionization cross section at the series limit. Aymar *et al* (1976) calculated the photoionization cross-section for s, p and d Rydberg states of Li, Na and K in the framework of a single electron model using a parametric central potential. Lahiri and Manson (1993) calculated the radiative-recombination rate coefficients for $e^-Li^+$ and the associated excited state photoionization cross section for lithium in the framework of the Central-Potential Model. Saha *et al* (1988) used the multiconfiguration Hartree-Fock calculations for the photoionization cross section of the 4d excited state of Na. Kupliauskiene (1997) applied the relaxed-orbital multiconfiguration Hatreee-Fock

approach to calculate the photoionization cross section of the ground and the excited states of sodium and potassium. The R-matrix technique is also one of the most widely used approaches (Tayal *et al* 1994, Rouvellou *et al* 1995) for the calculation of the photoionization properties for a wide variety of systems. R-matrix Floquet theory (Burke *et al* 1991, 1993) has proven to be a highly accurate technique for obtaining multiphoton ionization cross section for the complex atoms. Madine and van der Hart (2005) used this theoretical approach for calculating the single and two-photon ionization cross sections for Sr.

Rothe (1969, 1971), to our knowledge, first experimentally determined the photoionization cross section of the 3p excited state of sodium and the 2p excited state of lithium at threshold using absolute intensity measurements resulting from the radiative electron-ion recombination in to these states from the sodium and lithium-seeded plasma in the pressure driven shock tube. The high intensity, exceedingly small spectral width and tunability of the dye lasers made possible the selective excitation of any atomic state, and the subsequent photoionization from that state leads to measurement of the photoionization cross section of the selectively excited states. The thermionic diode is a very sensitive ion detector having gain up to $10^7$ (Thompson and Stoicheff 1982, Niemax 1985) and has been widely used (Kallenback *et al* 1988, Mende and Kock 1996, Griesmann *et al* 1992, Zhang *et al* 1992, Willke and Kock 1993, Amin *et al* (2006 a,b) for the measurement of the photoionization signals which have been used for the determination of the cross section of the excited states by employing the saturation technique. Bradley *et al* (1976) used a heat pipe oven and a set of electrodes in the heat pipe as ion collectors for measuring the photoionization cross-section of selectively excited magnesium. Triple atomic beam apparatus, which consists of an atomic beam oven, ion deflection electrodes and an ion detector, has also been extensively used for the measurements of the photoionization cross section of the excited states (Nygaard *et al* 1975, Smith *et al* 1980, Gerwert and Kollath 1983, Beterov and Ryabtsev 1993, Burkhardt *et al* 1988, Beterov *et al* 1996, Madsen *et al* 2000, He *et al* 1991). In the triple atomic beam apparatus, ions are produced only as a result of laser - atomic beam interaction and there are no collisions involved in the ion production as they are in the thermionic diode. Therefore, this apparatus provides a neat and clean environment for the

measurement of the photoionization cross-section and the related spectroscopic properties. Magneto-optical traps, which are pioneered by Dinneen *et al* (1992) are used for the measurement of the photoionization cross section of the excited states of trapped atoms or their specific isotopes (Gabbanini *et al* 1997, Marago *et al* 1998, Patterson *et al* 1999, Wippel *et al* 2001). Hussain *et al* (2006) reported the measurements of photoionization cross section of the excited states of He using a simple combination of DC discharge and two step photoionization.

The Time of Flight (TOF) mass spectrometer is a very sensitive ion detector (Castaldi and Senkan 1998) and is a widely applicable technique to probe the free neutral atoms in the specific atomic states (Hurst 1979, Letokhov 1987, Payne *et al* 1994). This has proven an alternate technique for the measurement of the photoionization cross section of the ground state (Sato *et al* 1985, Huang *et al* 1999, Wehlitz *et al* 2002, van der Hart and Greene 1998) as well as for the excited states (Lievens *et al* 1996, Philipsen *et al* 2000, Gisselbrecht *et al* 1999). The TOF mass spectrometer has the advantage over the thermionic diode and the triple atomic beam apparatus that it provides opportunities for the simultaneous measurement of different spectroscopic properties of the selected isotopic masses (Demtröder 1998). It makes sure that the emergence of the photoion signal is purely due to the isotope of interest. It also made it possible to investigate the singly, doubly, triply etc. photoionization states of atoms (Sato *et al* 1985, Wehlitz *et al* 2002b).

We have used our locally developed atomic beam-TOF mass spectrometer system, as described in the chapter 3, for the simultaneous measurements of the photoion signals of both the lithium isotopes as a function of the ionizing laser energy. This data is used to deduce the photoionization cross-section of the excited concerned state and the number density of the corresponding isotope. For pure two-step photoion signals, a relation between the number of ions and the photoionization cross section of the excited state can be deduced from the rate equations. If there are no collisions between the atoms, and the production of ions is only due to the two-step photoionization, then the following rate equations can be written, which are illustrated in figure (5.1) for the populations $N_0$, $N_{ex}$ and $N_{io}$ of each level:

$$\frac{dN_0}{dt} = -\sigma_a \phi_{ex}\left(N_0 - N_{ex}\right) \tag{5.1}$$

$$\frac{dN_{ex}}{dt} = \sigma_a \phi_{ex}\left(N_0 - N_{ex}\right) - \sigma(\lambda_{io})\phi_{io} N_{ex} \tag{5.2}$$

$$\frac{dN_I}{dt} = \sigma(\lambda_{io})\phi_{io} N_{ex} \tag{5.3}$$

Where $\sigma_a$ is the photoabsorption cross section, $\phi_{ex}$ is the photon flux of the exciter laser, $\sigma(\lambda_{io})$ is the photoionization cross section of the excited level at the ionizer laser wavelength $\lambda_{io}$, $\phi_{io}$ is the photon flux of the ionizer laser, $N_0$ is the population of the ground state, $N_{ex}$ is the population of the excited state and $N_I$ is the ions density produced as a result of two-step photoionization. The intensity of the exciting laser is sufficiently high throughout the laser pulse to saturate the excited state, where both the populations stay in equilibrium i.e. $N_0 \cong N_{ex}$.

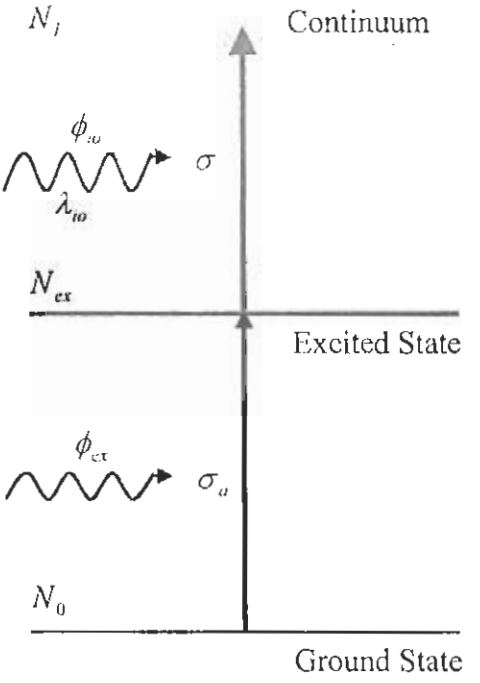


Figure 5.1 *Excitation/ionization scheme for selective two-step photoionization.*

Under this assumption, the total number density of atoms is

$$N_T = N_0 + N_{ex} = 2N_{ex}.$$

By adding equations (5.1) and (5.2), we get

$$\frac{d(N_0 + N_{ex})}{dt} = \frac{d(N_T)}{dt} = -\sigma(\lambda_{io})\,\phi_{io}\,N_{ex}$$

$$\Rightarrow \frac{dN_{ex}}{dt} = -\tfrac{1}{2}\sigma(\lambda_{io})\,\phi_{io}\,N_{ex}$$

$$\Rightarrow N_{ex} = \frac{N_0(t=0)}{2}\exp\left(-\frac{1}{2}\int_{-\infty}^{t}\sigma(\lambda_{io})\,\phi_{io}(t')\,dt'\right)$$

Integrating equation (5.3), we have

$$N_I = \int_{-\infty}^{\infty}\sigma(\lambda_{io})\,\phi_{io}(t)\,N_{ex}\,dt$$

Inserting the value of $N_{ex}$, we have

$$N_I = \int_{-\infty}^{\infty}\sigma(\lambda_{io})\,\phi_{io}(t)\;\frac{N_0}{2}\exp\left(-\frac{1}{2}\int_{-\infty}^{t}\sigma(\lambda_{io})\,\phi_{io}(t')\,dt'\right)dt \qquad (5.4)$$

Here the first term gives the total number of photons in the ionizing laser pulse and the second term containing $t'$ explains the decaying of the excited atoms due to the ionizing photons at any time $t$.

The solution of equation (5.4) yields

$$N_I = N_0\left[1-\exp\left(-\frac{1}{2}\int_{-\infty}^{\infty}\sigma(\lambda_{io})\,\phi_{io}(t)\,dt\right)\right]$$

Since at saturation $N_0 \cong N_{ex}$

$$N_I = N_{ex}\left[1-\exp\left(-\frac{1}{2}\sigma(\lambda_{io})\,\Phi_{io}\right)\right]$$

Here $\Phi_{io}$ is the fluence of the ionizing laser as seen by an atom at the beam center, as

$$\Phi_{io} = \int_{-\infty}^{\infty}\phi_{io}(t)dt$$

The fluence $\Phi_{io}$ is related with the energy $U$ of the ionizing laser as

$$\Phi_{io} = \frac{\lambda_{io}\,U}{h\,c\,A}$$

Here $h$ is the planck constant, $c$ is the velocity of light and $A(cm^2)$ is the cross sectional area of the interaction region. Hence

$$N_I = N_{ex}\left[1-\exp\left(-\frac{1}{2}\sigma(\lambda_{io})\frac{\lambda_{io}U}{hcA}\right)\right]$$

The ions density $N_I$ can be related with the total charge $Q$ that is produced in the ionizing volume $V(cm^3)$ as

$$N_I = \frac{Q}{eV}$$

Here $e$ is the electronic charge, hence

$$\frac{Q}{e} = N_{ex}\,V\,[1-\exp(-\tfrac{1}{2}\sigma(\lambda_{io})\frac{U\lambda_{io}}{hcA})] \qquad (5.5)$$

The photoions are always recorded as the voltage signal; hence the voltage signal can be related to the charge $Q$ as

$$Q = \left(\frac{Voltage\ signal}{R}\right)\times\Delta t \qquad (5.6)$$

Here $R$ is the terminating resistance at the oscilloscope and $\Delta t$ is the pulse width at the FWHM of the photoion signal peak in seconds. Equation (5.5) is applicable under three assumptions: the first one is that the transition remain saturated during the exciter laser pulse (i.e. $N_0 \approx N_{ex}$), the second one is that there are no spontaneous emissions during the exciter and the ionizer laser pulses and the last is that the intensity of the ionizer laser is higher i.e. in excess to that required for the complete ionization of the excited atoms from the corresponding excited state.

This technique of measuring the photoionization cross section is termed as the saturation technique. In this method, the photoion signal first increases with an increase in the energy of the ionizing laser and then stops for any further increase in the ionizing energy i.e. it gets saturated. The saturation technique was pioneered by Ambartzumian *et al* (1976) and has been used by many researchers (Bradley *et al* 1976, Heinzmann *et al* 1977, Smith *et al* 1980, Burkhardt *et al* 1988, Kallenbach *et al* 1988, He *et al* 1991, Willke and Kock 1993, Mende *et al* 1995, Amin *et al* 2006 a,b and Hussain *et al* 2006) for the measurement of the photoionization cross section of the excited states of alkali and alkaline earth metals. Burkhardt *et al* (1988), in addition, determined the atomic density for the resonance levels of sodium, barium and potassium. Mende *et al* (1995)

improved the theoretical part by taking the gaussian distribution function for determining the photon flux and measured the photoionization cross section of Sr $(5s5p)^1P_1$ excited state.

The first condition for measuring the photoionization cross section using equation (5.5) was fulfilled (experimentally) by varying the energy of the exciter laser to ensure the saturation of the exciting transition. The second condition is satisfied in all of our experiments because the lifetimes of the 2p $^2P_{1/2, 3/2}$, 3d $^2D$, 4s $^2S$, 3s $^2S$, 3p $^2P$, 4p $^2P$ and 4d $^2D$ excited states of lithium are 27 ns (McAlexander *et al* 1996), 14.9 ns (Hanson 1983), 56 ns (Boyd *et al* 1980), 27.9 ns, 200 ns, 450 ns and 33 ns (Radzig and Smirnov 1985) respectively which are much longer than the pulse duration (~5 ns) of the exciter laser. The ionizer laser was therefore delayed by ≈ 5 ns to the exciter laser to ensure a pure two-step photoion signal. The third requirement of the saturation technique is that the energy of the ionizer laser must be high enough to completely ionize all the excited atoms. This was achieved by focusing the ionizer laser with a plano convex lens of 250 mm focal length in the ionization region, which also served to constrain the ionizing volume small and cylindrical (Song *et al* 1999) over the ion collection length (atomic beam diameter of ~ 4.5 mm). This procedure also minimizes the problems associated with the spatial overlap of the exciter and the ionizer laser. Temporal overlapping is necessary only in the case if the lifetime of the excited state is comparable with the laser pulse duration.

Equation (5.5) illustrates that the accurate measurements of σ needs accurate determination of the cross sectional area of the ionizing laser beam at the atomic beam. The cross sectional area can be calculated (Demtröder 1998) as:

$$A = \pi\omega_0^2\left[1+\left(\lambda_{io}\, z \Big/ \pi\omega_0^2\right)^2\right] \tag{5.7}$$

Here $z$ is the distance on the beam propagation axis from the focus, $\omega_0 = f\lambda/\pi\omega_s$ is the diffraction limited radius at z = 0, $\omega_s$ is one half of the spot size of the ionizing laser beam on the focusing lens, and $\lambda_{io}$ is the wavelength of the ionizing laser. The accurate determination of $A$ therefore depends upon $z$ and $\omega_s$. For an accurate measurement of

$\omega_x$, the spatial profile of the ionizer laser beam was generated by scanning a PIN photodiode across its diameter. The spatial profile of the exciter laser at the ionization region of the TOF mass spectrometer was reproduced by placing a beam splitter before the entrance of the vacuum chamber (figure 2.1). The profiles of both the laser beams were gaussian, therefore their spot sizes were determined at which the irradiance (intensity) falls to $1/e^2$ of its axial value. The diameter of the exciter laser beam was found to be $\approx 4$ mm in the ionization region across the atomic beam and of the ionizer laser beam was also $\approx 4$ mm on the focusing lens.

Equation (5.5) predicts that the photoions get saturated only for $U \rightarrow \infty$, however every detection system has some limitations of sensing even very minute variations in the signals. We, however, made sure that the detector of the TOF mass spectrometer operates in the linear mode (explained in chapter 3) so that the actual changes of the photoion signals verses the energy density of the ionizer laser could be registered.

The signal heights of the isotopic signals were recorded simultaneously by varying the intensity of the ionizing laser by inserting the neutral density filters, keeping the intensity of the exciting laser fixed. In order to simultaneously saturate both the isotopic transitions, the exciter laser was tuned in the middle of the excited states of both the isotopes. The energy of the exciter laser was optimized to ensure the saturation of both transitions of the isotopes.

The polarization of the exciter and the ionizer laser plays an important role for the measurement of the photoionization cross section. Therefore, if both the exciter and the ionizer laser pulses are linearly polarized, then the measured cross section depends upon the angle θ between the two laser polarization directions (He *et al* 1991), as given by

$$\sigma(0) = \cos^2\theta\, \sigma^{\parallel} + \cos^2\theta\, \sigma^{\perp}$$

Where $\sigma^{\parallel}$ and $\sigma^{\perp}$ are the cross sections for parallel and perpendicular polarizations of the exciter and the ionizer laser beams respectively. In all of our experiments, both the exciter and the ionizer lasers were linearly polarized and the polarization vectors were parallel. Therefore, only the term $\cos^2\theta\, \sigma^{\parallel}$ will contribute in these measurements of the cross section. In addition, only transitions between the magnetic sublevels $\Delta m = 0$ are allowed under these conditions.

The equation (5.5) also yields the number density of the atoms being excited to a particular state. It is evident that the determination of $N_{ex}$ is independent of the photoionization cross-section. In other words, $N_{ex}$ is deduced from the asymptotic value of $Q/e$ while $\sigma$ is associated with the shape of the $Q/e$ verses $U/A$ experimental data. The accurate determination of $N_{ex}$ requires that both the transitions must be saturated and that the ionizing volume has been measured accurately. The ionizing volume is defined as the interaction volume of the overlap region of the exciter and the ionizer laser beams in the effective collection region (atomic beam size). In order to measure the true number density of the isotopes (explained in chapter 4), the corresponding photoion signals were divided with the gain of the channeltron (Galileo USA), which is used as the ion detector in the TOF mass spectrometer.

The experimental uncertainties in the measurements of the cross section include the energy measurements (± 3%), laser energy fluctuations (± 5%), atomic beam estimation (± 5%) and the cross sectional area of the interaction region (± 13%). Based on these experimental uncertainties, we estimate our reported values to be accurate (Topping 1962, Dunning and Stebbings 1974) to ± 15 %.

The literature reveals that only the 2p excited state of lithium has been used for the isotope separation of $Li^6$ and $Li^7$, that is why the cited literature contains only the photoionization cross-section of both the isotopes from the 2p excited state. The ionization yield of the isotope of interest can be quantified if the photoionization cross-section of the excited state involved in the enrichment process is precisely known. There are no experimentally measured photoionization cross-sections from the higher excited states of the lithium. We have, for the first time, measured the photoionization cross section of both the lithium isotopes from the $2p\ ^2P_{1/2,\ 3/2}$, $3s\ ^2S$, $3p\ ^2P$, $3d\ ^2P$, $4s\ ^2S$, $4p\ ^2P$ and $4d\ ^2D$ excited states.

We have resolved the fine structure components of the 2p-excited state, as shown in the figure (4.1). The linewidth of our exciter laser was not sufficiently narrow to selectively excite the $2p\ ^2P_{3/2}$ excited state of $Li^6$ and $2p\ ^2P_{1/2}$ excited state of $Li^7$, however the TOF mass spectrometer separated both the lithium isotopes on the time axis (see figure 4.1). This enabled us to simultaneously measure the photoion signals of the resolved fine structure components as a function of the intensity of the ionizing laser. Figure (5.2)

shows a schematic diagram for the two-step photoionization scheme used to measure the photoionization cross-section of the fine structure levels. The exciter laser (TDL-90) was tuned at 670.8 nm to populate the 2p-excited state via single photon excitation obeying the dipole selection rules. The exciter laser was tuned to the $^2P_{1/2}$ excited state of $Li^6$, between the $^2P_{3/2}$ of $Li^6$ and $^2P_{1/2}$ of $Li^7$ and $^2P_{3/2}$ of $Li^7$ while keeping the ionizer laser wavelength fixed for the measurement of the photoionization cross section for both the lithium isotopes from the said excited states.

As shown in the figure (4.1), the measurement of the cross sections from the 2p $^2P_{3/2}$ excited states of $Li^6$ and from the 2p $^2P_{1/2}$ excited state of $Li^7$ was possible only due to this alternate technique since both the excited states have not been excited selectively due to our broad band exciter laser. The photoionization cross-section from the 2p $^2P_{1/2}$ excited state of $Li^6$ and from the 2p $^2P_{3/2}$ excited states of $Li^7$ was also measured by tuning the exciter laser to the corresponding excited state. The energy of the exciter laser at any frequency was kept fixed and the energy of the ionizer laser was varied using neutral density filters in order to achieve the complete ionization of the excited isotopic atoms.

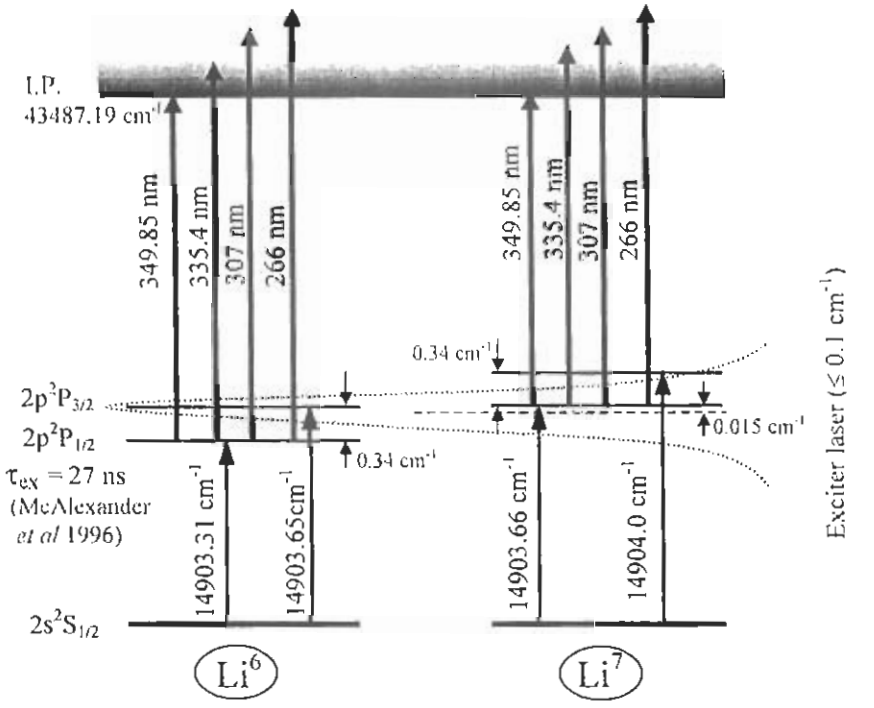


Figure 5.2 *Schematic diagram for the two-step photoionization of the lithium isotopes from the 2p $^2P_{1/2,\ 3/2}$ excited states.*

The ionizer laser at 335.4 nm was achieved by the frequency doubling of the exciter laser with a BBO type-1 crystal inside the TDL-90. Both the exciter and the ionizer lasers were separated by a Pellin Broca prism. The resulting photoion signals of $Li^6$ from the $2p\ ^2P_{1/2}$ excited state and of $Li^7$ from the $2p\ ^2P_{3/2}$ excited state verses the ionizing laser energy density at 335.4 nm is shown in figure (5.3). It is evident that the photoion current signals of both the isotopes increases with an increase in the energy density of the ionizer laser up to a certain value and then stops increasing further and finally saturation sets in.

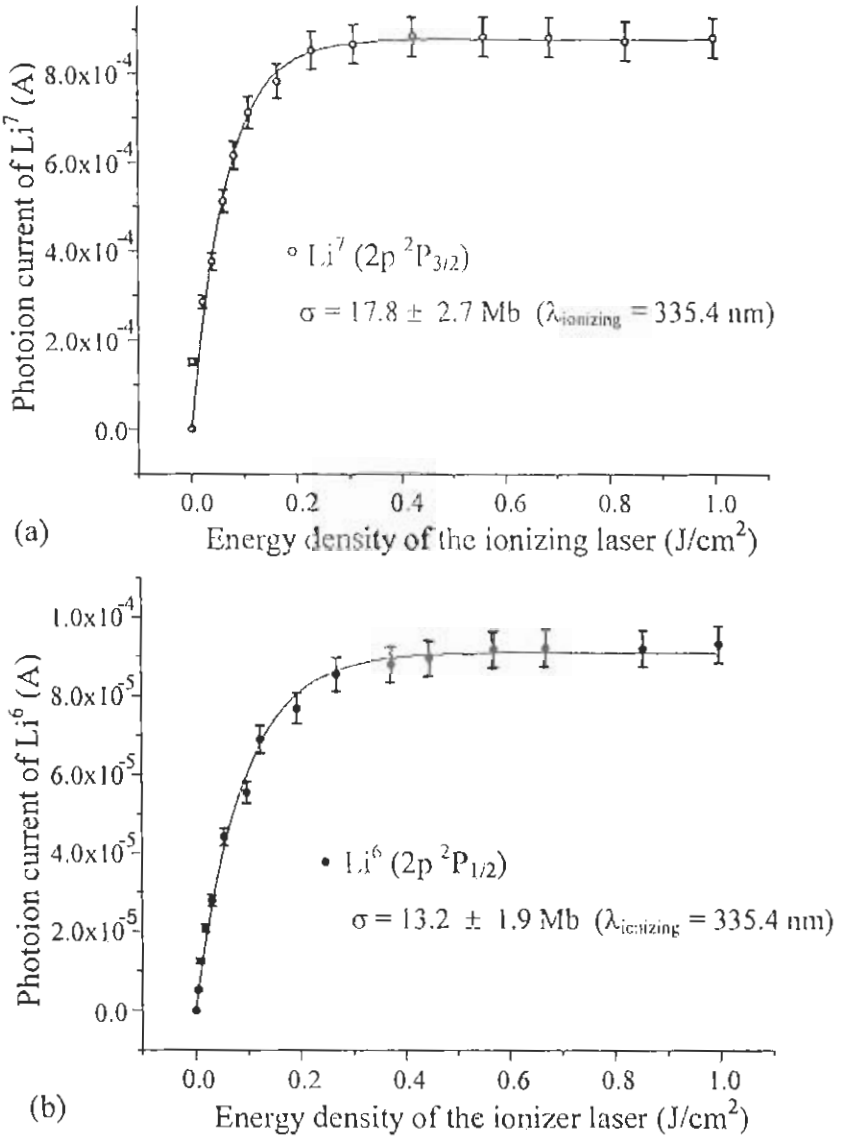


Figure 5.3 *Photoion current signals of (a) $Li^7$ from the $2p\ ^2P_{3/2}$ and (b) $Li^6$ from the $2p\ ^2P_{1/2}$ excited states verses the energy density of the ionizer laser at 335.4 nm. The error bars (5%) on the data points are due to the pulse-to-pulse fluctuations in the laser energy.*

Equation (5.5) is used for the least square fitting of the photoion current signals (shown in figure 5.3) for both the isotopes. The solid line that passes through the experimental data points is the least square fit to equation (5.5), which yields the absolute photoionization cross section of the 2p fine structure excited states for both the lithium isotopes. A similar procedure was adopted for the measurement of the cross section from the 2p $^2P_{3/2}$ excited state of $Li^6$ and the 2p $^2P_{1/2}$ excited state of $Li^7$ using the ionizer laser at 335.4 nm and three other ionizing laser wavelengths at 349.85, 307 and 266 nm. The measured values of the photoionization cross sections are listed in table (5.1). The ionizing laser wavelengths at 349.85 nm and 307 nm were achieved by the SHG of 699.7 and 614 nm with a BBO crystal. The lasers at 699.7 and 614 nm were achieved from the Hanna type dye laser by charging it with Pyridine-1 dissolved in PC (Propylene Carbonate) and Rhodamine 640 dissolved in methanol respectively. The laser at 266 nm was achieved by the frequency doubling of 532 nm (SHG of Nd:YAG) with a BBO crystal.

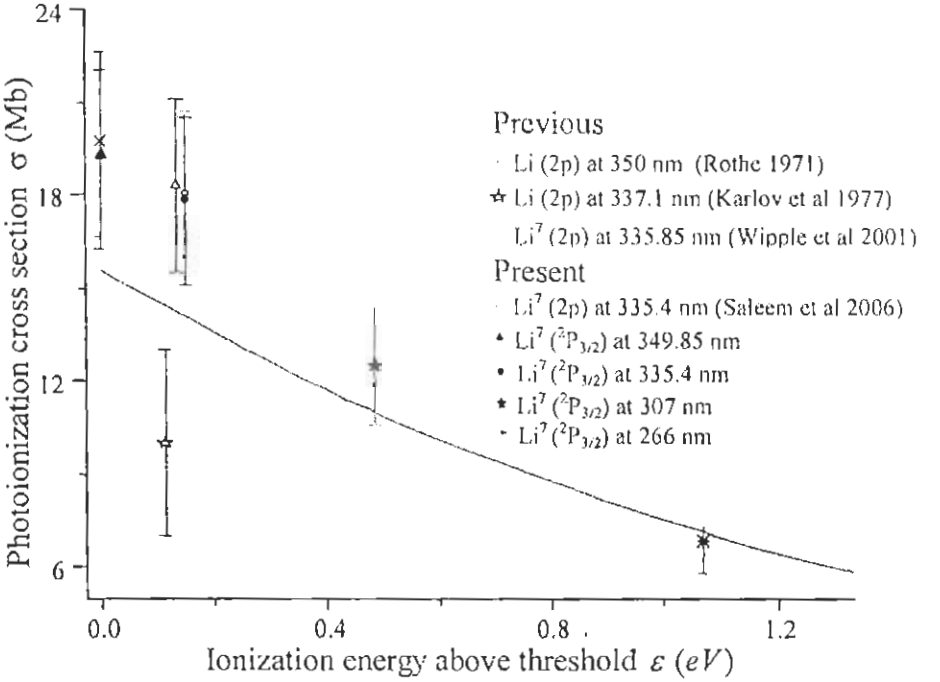


Figure 5.4 *Comparison of the experimentally measured values of the photoionization cross section at 2p $^2P_{3/2}$ of the $Li^7$ with the existing experimental and the theoretical literature. The continuous curve is the theoretical calculation of Lahiri and Manson (1993).*

Since $Li^7$ is 92.5 % abundant in the natural occurring lithium, therefore we have compared the measured cross sections of $Li^7$ with the existing theoretical and experimental values of the cross section for the lithium atoms as a whole.

Figure (5.4) shows a comparison of the measured values of the cross section from the 2p $^2P_{3/2}$ excited state for $Li^7$ at four ionizing laser wavelengths 335.4, 349.85, 307 and 266 nm with the known experimental and theoretical values. The continuous curve is the theoretical calculations of Lahiri and Manson (1993). It is evident from this figure that our measured values from the 2p $^2P_{3/2}$ excited state of $Li^7$ are very close to that reported by Wippel *et al* (2001) who used a much sophisticated experimental technique (MOT). More significantly, the last point of the measured photoionization cross-section at 266 nm lies at the theoretically calculated curve by Lahiri and Manson (1993).

Table (5.1)

*Experimentally determined photoionization cross-section of the lithium isotopes from the 2p $^2P_{1/2,\ 3/2}$ excited states for both isotopes as a function of the excess photon energy.*

| Lithium isotope | Excited state | Ionizing laser | Cross Section σ (Mb) | Reference |
|---|---|---|---|---|
| $Li^6$ | 2p $^2P_{1/2,\ 3/2}$ | 334.4 nm | 15 ± 15 | Wipple *et al* (2001) |
| | | 335.8 nm | 6 (-5, +20) | Wipple *et al* (2001) |
| | | 266 nm | (5 – 30) | Arisawa *et al* (1982) |
| | | 335.4 nm | 15.0 ± 2.3 | Saleem *et al* (2006) |
| | 2p $^2P_{3/2}$ | 349.85 nm | 15.4 ± 2.3 | This work |
| | | 335.4 nm | 14.8 ± 2.2 | |
| | | 307 nm | 10.5 ± 1.6 | |
| | | 266 nm | 6.8 ± 1.0 | |
| | 2p $^2P_{1/2}$ | 349.85 nm | 13.8 ± 2.0 | |
| | | 335.4 nm | 13.2 ± 1.9 | |
| | | 307 nm | 9.5 ± 1.4 | |
| | | 266 nm | 5.9 ± 0.9 | |
| $Li^7$ | 2p $^2P_{1/2,\ 3/2}$ | 334.4 nm | 16.2 ± 2.5 | Wipple *et al* (2001) |
| | | 335.8 nm | 18.3 ± 2.8 | Wipple *et al* (2001) |
| | | 335.4 nm | 18.0 ± 2.7 | Saleem *et al* (2006) |
| | 2p $^2P_{3/2}$ | 349.85 nm | 19.2 ± 2.9 | This work |
| | | 335.4 nm | 17.8 ± 2.7 | |
| | | 307 nm | 12.5 ± 1.9 | |
| | | 266 nm | 8.0 ± 1.2 | |
| | 2p $^2P_{1/2}$ | 349.85 nm | 16.5 ± 2.5 | |
| | | 335.4 nm | 15.5 ± 2.3 | |
| | | 307 nm | 10.8 ± 1.6 | |
| | | 266 nm | 6.8 ± 1.0 | |

Table (5.1) shows that the photoionization cross-section from the 2p $^2P_{3/2}$ excited state is higher than that of the 2p $^2P_{1/2}$ excited state for both the $Li^6$ and $Li^7$; this may be attributed to the transition line strength. The transition probability for $^2S_{1/2}$ to $^2P_{3/2}$ is higher (Cowan 1981, Sobel'man 1972) than for $^2S_{1/2}$ to $^2P_{1/2}$ transition.

The excitation of the 3s $^2S$, 3p $^2P$, 3d $^2D$, 4s $^2S$, 4p $^2P$ and 4d $^2D$ excited states of lithium have already been explained in the chapter 4. In this section, the measurements of the photoionization cross section of these excited states using different ionizing laser wavelengths above the first ionization threshold are presented. The reason for using different ionizing lasers is that by varying the frequency of the ionizing laser the electrons of different kinetic energies are produced and the behavior of the photoionization in different regions of the continuum can be investigated. The exciting and ionizing wavelengths used for these studies are shown in figure (5.5).

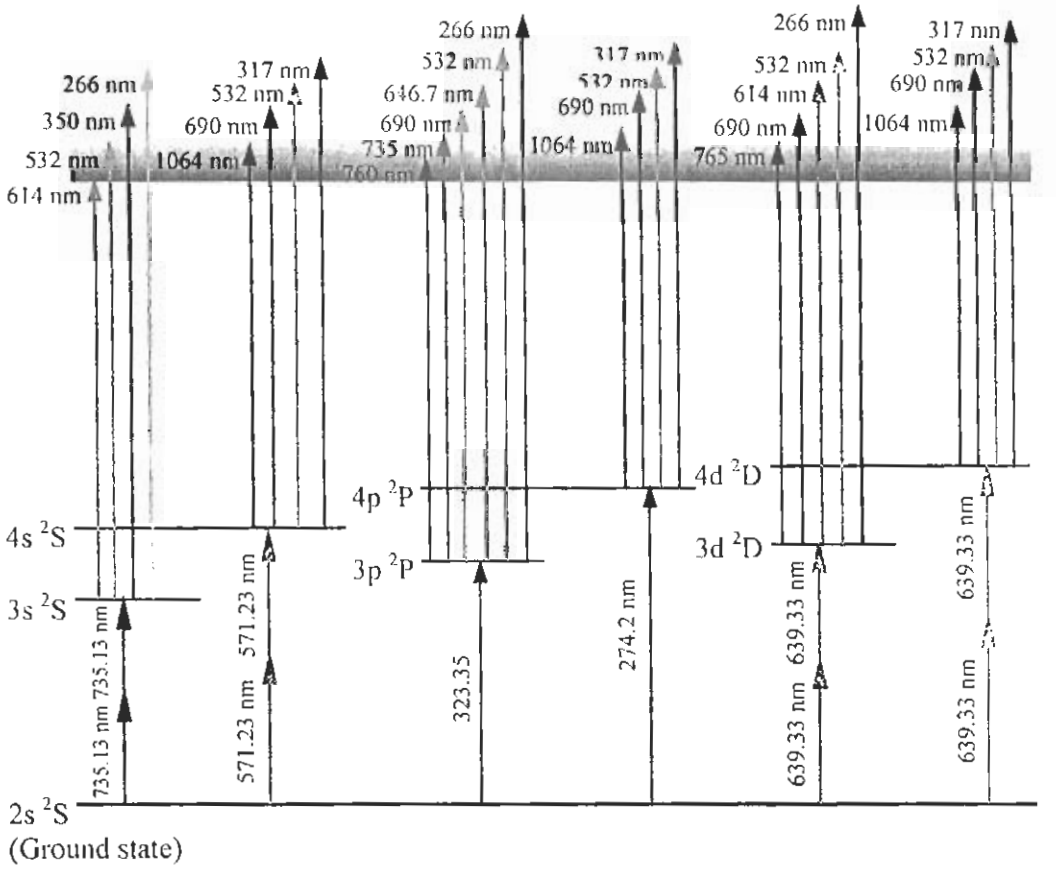


Figure 5.5 *Excitation/ionization scheme used for the measurement of the photoionization cross sections of both the lithium isotopes from the 3s $^2S$, 3p $^2P$, 3d $^2D$, 4s $^2S$, 4p $^2P$ and 4d $^2D$ excited states.*

All the exciting laser wavelengths were achieved with the TDL-90 dye laser, which delivered different laser wavelengths for the excitation of different excited states of lithium with sufficiently high laser intensity in order to saturate the excited states as described earlier. Most of the ionizing laser wavelengths were achieved by pumping a home made Hanna type (Hanna *et al* 1975) dye laser with 532 nm (SHG of 1064 nm) and charging it with different dyes, as shown in the table (5.2). The laser wavelength at 266 nm was achieved by the frequency doubling of 532 nm with a BBO crystal.

Table (5.2)

*A list of the ionizing laser wavelengths used to ionize the excited lithium isotopic atoms from the 3s, 3p, 3d, 4s, 4p and 4d excited states using the home made Hanna type dye laser pumped with the laser at 532 nm.*

| Ionizing laser wavelength | Dye | Solvent |
|---|---|---|
| 614 nm | Rhodamine 640 | Methanol |
| 690 nm / 700 nm | LDS 698 | Methanol |
| 765 nm / 760 nm / 735 nm | Pyridine – 2 | PC (Propylene Carbonate) |
| 634 nm | DCM | Methanol |

The ionizing laser at 646.7 nm was achieved through the dye laser TDL-90 by charging it with DCM dye dissolved in methanol, as its SHG was used to populate the 3p excited state. Both the laser wavelengths at 646.7 nm and its SHG at 323.35 nm were separated with a Pellin Broca prism. The lasers wavelengths at 700 and 634 nm were frequency doubled by the BBO crystal to achieve the required ionizing wavelengths at 350 and 317 nm. The energy of the exciter laser at any frequency was kept fixed and the ionizer laser energy was varied using neutral density filters in order to achieve the complete ionization of the excited isotopic atoms. For all these excited states, the exciter laser was tuned in the middle of the excited states of both the isotopes in order to simultaneously saturate both the isotopic transitions. The resulting photoion current signals of both the isotopes originating from all the aforementioned excited states versus energy density of the ionizer laser are shown in the figure (5.6). It is evident that the photoion current signals of both the isotopes first increase with an increase in the energy density of the ionizer laser and then stops for any further increase in the ionizing laser energy. That means a saturation in the photoion signals sets in except for the 3s and 4s excited states where more energy is

required for complete saturation. Equation (5.5) was used for the least square fitting of the photoionization data shown in these figures. The solid line that passes through the experimental data point is the least square fit which yields the photoionization cross sections of both the lithium isotopes from the 3s, 3p, 3d, 4s, 4p and 4d excited states and the deduced values are listed in the table (5.3).

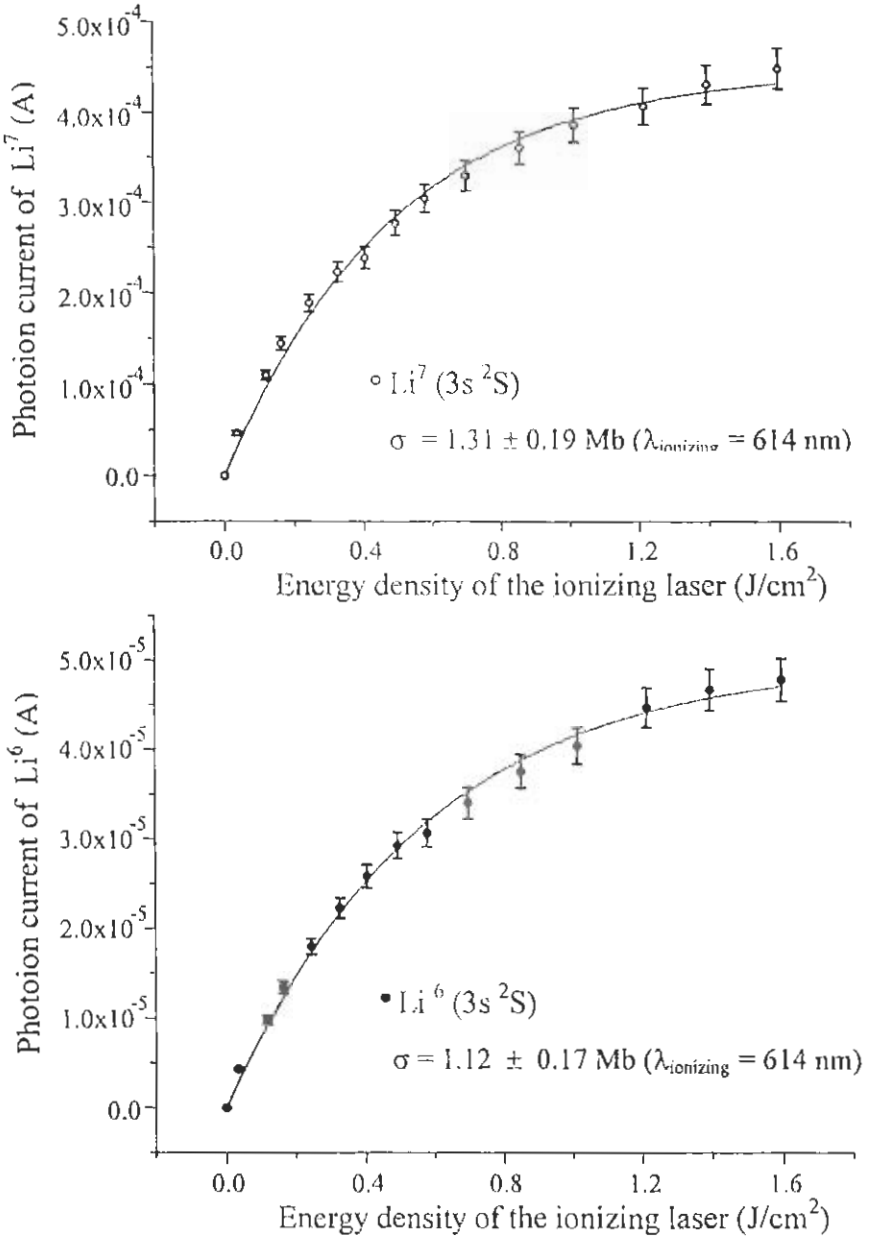


Figure 5.6(a) *The photoion current of the lithium isotopes measured simultaneously as a function of the energy density of the ionizer laser from the 3s excited state. The error bars (5%) result from pulse-to-pulse fluctuations in the photoion current signal due to the laser energy.*

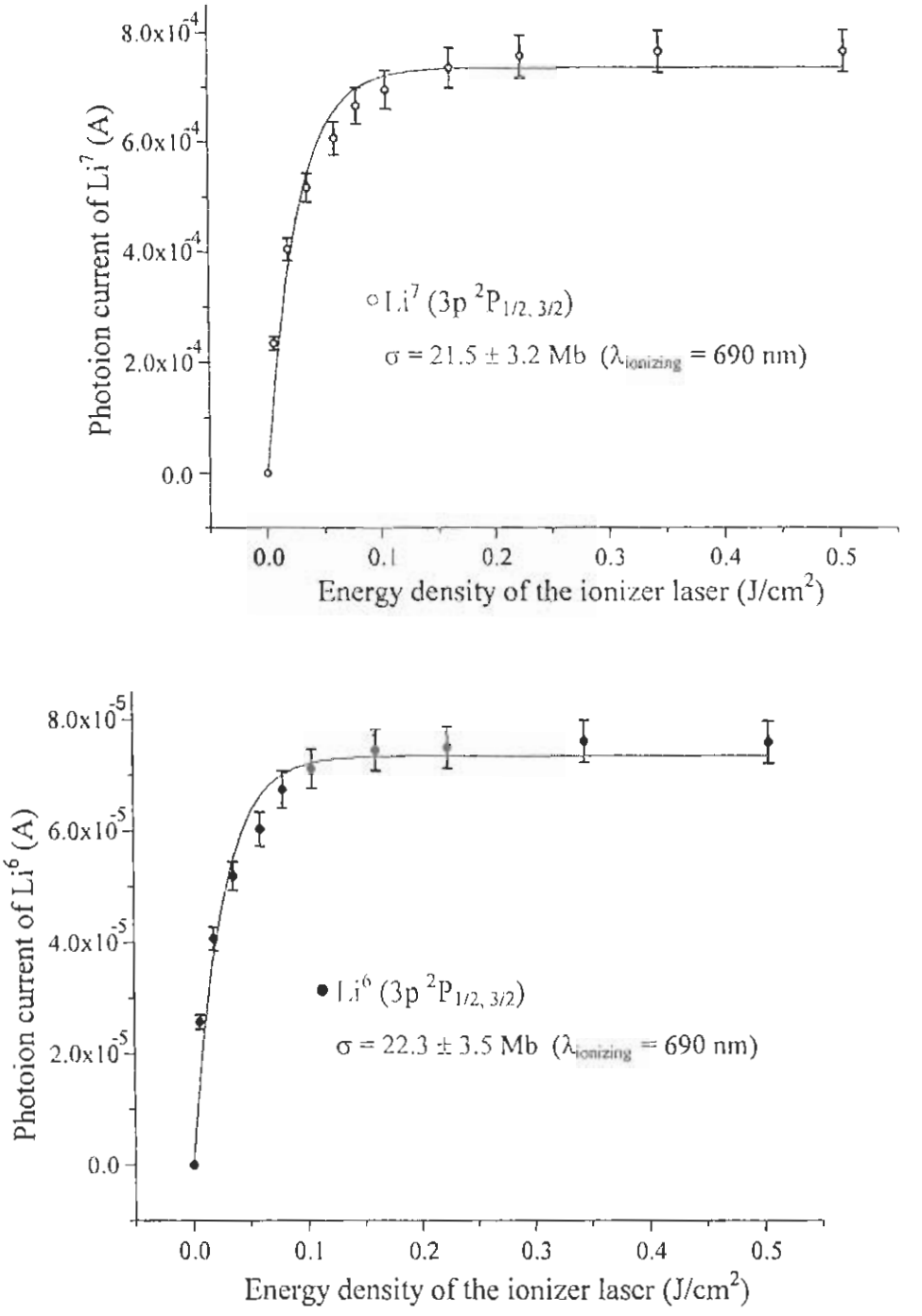


Figure 5.6(b) *The photoion current of the lithium isotopes measured simultaneously as a function of the energy density of the ionizer laser from the 3p excited state. The error bars (5%) result from pulse-to-pulse fluctuations in the photoion current signal due to the laser energy.*

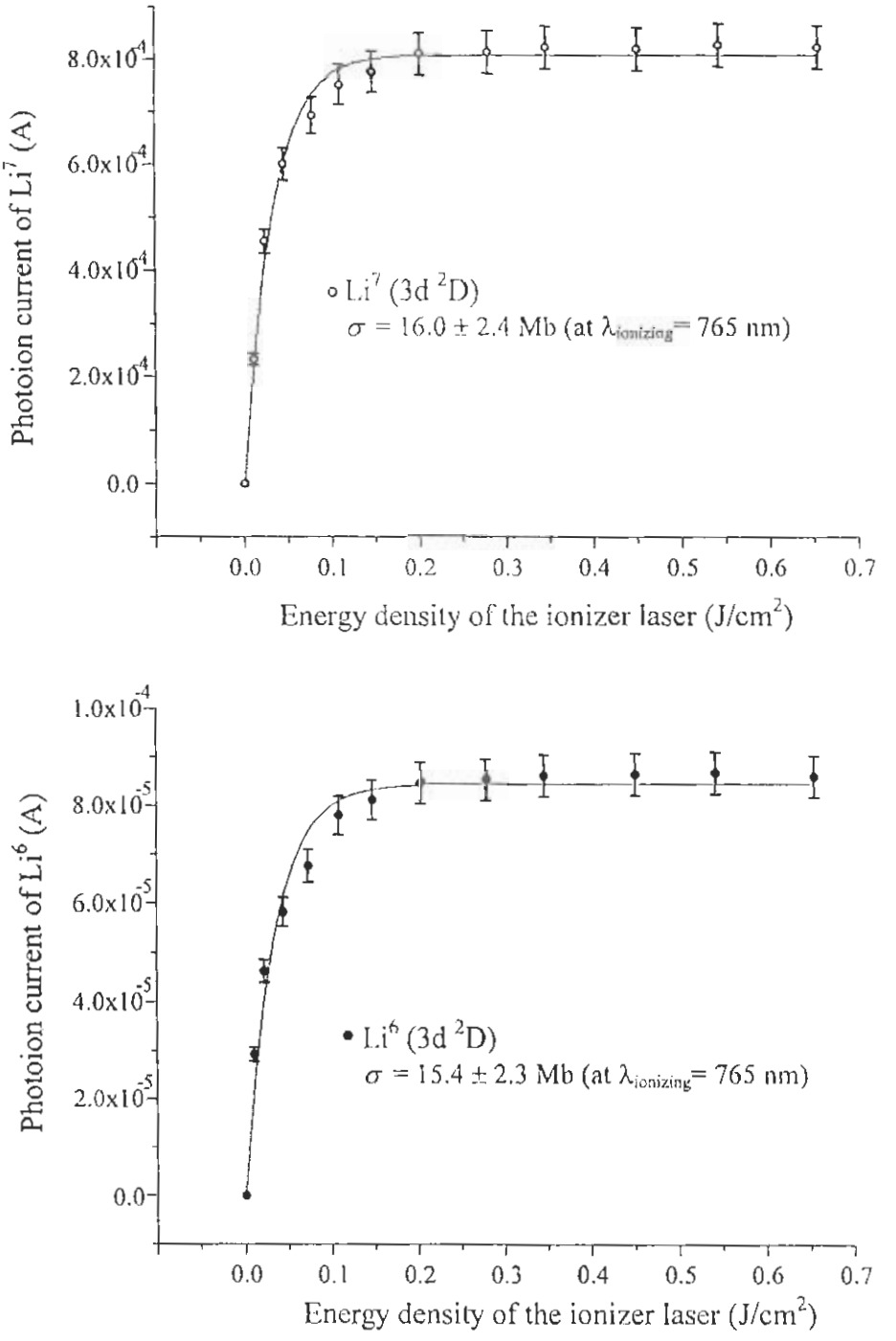


Figure 5.6(c) *The photoion current of the lithium isotopes measured simultaneously as a function of the energy density of the ionizer laser from the 3d excited state. The error bars (5%) result from pulse-to-pulse fluctuations in the photoion current signal due to the laser energy.*

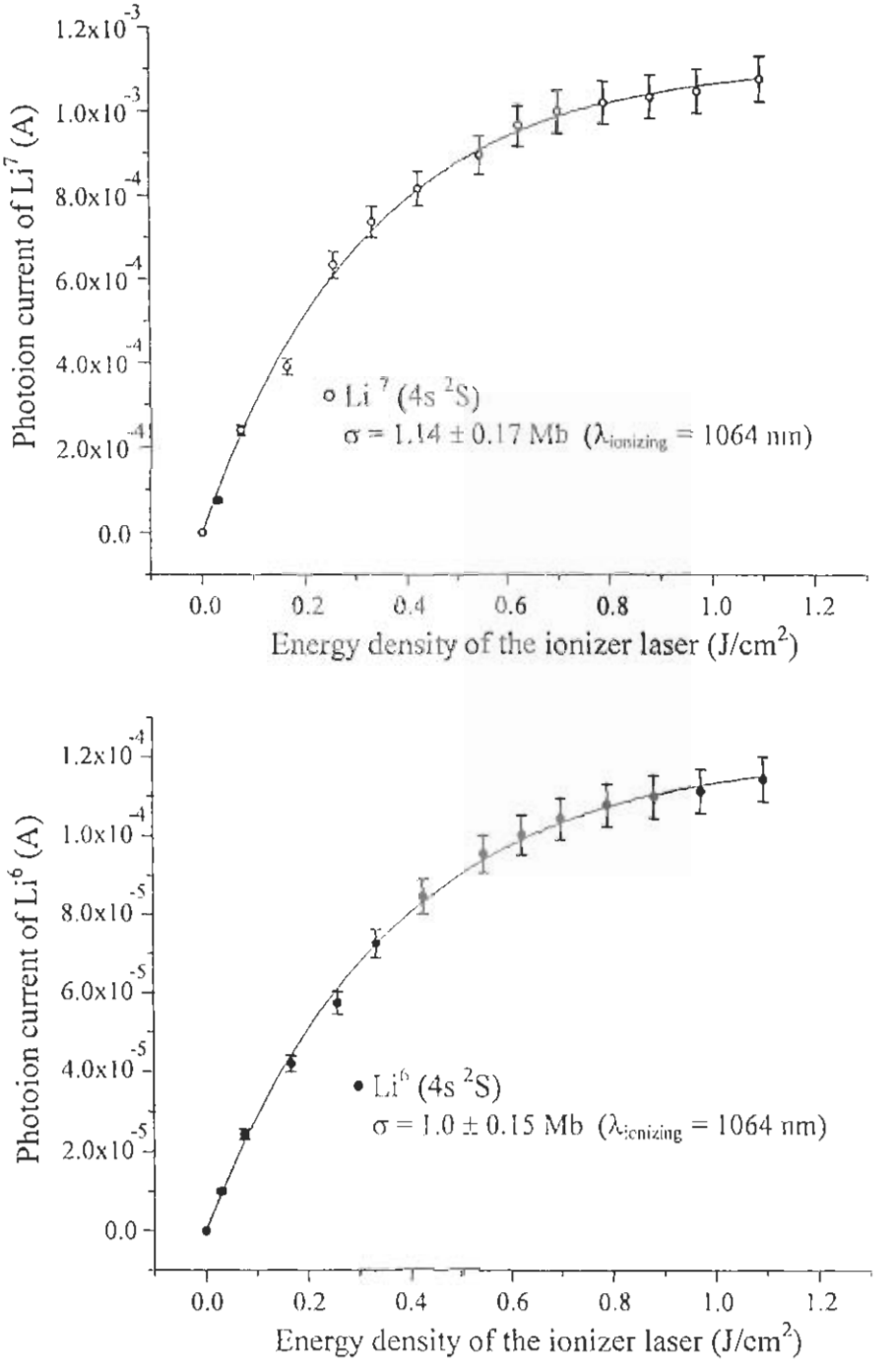


Figure 5.6(d) *The photoion current of the lithium isotopes measured simultaneously as a function of the energy density of the ionizer laser from the 4s excited state. The error bars (5%) result from pulse-to-pulse fluctuations in the photoion current signal due to the laser energy.*

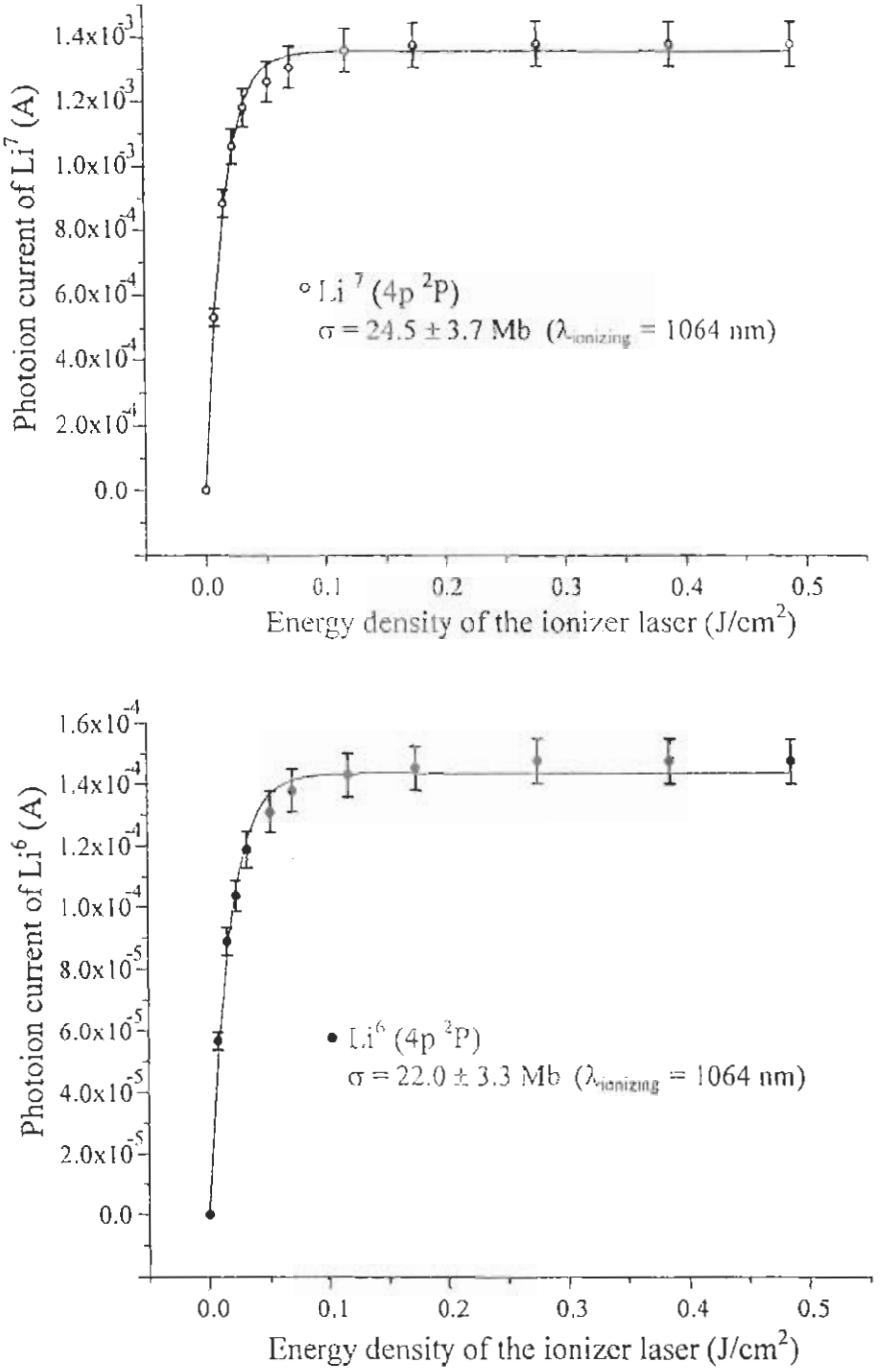


Figure 5.6(e) *The photoion current of the lithium isotopes measured simultaneously as a function of the energy density of the ionizer laser from the 4p excited state. The error bars (5%) result from pulse-to-pulse fluctuations in the photoion current signal due to the laser energy.*

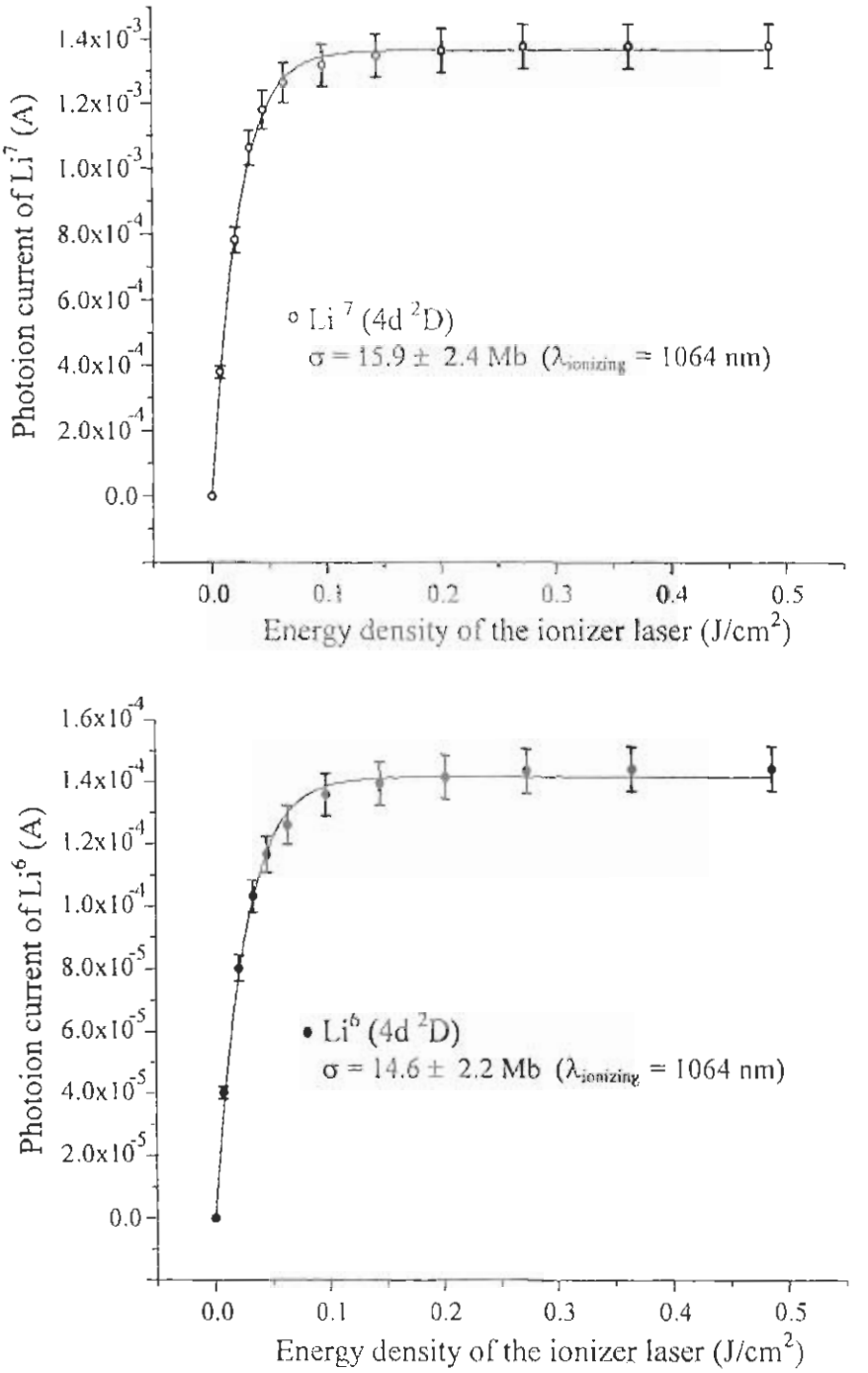


Figure 5.6(f) *The photoion current of the lithium isotopes measured simultaneously as a function of the energy density of the ionizer laser from the 4d excited states. The error bars (5%) result from pulse-to-pulse fluctuations in the photoion current signal due to the laser energy.*

It is clear from figure (5.6a to 5.6f) that for a higher value of the cross section the photoion signals get saturated even at a lower energy density of the ionizer laser.

Table (5.3)

*Experimentally determined absolute photoionization cross-sections of the lithium isotopes from the 3s, 3p, 3d, 4s, 4p and 4d excited states as a function of the excess photon energy above the first ionization threshold.*

| Excited state | Lithium/ Lithium isotopes | Ionizing laser wavelength | Photoionization cross section (Mb) | Reference |
|---|---|---|---|---|
| $3s\ ^2S$ | Li | 614 nm (Threshold) | 1.48<br>1.27<br>1.42<br>1.17<br>1.42 | Aymar *et al* 1976<br>Moskvin 1963<br>Ya'akobi 1967<br>Gezalov and Ivanova 1968<br>Caves and Dalgarno 1972 |
| | $Li^6$ | 614 nm | 1.12 ± 0.17 | This work |
| | | 532 nm | 1.20 ± 0.18 | |
| | | 350 nm | 1.13 ± 0.17 | |
| | | 266 nm | 0.80 ± 0.12 | |
| | $Li^7$ | 614 nm | 1.31 ± 0.19 | |
| | | 532 nm | 1.41 ± 0.21 | |
| | | 350 nm | 1.32 ± 0.19 | |
| | | 266 nm | 1.02 ± 0.15 | |
| $3p\ ^2P$ | Li | 796.1 nm (Threshold) | 28.1<br>10.0<br>28.2<br>28.0 | Aymar *et al* 1976<br>Ya'akobi 1967<br>Gezalov and Ivanova 1968<br>Caves and Dalgarno 1972 |
| | $Li^6$ | 760 nm | 28.5 ± 4.3 | This work |
| | | 735 nm | 26.8 ± 4.0 | |
| | | 690 nm | 22.3 ± 3.5 | |
| | | 646.7 nm | 18.6 ± 2.8 | |
| | | 532 nm | 10.5 ± 1.6 | |
| | | 266 nm | 4.3 ± 0.7 | |
| | $Li^7$ | 760 nm | 27.4 ± 4.1 | |
| | | 735 nm | 25.5 ± 3.8 | |
| | | 690 nm | 21.5 ± 3.2 | |
| | | 646.7 nm | 17.8 ± 2.7 | |
| | | 532 nm | 9.7 ± 1.5 | |
| | | 266 nm | 4.1 ± 0.6 | |

| | | | | |
|---|---|---|---|---|
| 3d $^2$D | Li | 819.4 nm (Threshold) | 18.2<br>15.0<br>17.5 | Aymar *et al* 1976<br>Ya'akobi 1967<br>Gezalov and Ivanova 1968 |
| | $Li^6$ | 765 nm | 15.4 ± 2.3 | This work |
| | | 690 nm | 8.5 ± 1.3 | |
| | | 614 nm | 5.2 ± 0.8 | |
| | | 532 nm | 3.5 ± 0.5 | |
| | | 266 nm | 1.0 ± 0.2 | |
| | $Li^7$ | 765 nm | 16.0 ± 2.4 | |
| | | 690 nm | 9.0 ± 1.4 | |
| | | 614 nm | 5.8 ± 0.9 | |
| | | 532 nm | 3.8 ± 0.6 | |
| | | 266 nm | 1.2 ± 0.2 | |
| 4s $^2$S | Li | 1180 nm (Threshold) | 1.40<br>1.31 | Aymar *et al* 1976<br>Gezalov and Ivanova 1968 |
| | $Li^6$ | 1064 nm | 1.0 ± 0.15 | This work |
| | | 690 nm | 1.07 ± 0.16 | |
| | | 532 nm | 0.77 ± 0.12 | |
| | | 317 nm | 0.45 ± 0.07 | |
| | $Li^7$ | 1064 nm | 1.14 ± 0.17 | |
| | | 690 nm | 1.25 ± 0.19 | |
| | | 532 nm | 1.05 ± 0.16 | |
| | | 317 nm | 0.54 ± 0.08 | |
| 4p $^2$P | Li | 1425 nm (Threshold) | 41.70<br>34.20 | Aymar *et al* 1976<br>Gezalov and Ivanova 1968 |
| | $Li^6$ | 1064 nm | 22.0 ± 3.3 | This work |
| | | 690 nm | 8.0 ± 1.2 | |
| | | 532 nm | 4.5 ± 0.7 | |
| | | 317 nm | 1.7 ± 0.3 | |
| | $Li^7$ | 1064 nm | 24.5 ± 3.7 | |
| | | 690 nm | 9.5 ± 1.4 | |
| | | 532 nm | 5.2 ± 0.8 | |
| | | 317 nm | 1.8 ± 0.3 | |
| 4d $^2$D | Li | 1456.9 nm (Threshold) | 36.20<br>30.60 | Aymar *et al* 1976<br>Gezalov and Ivanova 1968 |
| | $Li^6$ | 1064 nm | 14.6 ± 2.2 | This work |
| | | 690 nm | 3.0 ± 0.5 | |
| | | 532 nm | 1.7 ± 0.3 | |
| | | 317 nm | 0.5 ± 0.1 | |
| | | 1064 nm | 15.9 ± 2.4 | |

The fitting procedure yields the number densities for $Li^7$ as $\approx 1.2\times10^9$ atoms/cm$^3$ and for $Li^6$ as $\approx 1.2\times10^8$ atoms/cm$^3$ utilizing all the excited states provided both the transitions (from the ground state to the excited states and from the excited states to the ionization continuum) are saturated. The deduced values of the number densities are very close (within experimental error) to the natural abundance of both the lithium isotopes. This clearly reflects the simultaneous saturation ($N_0 = N_{ex}$) of the excited states of both the isotopes.

We have compared our measured values of the cross sections with the existing theoretical values. The cross sections of the excited states of lithium have been calculated by considering it as a whole atom and to our knowledge no measurements are available about the cross sections of its isotopes $Li^6$ and $Li^7$ separately. Figure (5.7) shows a comparison of the measured cross sections of $Li^7$ isotope from the 3s excited state. The solid line is the calculations of Lahiri and Manson (1993) that cover the excess energy range from the first ionization threshold up to 6.8 eV (1 eV = 8065.65 cm$^{-1}$).

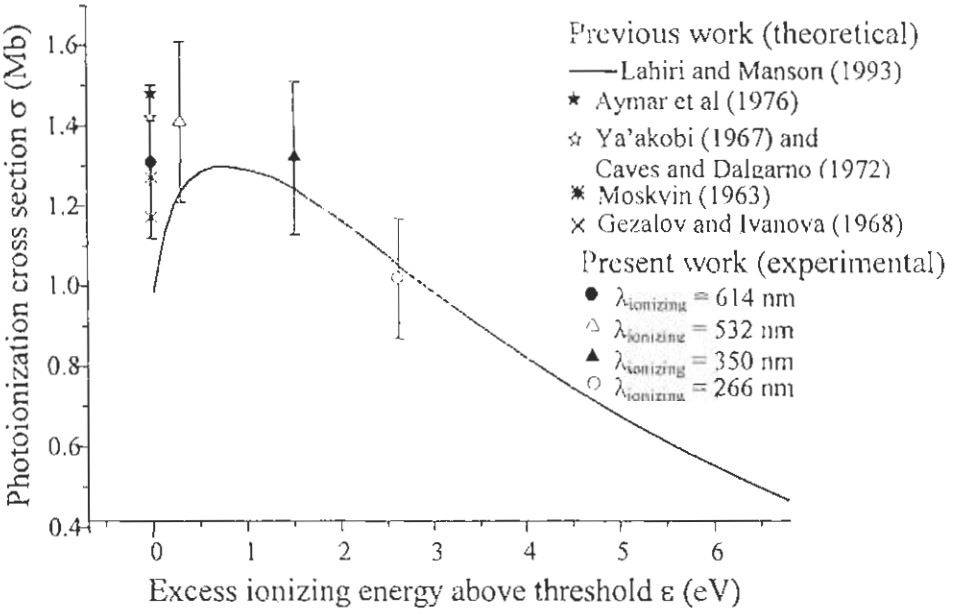


Figure 5.7 *Comparison of the measured values of the absolute photoionization cross section of the $Li^{7*}$ 3s with the theoretical cited literature. The continuous line is the calculations of Lahiri and Manson (1993).*

The figure also contains theoretically calculated values of the cross section at threshold by Aymar *et al* (1976), Moskvin (1963), Ya'akobi (1967), Gezalov and Ivanova (1968)

and Caves and Dalgarno (1972). It is evident that the cross section is lower at the threshold from where it first increases to a maximum value and then decreases smoothly. This figure shows that our measured values are in good agreement with the calculations of Lahiri and Manson (1993).

Similarly, the photoionization cross section of the $Li^7$ isotope from the 3p excited state measured at different ionizing laser wavelengths from the first ionization threshold up to 3.4 eV is shown in the figure (5.8) for comparison with the theoretical calculated values.

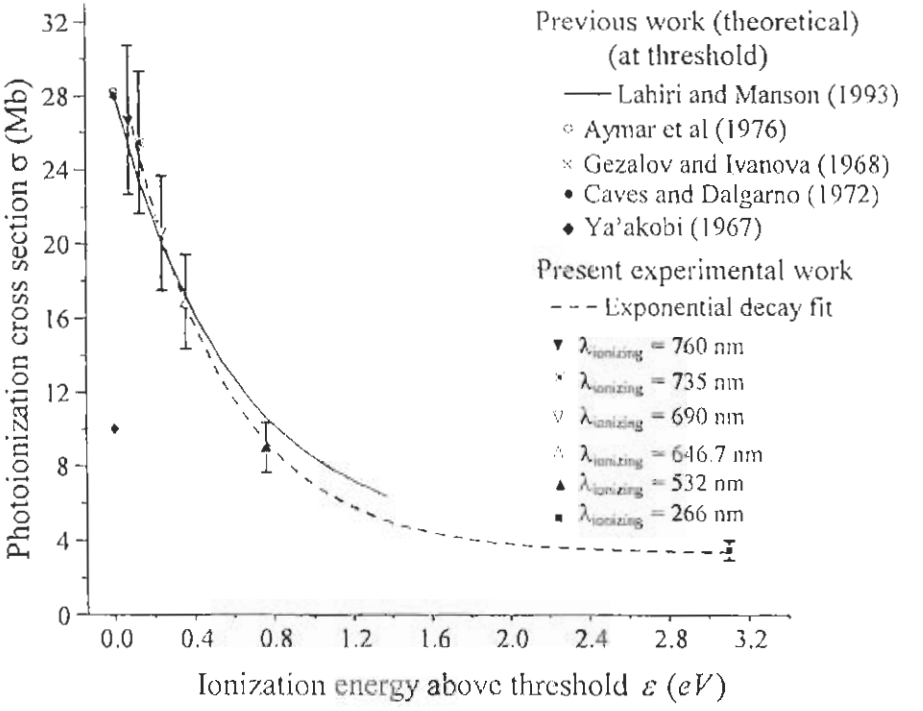


Figure 5.8 *Comparison of the measured values of the absolute photoionization cross section of $Li^{7*}$ 3p with the calculated ones. The solid line is the calculations of Lahiri and Manson (1993) and the dotted line is the exponential fit to the experimentally measured cross sectional values (present work).*

The continuous curve is the calculations of Lahiri and Manson (1993) who used the Central-Potential Model to calculate the cross section of the 3p excited state of lithium, which covers the energy range from the first ionization threshold up to 1.36 eV and the dotted line is the exponential fit to the experimentally measured values of the cross section. The cross section varies with the ionizing laser wavelength and displays an overall decrease from a maximum value ≈ 28 Mb (1Mb = $10^{-18}$ $cm^2$) near threshold to ≈ 4 Mb at 3.1 eV above the ionization threshold. The theoretical calculations exhibit an

excellent agreement with our measured photoionization cross-section in the considered energy range.

Figure (5.9) shows a comparison of our measured values of the cross section of the $Li^7$ from the 3d excited state with the existing literature values. There are only three theoretical values of the cross section at threshold available in the literature by Aymar *et al* (1976), Ya'akobi (1967) and Gezalov and Ivanova (1968) for comparison. There does not exist any experimental or theoretical value of the cross section of 3d excited state above the first ionization threshold. We have for the first time measured the cross sections from the 3d excited state above the threshold at different ionizing laser wavelengths. We used an exponential decay law to fit the experimentally measured cross sections for the $Li^7$ isotope just to show the decreasing trend of the photoionization cross section (figure 5.9). The wavelength range of the ionizing laser extends from just above the first ionization threshold of lithium ($1s^2\ ^1S_0$) to the energy of 3.1 eV. It is evident that for the $Li^7$ isotope, the cross section is maximum (17.2 Mb) at 765 nm (0.11 eV) and decreases to 2.0 Mb at 266 nm (3.1 eV). This figure demonstrates a rapid decay of the photoionization cross section above the ionization threshold.

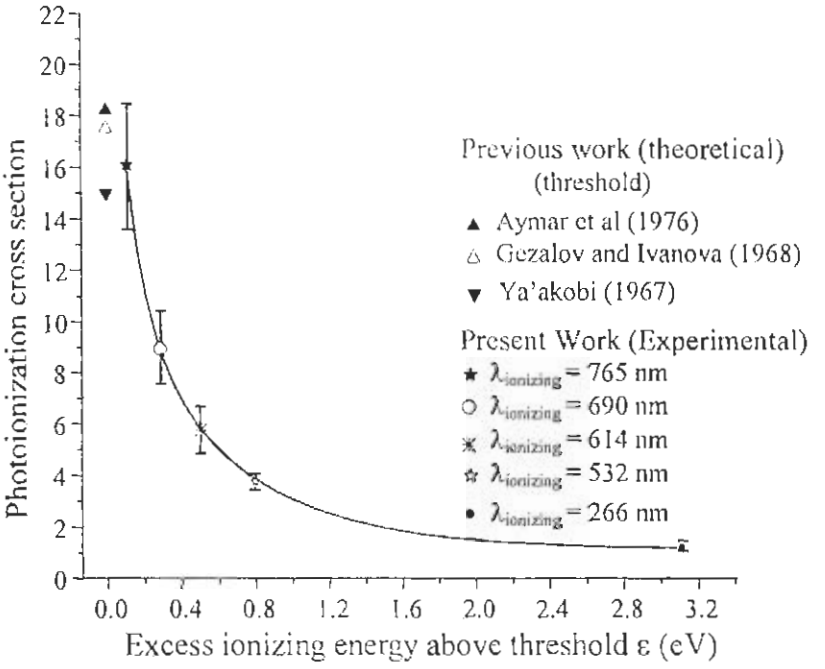


Figure 5.9 *Comparison of the present measured values (experimentally) of the absolute photoionization cross section of $Li^{7*}$ $3d\ ^2D$ with the theoretically calculated cited literature.*

Figure (5.10) shows a comparison of our measured values for $Li^7$ from the 4s excited state with the theoretical calculated values. It contains two theoretical values by Aymar *et al* (1976) and Gezalov and Ivanova (1968) and a continuous curve calculated by Lahiri and Manson (1993) based on the Central Potential Model. The continuous curve covers the energy range from the first ionization threshold up to 6.8 eV. It is evident that our measured values are in good agreement with the calculations of Lahiri and Manson (1993). Similar to the 3s excited state, the cross section of the $Li^7$ from the 4s excited state is also lower at threshold and then increases to a maximum value and after that a smooth decreased is observed.

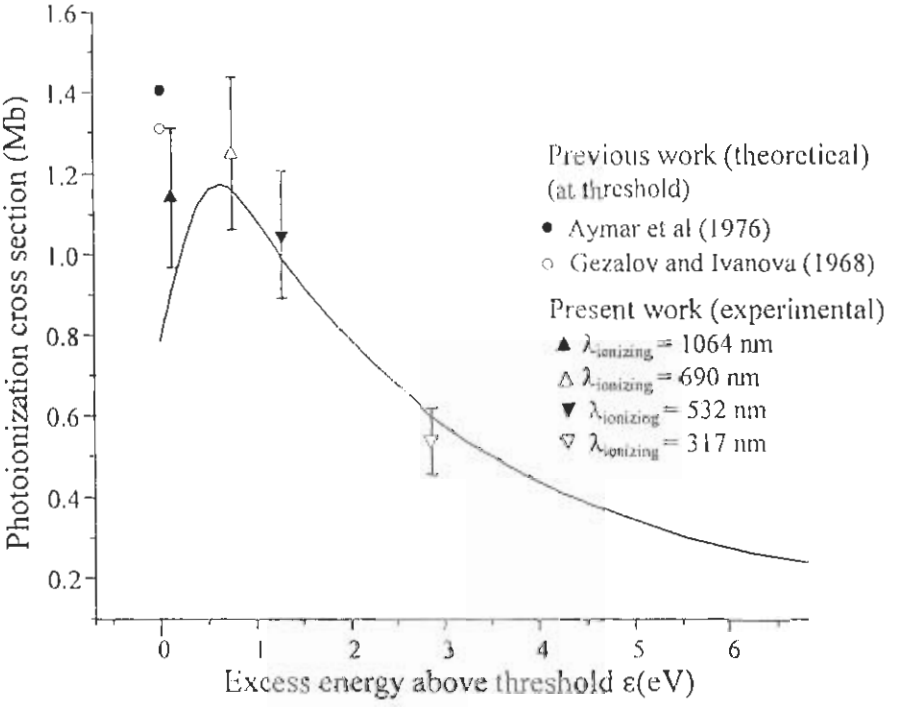


Figure 5.10 *Comparison of the present measured values of the absolute photoionization cross section of $Li^{7+}$ 4s $^2S$ with the theoretically calculated values as a function of the excess photon energy above the first ionization threshold. The solid line is the calculations of Lahiri and Manson (1993).*

The measured values of the cross-sections of $Li^7$ from the 4p excited state are shown in the figure (5.11) to give a comparison with the theoretically calculated values. The continuous curve is the calculations of Lahiri and Manson (1993) that covers the energy range from ionization threshold up to 1.36 eV, whereas the dotted line is the exponential decay fit to our measured cross sections up to 3.1 eV. The decreasing trend of our measured cross sections is in good agreement with the calculations of Lahiri and Manson.

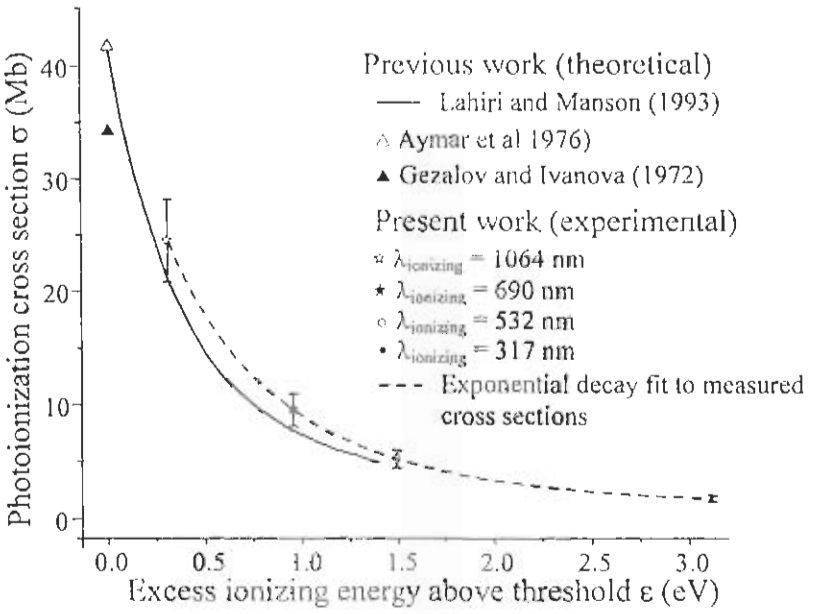


Figure 5.11 *Comparison of the measured values of the absolute photoionization cross section of the $Li^{7*}$ $4p\ ^2P$ with the theoretically calculated values. The solid line is the calculations of Lahiri and Manson (1993), whereas the dotted line is the exponential decay fit to the measured cross sections.*

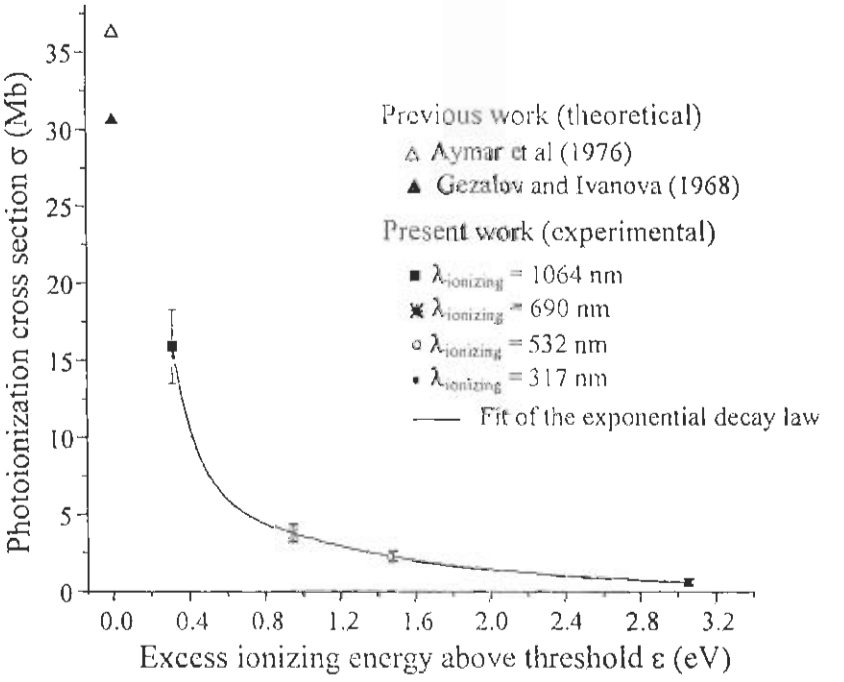


Figure 5.12 *Comparison of the present measured values (experimental) of the absolute photoionization cross section of $Li^{7*}$ $4d\ ^2D$ with the theoretically calculated values. The solid line is a fit of the exponential decay law to the experimentally measured cross sections.*

These are the first photoionization cross sections measurements of the lithium isotopes from the 4d $^2$D excited state using different ionizing laser wavelengths above the first ionization threshold. There are only two theoretical values of the cross section calculated at threshold from the 4d $^2$D excited state of lithium by Aymar *et al* (1976) and Gezalov and Ivanova (1968) that are shown in figure (5.12) for comparison. The exponential decay law fit on the measured data points for $Li^7$ is just to show the decrease of the cross section with the excess photon energy (figure 5.12). The decreasing trend of cross section from the 4d excited state is even faster than that from the 3d excited state.

The measured values of the photoionization cross sections from the 3s, 3p, 3d and 4s, 4p, 4d excited states are collectively presented in figure (5.13). The values of the cross section from the 3s and 4s excited states are multiplied by a factor of 25 just to compare the trends of photoionization cross sections with other states. The dotted lines passing through the values of the cross section of 3s and 4s excited states at different ionizing wavelengths are not the fitted curves. These are just drawn for the comparison with the 3p, 3d and 4p, 4d excited states. The solid lines are the exponential decay fit to the experimental data points for the photoionization cross section from the 3p, 3d and 4p, 4d excited states.

The behavior of the photoionization cross-section for the excited states can be correlated with the difference between the initial state quantum defect and the final continuum threshold phase shift. The quantum defects of s and p states of lithium are 0.4 and 0.05 respectively and are effectively zero for $\ell \geq 2$ (Lahiri and Manson 1993). Thus only transitions involving s or p states are nonhydrogenic while the remainders are entirely hydrogenic. It has been shown that a difference of about 0.5 is necessary to have a Cooper minimum in the continuum (Felfli and Manson 1990).

There is only one channel εp through which the electrons from the *n*s excited states can be promoted to the ionization continuum. The difference between the *n*s quantum defect and the threshold εp phase shift is 0.37, which is less than 0.5 therefore a minimum is expected in the discrete region near the threshold (Lahiri and Manson 1986). The presence of this minimum causes the *n*s cross section to be anomalously small at threshold (Lahiri and Manson 1993). Our measured values of the cross-section for the 3s and 4s excited states at threshold are close to those calculated by Lahiri and Manson

(1993) in comparison with Aymar *et al* (1976), Moskvin (1963), Ya'akobi (1967), Gezalov and Ivanova (1968) and Caves and Dalgarno (1972). This confirms the theoretical prediction of Lahiri and Manson (1993) about the behavior of cross sections of the *n*s excited states of lithium. It is also evident that for the 3s $^2$S and 4s $^2$S excited states, the photoionization cross section first increases to a maximum value and then decreases with the increase in the ionizing laser photon energy, also deviating from the hydrogenic behavior. In addition, the decreasing trend of the cross section from the 4s $^2$S excited state is faster than the 3s $^2$S excited state, which indicates that with an increase in the principal quantum number *n*, the effects of the inner, nonhydrogenic region of the potential becomes less important.

A smooth decrease in the photoionization cross section above the ionization threshold attributes to the fact that when the ionizing electron gains high kinetic energy, its electron wave becomes more oscillatory and as a result the vacated orbital and the photoelectron wave are no more in the same spatial region and consequently the photoionization cross section for that ionizing photon decreases (Green and Decleva 2005).

The behavior of the photoionization cross section from the np-excited states is completely different from that of the ns or nd excited states. The excited electrons from the p-states can be promoted to the ionization continuum through two different channels $np \rightarrow \varepsilon s$ and $np \rightarrow \varepsilon d$. The contribution of the $np \rightarrow \varepsilon s$ channel towards the photoionization cross section is very small while the most dominating channel is the $np \rightarrow \varepsilon d$ according to the transition intensity selection rules (Cowan 1981). The contribution of S and D waves cannot be verified on the experimental basis because experimentally we can only determine the total absolute cross section of the excited state. The threshold phase shift difference for $np \rightarrow \varepsilon d$ is only 0.5, which discards any possibility of a minimum. The figure (5.14) shows a comparison of our measured cross sections of the 2p $^2P_{3/2}$, 3p $^2$P and 4p $^2$P excited states for the $Li^7$ as a function of the excess ionizing photon energy.

It is evident that no minimum is present in the photoionization cross section from the 2p $^2P_{3/2}$, 3p $^2$P and 4p $^2$P excited states near threshold. The cross sections decrease monotonically with the increase in the ionizing laser wavelength above the first ionization threshold but this falloff of the cross section is not hydrogenic due to the small quantum defects for the p-states. Furthermore, near threshold, the cross section increases

with $n$ and then falloff more rapidly with the excess photon energy. The rapid decay of the cross section near threshold with the increase in $n$ indicates the decreasing contribution of the non-hydrogenic region of the potential.

For the photoionization of the atoms from the $n$d-excited states, there are two possible ionization channels εp and εf through which the excited electrons from these states can be uplifted to the ionization region. The $n$d → εp cross section is slightly different from hydrogenic, owing to the small p-wave phase shift, but the $n$d → εf is completely hydrogenic because for $l \geq 2$, the quantum defects or phase shifts are effectively zero. In addition the contribution of the $n$d → εf channel towards the photoionization cross section dominates so that the contribution of $n$d → εp channel is not of great interest (Lahiri and Manson 1993). The fitted curves through the measured data points for the 3d $^2$D and 4d $^2$D excited states (figure 5.13) decrease more sharply with the increase in the ionizing laser photon energy. This decreasing behavior of the cross section from the $n$d excited states is purely hydrogenic as compared to that of the $n$s or $n$p excited states. In addition, the cross sections from the 4d $^2$D excited state decay faster than the cross sections from the 3d $^2$D state with the increase in the ionizing laser photon energy, which is in accordance with the theoretical prediction.

The radiative recombination is a process in which a continuum electron (free electron) is captured by the ion via a spontaneous emission of a photon. It is therefore an inverse process of photoionization. The radiative recombination process plays an important role in the measurements of the photoionization cross section near the ionization threshold. The cross section for the radiative recombination can be extracted from the detailed balance principle as described by Lahiri and Manson (1993). A comparison in figure (5.13) shows that the photoionization cross sections of the np-excited states are slightly greater than the cross sections of the nd states but are larger by more than an order of magnitude to those of the $n$s excited states. Thus the radiative recombination cross section for the $n$p excited states is greater than for the $n$d and much greater for the ns excited states.

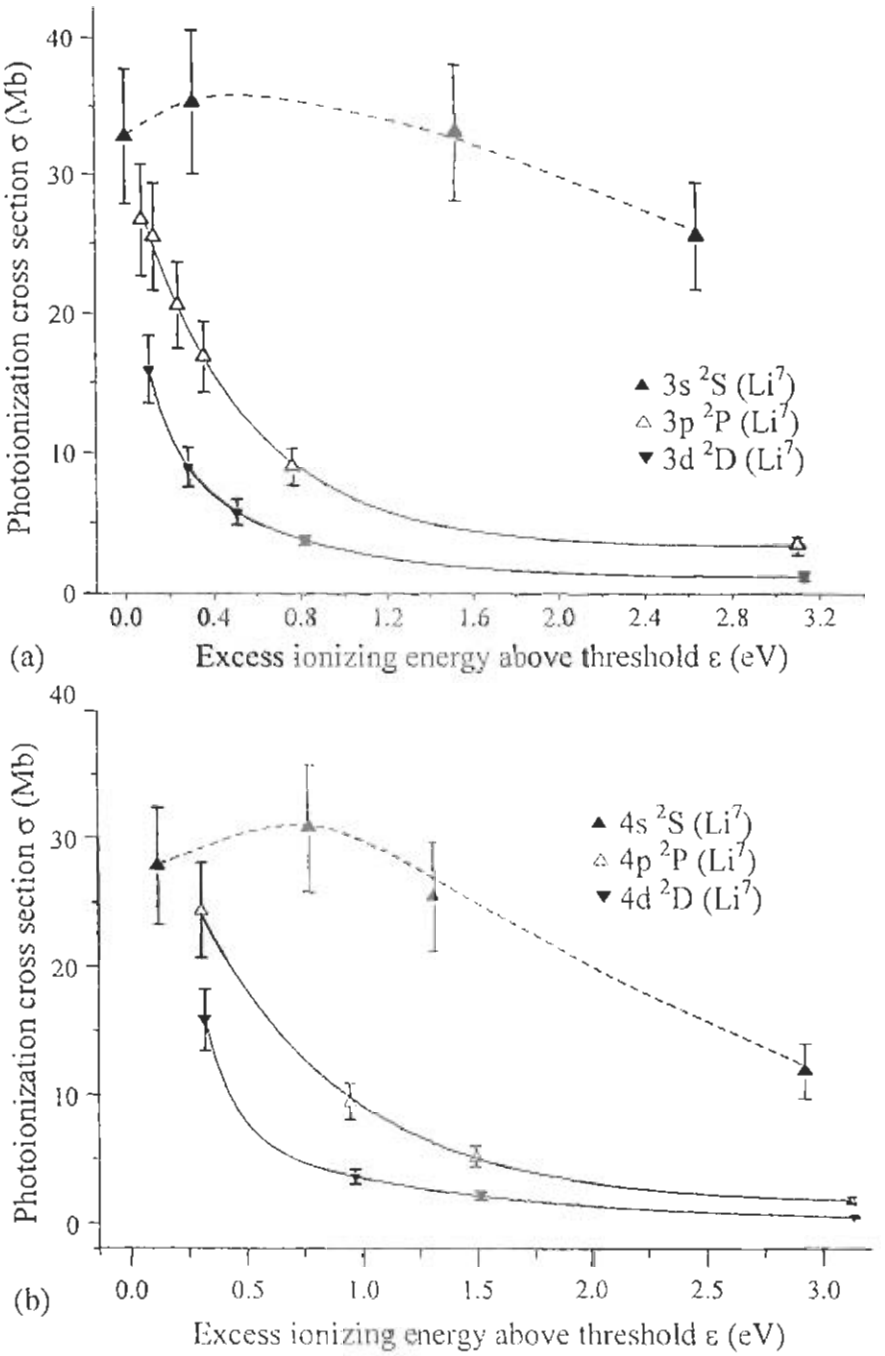


Figure 5.13 *A comparison of the energy dependent behavior of the measured values of the photoionization cross section from the (a) 3s $^2S$, 3p $^2P$, 3d $^2D$ and (b) 4s $^2S$, 4p $^2P$, 4d $^2D$ excited states of lithium. The photoionization cross sections of the 3s $^2S$ and 4s $^2S$ excited state are multiplied by 25 just to compare with the other excited states. The dotted lines passing through the cross sections of the 3s $^2S$ and 4s $^2S$ excited states are not the fitted curve. The solid lines are the exponential decay fit to the experimental data points for the photoionization cross section from the 3p $^2P$, 3d $^2D$ and 4p $^2P$, 4d $^2D$ excited states.*

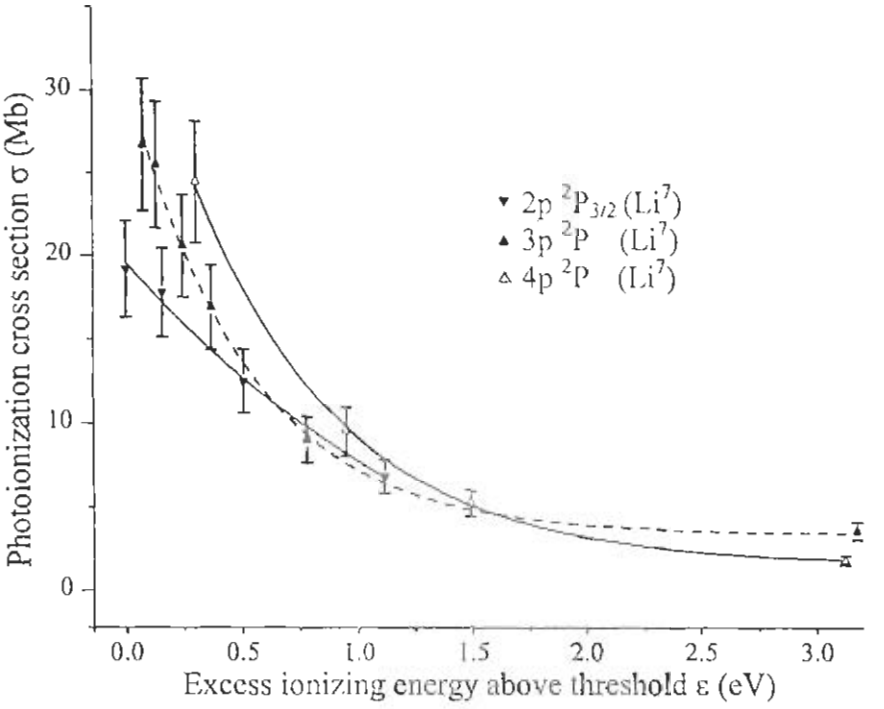


Figure 5.14 *A comparison of the energy dependent behavior of the measured values of the photoionization cross sections from the 2p $^2P_{3/2}$, 3p $^2P$ and 4p $^2P$ excited states of $Li^7$. The solid/dotted lines are the exponential decay fit to the experimental data points.*

# Conclusion

A well collimated atomic beam apparatus and a Time of Flight (TOF) mass spectrometer is designed and fabricated locally. The atomic beam source is simple, versatile and can be operated at a stable temperature up to 1000 K. The Time of Flight mass spectrometer provides a two-stage acceleration and one-meter field free length for separating isotopic masses. The optimum performance of this system has been demonstrated by the isotopic separation of lithium. The observed TOF signals are correlated with the flight times for different isotopic masses. The TOF mass spectrometer is capable of detecting different isotopes with their natural abundance and can be used for the simultaneous measurement of the spectroscopic properties of the isotopic masses.

An alternate technique for the simultaneous measurements of the photoionization cross section of the excited states of the isotopic masses has been successfully applied for the determination of the cross sections and the number densities of both the lithium isotopes from the $2p\ ^2P_{1/2,\ 3/2}$, $3s\ ^2S$, $3p\ ^2P$, $3d\ ^2D$, $4s\ ^2S$, $4p\ ^2P$ and $4d\ ^2D$ excited states for the first time. The measured values of the cross sections have been found in good agreement with the existing experimental and theoretical work. The different regions of the ionization continuum have been investigated by promoting the excited electrons to different regions of the continuum from the aforementioned excited states by using different ionizing laser wavelengths. It is found that the cross sections of both the lithium isotopes are maximum at the ionization threshold for the 3p, 3d, 4p and 4d excited states and decreases monotonically with the increase of the excess photon energy above the first ionization threshold except for the 3s and the 4s excited states, where the cross section is lower at the ionization threshold due to the existence of the minima in the discrete region near threshold and then increases to a maximum value and then again decreases smoothly.

Utilizing the combination of the two-step photoionization and atomic beam – TOF mass spectrometer, we have resolved the fine structure of the 2p excited state for both the lithium isotopes using the exciter laser having linewidth ~ 0.1 $cm^{-1}$ that is not sufficiently narrow to selectively excite the isotopic level. However, the use of a TOF mass spectrometer enabled us to resolve these levels because it resolves the ionic masses on the time axis without knowing how they have been produced. The effect of the laser power

broadening on the 2p excited state is also observed that affects the resolution of the fine structure levels and limits the quantitative yield of $Li^6$.

In addition, the ionization yield of the $Li^6$ isotope has been investigated as a function of the exciter laser frequency from all the aforementioned excited states. It was found that the enrichment of $Li^6$ isotope can be enhanced up to 60% by tuning the exciter laser to the 3s $^2S$ and the 3p $^2P$ excited states of the $Li^6$ isotope by using an appropriate exciting laser frequencies respectively. The measured values of the photoionization cross section of the $Li^6$ isotope from the 3s excited state is 1.31 Mb at the threshold and from the 3p is 26.7 Mb just above the threshold, which reveals that the $Li^6$ has very low value of the cross section from the 3s excited state, therefore cannot be used for the quantitative yield. However, $Li^6$ has a large value of the cross section from the 3p excited state, which can however be used very efficiently for the quantitative yield.

Further work in this direction is in progress at this laboratory as the basic experimental set up has been established. In particular, work on the oscillator strength of the Rydberg states and the photoionization cross section at and above the first ionization potential will provide more information about the photoionization processes.

# References


Alpine R D and Evan D K 1985 Adv. Chem. Phys. **60** 31

Amin N, Mahmood S, Anwar-ul-Haq M, Riaz M and Baig M A 2006a European Physical J. D **37** 23

Amin N, Mahmood S, Saleem M, Kalyar M A and Baig M A 2006b European Physical J. D (on line August 2006)

Ambartzumian R V, Furzikov N P, Letokhov V S and Puretsky A A 1976 *Appl. Phys.* **9** 335

Arisawa T, Maruyama Y, Suzuki Y and Shiba K 1982a Appl. Phys. B **28** 73

Arisawa T, Suzuki Y, Maruyama Y and Shiba K 1982b J. Phys. D: Appl. Phys.**15** 1955

Arisawa T, Maruyama Y, Suzuki Y, and Naruse Y 1982 J. Phys. D: Appl. Phys.**16** 2415

Arisawa T, Suzuki Y, Maruyama Y and Shiba K 1983 Chem. Phys. **81** 473

Aushev V E, Zaika N I and Mokhnach A V 1982 Sov. Phys. Tech. Phys. **27** 878

Aymar M, E. Koening L and Farnoux F C 1976 J. Phys. B: At. Mol. Phys. **9** 1279

Azuma Y 1998 Phys. Rev. Lett. **81** 1813

Bass I L, Bonanno R E, Hackel R P and Hammond P R 1992 Appl. Opt. **31** 6993

Balz J G, Bernheim R A and Gold L P 1987 J. Chem. Phys. **86** 6

Bergmann T, Martin T P and Schaber H 1989 Rev. Sci. Instrum. **60** 347

Berkowitz J 1979 *Photoabsorption, Photoionization and Photoelectron Spectroscopy* (New York: Academic Press)

Berkowitz J 2002 *Atomic and Molecular Photoabsorption, Absolute Total Cross sections* (New York: Academic Press)

Bernhardt A F, Duerre D E, Simpson J R and Wood L L 1974 Appl. Phys. Lett. **25** 617

Beterov I M and Ryabtsev I I 1993 Opt. Spectrosc. **75** 313

Bloembergen N and Levenson M D 1976 *High Resolution Spectroscopy* Editor: Shimoda K (Germany: Springer-Verlag)

Bokhan P A, Buchanov V V, Fateev N V, Kalugin M M, Kazaryan M A, Prokhorov A M, Zakrevskii D E 2006 *Laser Isotope Separation in Atomic Vapor* (N:John Wiley)

Boyd R W, Dodd J G, Krasinski J and Stroud C R 1980 Optics Lett. **5** 117

Bradley D J, Dudan C H, Ewart P and Purdie A F 1976 Phys. Rev. A **13** 1416

Bransden B H and Joachain C J 1983 *Physics of Atoms and Molecules* (New York: Longman Inc.)

Burgess A and Seaton M J 1960 Monthly Notices Roy. Astron Soc. **120**, 121

Burke P G, Francken P and Joachain C J 1991 J. Phys. B: At. Mol. Opt. Phys. **24** 751

Burke P G, Berrington K A 1993 *Atomic and Molecular Processes: An R-matrix Approach* ( Bristol: Institute of Phys.)

Burkhardt C E, Libbert J L, Xu J and Leventhal J J 1988 Phys. Rev. A **38** 5949

Cameron A E and Eggers D F 1948 Rev. Sci. Instrum. **19** 605

Cantrell C D, Freund S M and Lyman J L 1979 *Laser Handbook*, vol. 3 ed. by Stitch M L (North Holland, Amsterdam)

Castaldi M J and Senkan S M 1998 J. of Air & Waste Management Association **48** 77

Caves T C and Dalgarno A 1972 J. Quant. Spectrosc. Radiat. Transfer **12** (1972) 1539

Chang T N and Kim Y S 1982 J. Phys. B: At. Mol. Phys. **15** L835

Compbell I E and Shewood E M 1967 *High Temperature Materials and Technology* (New York: Wiley)

Cowan R D 1981 *The Theory of Atomic Structure and Spectra* (University of California Press)

Dawson J M, Kim H C, Arnush D, Fried B D, Gould R W, Heflinger L O, Kennel C F, Romesser T E, Stenzel R L, Wong A Y and Wuerker 1976 Phys. Rev. Lett. **37** 1547

Demtröder W 1998 *Laser spectroscopy: basic concepts and instrumentation* (Berlin: Springer-Verlag)

Dinneen T P, Wallace C D, Tan K -Y N, Gould P L 1992 Opt. Lett. **17** 1706

Dirac P A M 1958 *The Principles of Quantum Mechanics* (Oxford, Clarendon Press)

Duarte F J and Piper J A 1980 Optics Commun. **35** 100

Duarte F J and Piper J A 1984 Appl. Opt. **23** 1391

Duarte F J 1995 *Dispersive external-cavity semiconductor lasers* in *Tunable Laser Applications* Editor: Duarte F J (New York: Marcel-Dekker)

Dunning F B and Stebbings R F 1974 Phys. Rev. Lett. **32** 1286

Dushman 1966 *Scientific Foundation of Vacuum Technology* (John Wiley)

Ehrfeld W 1983 *Elements of Flow and Diffusion Processes in Separation Nozzles* (Springer-Verlag)

Estermann I 1946 *Rev. Modern Phys.* **18** 300

Felfli Z and Manson S T 1990 Phys. Rev. A **41** 1709

Fraser R G J 1931 *Molecular Rays* (London: Cambridge University Press)

Gabbanini C, Gozzini S and Lucchesini A 1997 Opt. Commun. **141** 25

Gerwert K and Kollath K J 1983 J. Phys. B: At. Mol. Phys. **16** L217

Gezalov Kh B and Ivanova A V 1968 High Temp. **6** 400

Giormaine J A and Wang T C 1960 *J. Appl. Phys.* **31** 463

Gisselbrecht M, Descamps D, Lynga C, L'Huillier A, Wahlstrm C –G and Meyer M 1999 Phys. Rev. Lett. **82** 4607

Goeppert-Mayer M 1931 Ann. Physik **9** 273

Gomide J V B, Garcia G A, Cruz F C, Polaquini A J, Arruda M P, Pereira D, Scalabrin A 1997 Brazilian Journal of Physics **27** 266

Green J C and Decleva P 2005 Coordination Chemistry Reviews **249** 209

Griesmann U, Esser B and Baig M A 1992 J. Phys. B: At. Mol. Opt. Phys. **25** 3475

Guilhaus M 1995 J. Mass Spectrometry **30** 1519

Hanna D Karkainen, P and Wyatt R 1975, Opt. Quantum Electron.**7** 115

Hansch T W 1972 Appl. Opt. **11** 895

He L -W, Burkhardt C E, Ciocca M, Leventhal, Manson S T 1991 Phys. Rev. Lett. **67** 2131

Heinzmann U, Schinkowski D and Zeman H D 1977 Appl. Phys. **12** 113

Hollberg L 1990 *CW dye lasers* in *Dye Laser Principles* Editor: Duarte F J and Hillman L W (New York: Academic)

Huang M T, Wehlitz R, Azuma Y, Pibida L, I. Sellin A, Cooper J W, Koide M, Ishijima H and Nagata T 1999 Phy. Rev. A **59** 3397

Hurst G S, Payne M G, Kramer S D and Young J P 1979 Rev. Mod. Phys, **51** 767

Hussain S, Saleem M, Rafiq M and Baig M A 2006 Phys. Rev. A **74** 022715

Kallenback A, Kock M and Zierer G 1988 Phys. Rev. A **38** 2356

Karlov N V, Krynetskii B B and Stel'makh O M 1977 Sov. J. Quantum Electron. **7** 1305

Karlov N V, Krynetskii B B, Mishin V A and Prokhorov A M 1978 Appl. Opt. **17**, 856

Karlov N V, Krynetskii B B, Mishin V A and Prokhorov A M 1979 Sov. Phys. Usp. **22** 220

Kupliauskiene A 1997 J. Phys. B: At. Mol. Opt. Phys. **30** 1865

Lahiri J and Manson S T 1986 Phys. Rev. A **33** 3151

Lahiri J and Manson S T 1993 Phys. Rev. A **48** 3674

Letokhov V S 1987 *Laser Photoionization Spectroscopy* (Orlando: Academic Press)

L. Li, Y. Wang, M. Li, Chin. Phys. **3**, 155 (1983)

Lievens P, Vandeweert E, Thoen P and Silverans R E 1996 Phys. Rev. A **54**, 2253

Littmam M G and Metcalf H J 1978 Appl. Opt. **17** 2224

Lorenzen C J and Niemax K 1982 J. Phys. B: At. Mol. Phys. **15** L139

Madine M and van der Hart H W 2005 J. Phys. B: At. Mol. Opt. Phys. **38** 1895

Madsen D N, Balslev S, Drewsen M, Kjaergaard N, Videnscn Z and Thomsen J W 2000 J. Phys. B: At. Mol. Opt. Phys. **33** 4981

Maissel L I and Glang R 1970 *Handbook of Thin Film Technology* (New Yark: Mc Graw-Hill)

Mamyrin B A, Schmikk D V and Zagulin V A 1973 Soviet Phys. JETP **37** 45

Marago O, Ciampini D, Fuso F, Arimondo E, Gabbanini C, Manson S T 1998 Phys. Rev. A **57** R4110

Mariella R P 1982 U. S. patent 4320300

Marr G V 1967 *Photoionization Processes in Gases* (New York: Academic Press)

Maruyama Y, Kato M, Arizawa T 1996 Opt. Eng. **35** 1084

McAlexander W I, Abraham E R I and Hulet R G 1996 Phys. Rev. A **54**, R5

Mende W, Bartschat K and Kock M 1995 J. Phys. B: At. Mol. Opt. Phys. **28** 2385

Mende W and Kock M 1996 J. Phys. B: At. Mol. Opt. Phys. **29** 655

Moskvin Yu V 1963 Optics Spectrosc. **15** 316

Msezane A Z and Manson S T 1984 Phys. Rev. A **30** 1795

Myers E G, Murnick D E and Softky W R 1987 Appl. Phys. B: **43** 247

Nahar S N and Manson S T 1989 Phys. Rev. A **40** 6300

Niemax K 1985 Appl. Phys. B **38** 147

Nygaard K J, Hebner R E, Jones J D and Crbin R J 1975 Phys. Rev. A **12** 1440

O'Hanlon J F 1989 *A user's guide vacuum technology* (N York: John Wiley)

Olivares I E and Duarte A E 1999 Appl. Opt. **38** 7481

Olivares I E, Duarte A E, Saravia E A and Duarte F J 2002 Appl. Opt. **41** 2973

Patterson B M, Takekoshi T and Knize R J 1999 Phys. Rev. A **59** 2508

Payne M G, Deng L, Thonnard N 1994 Rev. Sci. Instrum. **65** 2433

Philipsen V, Bastiaansen J, Verschoren G, Lievens P, Vandeweert E, Silverans R E, Telle H H 2000 Spectrochimica Acta Part B **55** 1539

Radzig A A and Smirnov B M 1985 *Reference Data on Atoms, Molecules and Ions* (Springer Verlag).

Ramsey N F 1956 *Molecular Beams* (Oxford Press)

Ready J F 1965 *J. Appl. Phys.* **36** 462

Ross K J and Sonntag B 1995 *Rev. Sci. Instrum.* **66** 4409

Rothe D E 1969 J. Quant. Spectrosc. Radiant. Transfer **9** 49

Rothe D E 1971 J. Quant. Spectrosc. Radiant. Transfer **11** 355

Rouvellou B, Bizau J –M, Cubaynes D, Novak J, Pahler M, Journel, Wuilleumier F J, Saha H P, Pindzola M S and Compton R N 1988 Phys. Rev. A **38** 128

Saleem M, Amin N, Hussain S, Rafiq M, Mahmood S and Baig M A 2006 Eur. Phys. J. D **38** 277

Saleem M, Hussain S, Rafiq M and Baig M A 2006 J. Appl. Phys. **100** 053111

Saleem M, Hussain S, Rafiq M and Baig M A 2006 J. Phys. B: At. Mol. Opt. Phys. **39** 5025

Sansonetti C J, Richou B, Engleman R, Radziemski L J 1995 Phys. Rev. A **52** 2682

Sato Y, Hayaishi T, Itikawa Y, Itoh Y, Murakami J, Nagata T, Sasaki T, Sonntag B, Yagishita A and Yoshino M 1985 J. Phys. B: At. Mol. Phys. **18** 225

Seaton M J 1951 Proc. Roy. Soc. A **208** 418

Schafer F P, Schmidt W and Volze J 1966 Appl. Phys. Lett. **9** 306

Selby D S, Mlynski V and Guilhaus M 2001 Int. Journal of Mass Spectrometry **206** 201

Singh S, Dasgupta K, Kumar S, Manohar K G, Nair L G and Chatterjee U K 1994 Opt. Eng. **33** 1894

Shimazu M, Takubo Y and Maeda Y 1977 Japan J. Appl. Phys. **16** 1275

Shoshan I, Danon N N and Oppenheim U 1977 J. Appl. Phys. **48** 4495

Smith A V, Goldsmith J E M, Nitz D E and Smith S J 1980 Phys. Rev. A **22** 577

Sobel'man I I 1972 *Introduction to the Theory of Atomic Spectra* (N: Pergamon Press)

Song J M, Inoue T, Kawazumi H and Ogawa T 1999 Anal. Sciences **15,** 601

Sorokin P P and Lankard J P 1966 IBM J. Res. Dev. **10** 162

Stephens W I 1946 Phys. Rev. **69** 691

Stewart A L 1954 Proc. Roy. Soc. A **67** 917

Sugiyama A, Nakayama T, Kato M, Maruyama Y, Arisawa T 1996 Opt. Eng. **35** 1093

Symons E A 1985 Sep. Sci. Technol. **20** 633

Tayal S S, Msezane A Z and Manson S T 1994 Phys. Rev. A **49** 956

Thompson D C and Stoicheff B P 1982 Rev. Sci. Instrum. **53** 822

Thorne A P 1988 Spectrophys (London : Chapman)

Topping J 1962 *Errors of observation and their treatment* (London: Chapman and Hall)

Villani S 1979 *Uranium Enrichment* (Springer-Verlag)

Van der Hart H W and Greene C H 1998 Phys. Rev. Lett. **81** 4333

Voky L, Faucher P, Hilbbert A, Berrah N 1995 Phys. Rev. Lett. **75** 33

Walls J, Ashby R, Clarke J J, Lu B and van Wijngaarden W A 2003 European Physical J. D **22** 159

Wehlitz R, Bluett J B and Whitfield S B 2002 Phys. Rev. A **66** 012701

Wehlitz R, Luckić D, Koncz C and Sellin I A 2002 Rev. Sci. Instrum. **73** 1671

Weissler G L and Carlson R W 1979 *Methods of Experimental Physics: Vacuum Physics and Technology* vol. 14 (London: Academic Press)

Wiley W C and McLaren I H 1955 Rev. Sci. Instrum. **26** 1150

Willke B and Kock M 1993 J. Phys. B: At. Mol. Opt. Phys. **26** 1129

Windholz L 1995 Appl. Phys. B **60** 573

Wippel V, Binder C, Huber W, Windholz L, Allegrini M, Fuso F and Arimondo E 2001 Eur. Phys. J. D **17** 285

Xiwen Z, Guilong H, Ganghua M and Delin Y 1999 J. Phys. B: At. Mol. Opt. Phys. **25** 3307

Ya'akobi B 1967 Pro. Phys. So. **92** 100

Yamashita M and Kashiwagi H 1979 U. S. patent 4149 077

Yan Z C and Drake G W F 2002 Phys. Rev. A **66** 042504

Yang F and Hamilton J H 1996 *Modern Atomic and Nuclear Physics* (New York: McGraw-Hill)

Zare R N 1977 Sci. Am. **236** 86

Zorabedian P 1995 *Tunable external-cavity semiconductor lasers* in *Tunable Lasers Handbook* Editor: F. J. Duarte (New York: Academic)

Zhang J, Lambropoulos P, Zei D, Compton R N and Stockdale J A D 1992 Z. Phys. D-Atoms, Molecules and Clusters **23** 219

Zhou H L, Kim D S, Felfli Z and Manson S T 1993 Phys. Rev. A **47** 4496